



ERNEST ORLANDO LAWRENCE BERKELEY NATIONAL LABORATORY

Suppression of Bremsstrahlung and Pair Production due to Environmental Factors

Spencer Klein
Nuclear Science Division

February 1998

Submitted to
Reviews of Modern Physics



Lawrence Berkeley National Laboratory
Bldg. 50 Library - Ref.
REFERENCE COPY
Does Not Circulate
COPY 1

DISCLAIMER

This document was prepared as an account of work sponsored by the United States Government. While this document is believed to contain correct information, neither the United States Government nor any agency thereof, nor the Regents of the University of California, nor any of their employees, makes any warranty, express or implied, or assumes any legal responsibility for the accuracy, completeness, or usefulness of any information, apparatus, product, or process disclosed, or represents that its use would not infringe privately owned rights. Reference herein to any specific commercial product, process, or service by its trade name, trademark, manufacturer, or otherwise, does not necessarily constitute or imply its endorsement, recommendation, or favoring by the United States Government or any agency thereof, or the Regents of the University of California. The views and opinions of authors expressed herein do not necessarily state or reflect those of the United States Government or any agency thereof or the Regents of the University of California.

**Suppression of Bremsstrahlung and
Pair Production due to Environmental Factors**

Spencer Klein

Nuclear Science Division
Ernest Orlando Lawrence Berkeley National Laboratory
University of California
Berkeley, California 94720

February 1998

Suppression of Bremsstrahlung and Pair Production due to Environmental Factors

Spencer Klein

Lawrence Berkeley National Laboratory, Berkeley, CA 94720

Abstract

The environment in which bremsstrahlung and pair creation occurs can strongly affect cross sections for these processes. Because ultra-relativistic electromagnetic interactions involve very small longitudinal momentum transfers, the reactions occur gradually, spread over long distances. During this time, even relatively weak factors can accumulate enough to disrupt the interaction.

This review will discuss a variety of factors which can suppress bremsstrahlung and pair production, as well as related effects involving beamstrahlung and QCD processes. After surveying different theoretical approaches, experimental measurements from the early cosmic ray studies to the recent detailed measurements by the SLAC E-146 collaboration will be discussed.

(Submitted to *Reviews of Modern Physics*)

Typeset using REVTeX

I. INTRODUCTION

Bremsstrahlung and pair creation are two of the most common high energy electromagnetic processes, and the interaction cross sections are well known (Bethe and Heitler, 1934). However, it is much less well known that these cross sections can change dramatically depending on the medium in which the interaction occurs. The SLAC E-146 collaboration observed photon intensities as low as 1/4 of that predicted by Bethe and Heitler, and much larger suppression is possible.

This happens because the kinematics of the processes dictates that they be spread over a significant distance; in contrast to the common picture where reactions occur at a point. The momentum transfer between a highly relativistic interacting particle and the target nucleus is small, especially along the direction of particle motion. When this longitudinal momentum transfer is small, the uncertainty principle dictates that the interaction is spread out over a distance, known as the formation length for particle production, or, more generally, as the coherence length.

If the medium in the neighborhood of the interaction has a large enough influence on the interacting particle during its passage through the formation zone, then the pair production or bremsstrahlung can be suppressed. Because the formation length can be quite long, weak, cumulative factors can have a large effect. Some of the factors that may suppress electromagnetic radiation are multiple scattering, photon interactions with the medium (coherent forward Compton scattering), and magnetic fields. In crystals, where the atoms are arranged in ordered rows, a large variety of effects can suppress or enhance radiation.

The formation length has a number of interesting physical interpretations. It is the wavelength of the virtual photon that was exchanged. It is also the distance required for the final state particles to separate enough (by a Compton wavelength) that they act as separate particles. It is also the distance over which the amplitudes from several interactions can add coherently to the total cross section. All of these pictures can be helpful in understanding different aspects of suppression mechanisms.

The formation length occurs in both classical and quantum mechanical calculations. Classically, any electromagnetic process has a phase factor

$$\Phi = \exp \{i[\omega t - \mathbf{k} \cdot \mathbf{r}(t)]\} \quad (1)$$

where ω is the photon frequency, t is the time, \mathbf{k} is the photon wave vector, and $\mathbf{r}(t)$ is the electron position. The formation length is the distance over which this phase factor maintains coherence. Coherence is maintained over a pathlength for which $\omega t - \mathbf{k} \cdot \mathbf{r}(t) \sim 1$, given by

$$l_{f0} = \frac{E^2}{\omega m^2 c^3} \quad (2)$$

where E is the electron energy, m is the electron mass, and c the speed of light. The f_0 subscript denotes the unsuppressed (free space) formation length. Electromagnetic interactions are spread over this distance. In many kinematic regions, l_{f0} can be very long. For example, for a 25 GeV electron radiating a 10 MeV bremsstrahlung photon, $l_{f0} = 100 \mu\text{m}$. This classically derived distance was the basis for the initial suppression calculations by Landau and Pomeranchuk, discussed in Sec. II.

The formation length also occurs in quantum calculations. Here, it is useful to start with a simple reaction like electron bremsstrahlung, in which an electron interacts with a nucleus and emits a real photon; when the electron accelerates, part of its surrounding virtual photon field shakes loose. Neglecting the photon emission angle and electron scattering, the momentum transfer in the longitudinal (+z) direction is

$$q_{\parallel} = p_e - p'_e - k/c = \sqrt{(E/c)^2 - (mc)^2} - \sqrt{((E-k)/c)^2 - (mc)^2} - k/c \quad (3)$$

where p_e and p'_e are the electron momenta before and after the interaction respectively and $k = \omega/\hbar$ is the photon energy. For $\gamma = E/mc^2 \gg 1$ this simplifies to

$$q_{\parallel} \sim \frac{m^2 c^3 k}{2E(E-k)}. \quad (4)$$

Here, we have used the small y approximation $\sqrt{1-y} \sim 1-y/2$. For high energy electrons emitting low energy photons, q_{\parallel} can become very small. For the above example, $q_{\parallel} = 0.03$ eV/c. Because q_{\parallel} is so small, the uncertainty principle requires that the radiation must take place over a long distance:

$$l_{f0} = \frac{\hbar}{q_{\parallel}} = \frac{2\hbar E(E-k)}{m^2 c^3 k}. \quad (5)$$

For $k \ll E$, this matches Eq. (2); the quantum mechanical calculation is needed only for $k \sim E$.

This formation length appears in most electromagnetic processes including pair production, transition radiation, Čerenkov radiation and synchrotron radiation. Usually, Eq. (5) is modified because q_{\parallel} acquires additional terms to account for specific interactions with the target medium. The body of this review will discuss a number of these additional terms, and show how they affect bremsstrahlung and pair production. Formation lengths apply to many processes involving other forces; this review will discuss a few non-electromagnetic interactions, showing how diverse reactions share many fundamental traits that stem from the kinematics.

The formation length affects radiation because it is the distance over which the interaction amplitudes can add coherently. So, if an external force doubles q_{\parallel} , thereby halving l_f , then the radiation intensity is reduced from $\sim l_f^2$ to $\sim 2 \cdot (l_f/2)^2$, a factor of 2, as the path-length splits into two independent emitters. If there is emission from an electron traversing a distance D , the trajectory acts as D/l_f independent emitters, each with a strength that scales as $|l_f|^2$, giving a total radiation proportional to l_f . As external factors increase q_{\parallel} and reduce l_f , the radiation drops proportionally.

A similar coherence distance \hbar/q_{\perp} limits the perpendicular distance over which coherent addition is possible. However, because $q_{\perp} \gg q_{\parallel}$, this dimension is much smaller, and of lesser interest here.

This article begins by considering separate classical and quantum calculations of suppression due to multiple scattering. Suppression due to photon interactions with the medium, pair creation and external magnetic fields will then be similarly considered.

More detailed calculations have considered the multiple scattering in more detail, as producing transverse diffusion of the electron. Migdals 1956 calculation, discussed in Sec.

III, was the earliest work; it will be considered a standard here. There have been a number of recent calculations of suppression, discussed in Secs. V to VII.

Experimental work is surveyed in Sec. IX, beginning with the first limited cosmic ray studies of Landau-Pomeranchuk-Migdal (LPM) suppression shortly after Migdals paper. These all suffered from very limited statistics, and hence had limited significance. In the 1970's and 1980's, a few accelerator experiments provided some data, but with limited detail. In 1993, SLAC experiment E-146 made detailed measurements of suppression due to multiple scattering and photon-medium interactions. E-146 confirmed Migdals formula to good accuracy, and at least partly inspired the more recent calculations in Secs. V to VII; because of this timing, some reference will be made to E-146 in the theory discussion before the experiment has been discussed.

Some more specialized topics will also be considered. Section X considers suppression in plasmas, where particles with similar energies interact with each other. Section XI will show how suppression mechanisms can affect electromagnetic showers, with a special focus on air showers. Section XII surveys the application of LPM formalism to hadrons scattering inside nuclei, where color charge replaces electric charge, and gluons replace photons. Finally, a number of open questions will be presented.

Earlier reviews (Feinberg and Pomeranchuk, 1956) (Akhiezer and Shulga, 1987) and a monograph (Ter-Mikaelian, 1972) have discussed these topics. Unless otherwise indicated, energies will be given in electron volts (eV) and momentum in eV/c; $\hbar c$ is 1.97×10^{-7} eV m and the fine structure constant $\alpha = e^2/\hbar c \approx 1/137$, where e is the electric charge. For both bremsstrahlung and pair conversion, E will represent electron/positron energy and k photon energy.

II. CLASSICAL AND SEMI-CLASSICAL FORMULATIONS

Landau and Pomeranchuk (1953a) used classical electromagnetism to demonstrate bremsstrahlung suppression due to multiple scattering; the suppression comes about because of the interference between photons emitted by different elements of electron path-length. For those with quantum tastes, subsection II.B gives a simpler derivation based on the uncertainty principle.

A. Classical Bremsstrahlung - Landau and Pomeranchuk

The classical intensity for radiation from an accelerated charge in the influence of a nucleus with charge Z is

$$\frac{d^2 I}{d\omega d\Omega} = \frac{Z^2 e^2 \omega^2}{4\pi^2 c^2} \left| \int \mathbf{n} \times d\mathbf{r} \exp \{i[(\omega t - \mathbf{k} \cdot \mathbf{r}(t))]\} \right|^2 \quad (6)$$

where $d\mathbf{r} = \mathbf{v}(t)dt$, \mathbf{n} is the photon direction and $\mathbf{v}(t)$ the electron velocity. The angular integration $d\Omega$ is over all possible photon and outgoing electron directions. The classical bremsstrahlung spectrum can be found by assuming that \mathbf{v} changes abruptly during the collision. Then, the integral splits into two pieces and the emission is easily found:

$$\frac{d^2 I}{d\omega d\Omega} = \frac{Z^2 e^2}{4\pi^2 c} \left| \frac{\mathbf{k} \times \mathbf{v}_1}{\mathbf{k} \cdot \mathbf{v}_1 - kc} - \frac{\mathbf{k} \times \mathbf{v}_2}{\mathbf{k} \cdot \mathbf{v}_2 - kc} \right|^2 \quad (7)$$

where \mathbf{v}_1 and \mathbf{v}_2 are the electron velocity before and after the interaction respectively. With the small angle approximations, $\mathbf{k} \cdot \mathbf{v} = k(1 - 1/\gamma^2)(1 - \theta_\gamma^2/2)$, where θ_γ is the angle between the photon and incident electron direction and $\mathbf{k} \times \mathbf{v} = k|\mathbf{v}|\theta_\gamma$, the bremsstrahlung angular distribution may be derived (for $\gamma \gg 1, k \ll E$):

$$\frac{dI^2}{d\omega d\Omega} = \frac{Z^2 e^2 \gamma^4 |\Delta \mathbf{v}|^2 (1 + \gamma^4 \theta_\gamma^4)}{\pi^2 c^3 (1 + \gamma^2 \theta_\gamma^2)^4} \quad (8)$$

The overall emission intensity can be removed by integrating over $d\Omega$, and $\Delta \mathbf{v} = \mathbf{v}_1 - \mathbf{v}_2$ expressed in terms of the change in electron momentum $q = \gamma m |\Delta \mathbf{v}|$. Then,

$$\frac{dI}{d\omega} = \frac{2Z^2 e^2 q^2}{3\pi m^2 c^3}. \quad (9)$$

The complete bremsstrahlung cross section can be found by multiplying this by the elastic scattering cross section, as a function of q and converting from classical field intensity to cross section with $d\sigma/dk = k/\hbar(dI/d\omega)$:

$$\frac{d\sigma}{dk} = \frac{16Z^2 \alpha r_e^2}{3k} \int_{q_{min}}^{q_{max}} \frac{dq}{q} \quad (10)$$

where $r_e = e^2/mc^2 = 2.8 \times 10^{-15}$ m is the classical electron radius. The integral evaluates to $\ln(q_{max}/q_{min})$, often called the form factor. This form factor is roughly equivalent to $\ln(\theta_{max}/\theta_{min})$, where θ is the electron scattering angle; this representation is convenient here, because the distributions of angles depend on the suppression. The use of α , and implicitly \hbar is needed to convert from field intensity to number of photons.

The minimum and maximum momentum transfers roughly correspond to maximum and minimum effective impact parameters respectively. For a bare nucleus, the minimum impact parameter is the electron Compton wavelength $\lambda_e = \hbar/mc = r_e/\alpha = 3.8 \times 10^{-13}$ m, so $q_{max} = 2mc$. When the momentum transfer q_{max} is larger than $2mc$, the electron scatters by an angle larger than $1/\gamma$. Then, coherence between the incoming and outgoing electron pathlength (implied in Eq. (7)) is lost and the cross section drops. The probability of such a large scatter is very small. This loss of coherence, however, foreshadows how multiple scattering affects the electron trajectory and hence the radiation. The minimum momentum transfer occurs when $q_\perp = 0$ so $q_{min} = q_\parallel$ as given in Eq. (3).

However, nuclei are generally surrounded by electrons which screen the nuclear charge. For ultrarelativistic electrons, screening is important over almost the entire range of k . Screening shields the radiating electron from the nucleus at large distances, so the maximum impact parameter is given by the typical (Thomas-Fermi) electron radius $a = 0.8Z^{-1/3}a_0$, for $Z \gg 1$ (Tsai, 1974), where the Bohr radius $a_0 = \hbar/\alpha mc = r_e/\alpha^2 = 5.3 \times 10^{-9}$ m. Then, $q_{min} = 1.25\hbar/\alpha mc Z^{1/3}$ and $\ln(q_{max}/q_{min}) = \ln(2.5/\alpha Z^{-1/3})$. A more detailed calculation finds the form factor is $\ln(184Z^{-1/3})$ (Bethe and Heitler, 1934).

This classical calculation is valid only for $y = k/E \ll 1$. A Born approximation quantum mechanical calculation gives a similar result, but covers the entire range of $y = k/E$. The result is (Bethe and Heitler, 1934)

$$\frac{d\sigma_{BH}}{dk} = \frac{4\alpha r_e^2}{3k} \left(y^2 + 2[1 + (1 - y)^2] \right) Z^2 \ln(184Z^{-1/3}) = \frac{1}{3nX_0 k} \left(y^2 + 2[1 + (1 - y)^2] \right) \quad (11)$$

where $X_0 = [4n\alpha r_e^2 Z^2 \ln(184Z^{-1/3})]^{-1}$ is the radiation length, with n the number of atoms per unit volume. More sophisticated calculations, discussed in Section IV, include additional terms in the cross section and radiation length. With a different approach to screening, in particular, a small constant may be subtracted from the form factor. However, Eq. (11) is a good semi-classical benchmark.

If the interaction occurs in a dense medium, however, this treatment may be inadequate. The interaction is actually spread over the distance l_{f0} ; if the electron multiple scatters during this time, it can affect the emission. The multiple scattering changes the electron path, so that

$$\mathbf{v}(t) = \mathbf{v}_z(t) + \mathbf{v}_\perp(t) = \mathbf{v}(0)(1 - \theta_{MS}(t)^2/2) + \theta_{MS}(t)\Theta \quad (12)$$

where Θ is a unit vector perpendicular to the initial direction of motion. The particle trajectory is then $\mathbf{r}(t) = \int \mathbf{v}(t)dt$, so that

$$\mathbf{k} \cdot \mathbf{r}(t) = \mathbf{v}_z \mathbf{k}_z + \mathbf{k}_\perp \mathbf{v}_\perp = v(0)k(1 - \frac{\theta_\gamma^2}{2}) \int_0^t (1 - \frac{\theta_{MS}^2}{2}) dt + k\theta_\gamma \cdot \int_0^t \theta_{MS}(t) dt \quad (13)$$

where θ_γ is the angle between the photon and the initial electron direction and θ_{MS} is the electron multiple scattering in the time interval 0 to t . Landau and Pomeranchuk took $\theta_{MS}^2 = \langle \theta_{MS}^2 \rangle$. Over a distance $d = \mathbf{v}_z t$, the rms multiple scattering is (Rossi, 1952)

$$\langle \theta_{MS}^2 \rangle = \left(\frac{E_s}{E}\right)^2 \frac{d}{X_0} \quad (14)$$

where X_0 is the radiation length and $E_s = mc^2 \sqrt{4\pi/\alpha} = 21.2 \text{ MeV}$.

The effect of multiple scattering can be found by inserting the trajectory of Eq. (12) into Eq. (6). This calculation simplifies with a clever choice of coordinate system. If the origin is centered on the formation zone, with $\mathbf{v}_\perp = 0$ at $z = 0$, then the multiple scattering distributes evenly before and after the 'interaction'. Then, \mathbf{v}_1 and \mathbf{v}_2 are equally affected by multiple scattering, with

$$\mathbf{k} \cdot \mathbf{v}_1 = \mathbf{k} \cdot \mathbf{v}_2 = k(1 - 1/\gamma^2)(1 - \theta_\gamma^2/2)(1 - \theta_{MS/2}^2/2) \quad (15)$$

and

$$\mathbf{k} \times \mathbf{v}_1 = \mathbf{k} \times \mathbf{v}_2 = k|\mathbf{v}| \sqrt{\theta_\gamma^2 + \theta_{MS/2}^2} \quad (16)$$

where $\theta_{MS/2}$ is the multiple scattering in half of the formation length. The angular addition in Eq. (16) is in quadrature because the angles are randomly oriented in the plane perpendicular to the electron direction. If the multiple scattering occurs on the same time scale as the interaction, then Eq. (8) becomes

$$\frac{dI^2}{d\omega d\Omega} = \frac{e^2 \gamma^4 |\Delta \mathbf{v}|^2 [1 + \gamma^4 (\theta_\gamma^2 + \theta_{MS/2}^2)^2]}{\pi^2 c^3 [1 + \gamma^2 (\theta_\gamma^2 + \theta_{MS/2}^2)]^4} \quad (17)$$

For $\theta_{MS/2}^2/2 > 1/\gamma^2 + \theta_\gamma^2/2$, the radiation will be reduced and the angular distribution changed; if there is enough multiple scattering while traversing the formation zone, emission is suppressed. For $\theta_\gamma \ll 1/\gamma$, this happens when

$$\omega < \frac{E_s^2 c}{E^2 X_0}. \quad (18)$$

Photons with lower energies will be suppressed. Equation (16) also shows that the angular distributions will be affected. Because multiple scattering can reduce the coherence length, a more detailed complete calculation is required to find the degree of suppression. Landau and Pomeranchuk (1953b) started with the expression

$$\frac{dI}{d\omega} = \frac{Z^2 e^2 \omega^2}{4\pi^2 c^3} \int_{-\infty}^{\infty} (\mathbf{n} \times d\mathbf{r}_1) \cdot \int_{-\infty}^{\infty} (\mathbf{n} \times d\mathbf{r}_2) \int d\mathbf{n} \exp \{i\omega[(t_1 - t_2) - \mathbf{n} \cdot (\mathbf{r}_1 - \mathbf{r}_2)]\} \quad (19)$$

This simplifies to

$$\frac{dI}{d\omega} = \frac{Z^2 e^2 \omega}{\pi c^2} \int_{-\infty}^{+\infty} dt_1 \int_{-\infty}^{+\infty} dt_2 \frac{\exp [ik(t_1 - t_2)/\hbar]}{|\mathbf{r}_{12}|} (J_1 + J_2) \quad (20)$$

where

$$J_1 = \mathbf{v}_1 \cdot \mathbf{v}_2 - \frac{(\mathbf{v}_1 \cdot \mathbf{r}_{12})(\mathbf{v}_2 \cdot \mathbf{r}_{12})}{r_{12}^2} \left(\sin(g) + \frac{3g \cos(g) - \sin(g)}{g^2} \right) \quad (21)$$

and

$$J_2 = (-2\mathbf{v}_1 \cdot \mathbf{v}_2) \left(\frac{g \cos(g) - \sin(g)}{g^2} \right) \quad (22)$$

where $g = \omega|\mathbf{r}_{12}|/c$ and $\mathbf{r}_{12} = \mathbf{r}(t_1) - \mathbf{r}(t_2)$. The first integral was evaluated by Landau and Pomeranchuk (1953b), while J_2 , neglected by Landau and Pomeranchuk was evaluated by Blankenbecler and Drell (1996), who found $J_1 = J_2$. Landau and Pomeranchuk still found the 'right' result, compensating by using a perpendicular momentum transfer due to multiple scattering twice the usual one.

These integrals can be evaluated by using the electron trajectory given in Eqs. (12) and (13). With appropriate substitutions,

$$\frac{dI}{d\omega} = \frac{e^2 \omega}{\pi c} \int_{-\infty}^{\infty} dT \int_{-\infty}^{\infty} \frac{dt}{t^3} e^{i\omega t} \left[\left(\int_0^t \theta_{MS}(t) dt \right)^2 - t \theta_{MS} \int_0^t \theta_{MS}(t) dt \right] \times \sin \left[\frac{\omega}{c} \left(vt - \frac{1}{2} \int_0^t \theta_{MS}^2(t) dt + \frac{1}{2t} \left(\int_0^t \theta_{MS} dt \right)^2 \right) \right] \quad (23)$$

This integral is evaluated by replacing the angular quantities by their average values. For example,

$$\left\langle \int_0^t \theta_{MS}(t) dt \right\rangle = \frac{E_s^2 ct |t|}{2E^2 X_0} \quad (24)$$

Landau and Pomeranchuk express their results in emission per unit time. In terms of the more commonly used total emission,

$$\frac{dI}{d\omega} = \frac{4e^2}{3c} \int_0^{\infty} dX \sin \left(X + \frac{E^2 E_s^2 X^2}{3m^4 c^7 \omega X_0} \right) \quad (25)$$

For $\omega \ll E_s^2 c / E^2 X_0$, the emission is

$$\frac{dI}{d\omega} = \sqrt{\frac{2\pi}{3}} \frac{e^2 m^2 c^3}{E_s E} \sqrt{\frac{\omega X_0}{c}} \quad (26)$$

In the strong suppression regime, the field intensity $dI/d\omega \sim \sqrt{\omega}$, compared to an isolated interaction, where dI/ω is independent of ω ; the corresponding cross sections scale as $1/\sqrt{\omega}$ and $1/\omega$ respectively. The following subsection will present a simple semi-classical derivation of the same result, and also discuss some of its implications.

B. Bremsstrahlung - Quantum approach

Bremsstrahlung suppression due to multiple scattering can be found by starting with Eq. (5). Multiple scattering can suppress bremsstrahlung if it contributes significantly to q_{\parallel} (Feinberg and Pomeranchuk, 1956). For a rough calculation, the multiple scattering angle can be taken as the average scattering angle. Multiple scattering affects q_{\parallel} by reducing the electron longitudinal velocity; the acquired perpendicular velocity components are unimportant here. As before, the multiple scattering is divided into two regions: before and after the interaction, so

$$q_{\parallel} = \sqrt{(E \cos \theta_{MS/2}/c)^2 - (mc)^2} - \sqrt{[(E - k) \cos \theta_{MS/2}/c]^2 - (mc)^2} - k/c \quad (27)$$

where $\theta_{MS/2}$ is the multiple scattering in half the formation length, $(E_s/E)\sqrt{l_f/2X_0}$. The scattering after the interaction is based on the outgoing electron energy $E - k$. The inclusion of electron energy loss is a significant advantage of the quantum formulation. With some small angle approximations,

$$q_{\parallel} = \frac{km^2 c^3}{2E(E - k)} + \frac{k\theta_{MS/2}^2}{2c} \quad (28)$$

Multiple scattering is significant if the second term is larger than the first. This happens if $\theta_{MS/2} > 1/\gamma$, or for

$$y = k/E < (E - k)/E_{LPM} \quad (29)$$

where E_{LPM} is a material dependent constant, given by

$$E_{LPM} = \frac{m^4 c^7 X_0}{\hbar E_s^2} = \frac{m^2 c^3 X_0 \alpha}{4\pi \hbar} \approx 7.7 \text{ TeV/cm} \cdot X_0. \quad (30)$$

Table I gives E_{LPM} in a variety of materials. This definition of E_{LPM} was used by Landau and Pomeranchuk (1953a,b), Feinberg and Pomeranchuk (1956) and others, but is twice that used in some papers (Anthony, 1995, 1997) (Baier, 1996), and 1/8 of that in others (Stanev, 1982). The last choice is convenient when working with Migdals equations (Sec. III), but not for the semi-classical derivation.

TABLE I. Suppression thresholds in a variety of materials. Listed are Z , X_0 , density, E_{LPM} , y_{die} and E_p . The carbon numbers is an average for graphite. BP stands for boiling point at atmospheric pressure. STP (standard temperature and pressure) is 20° C at 1 atmosphere. Standard rock, used to compare underground cosmic ray experiments, is defined as $Z = 11$, $A = 22$ and $\rho = 2.65\text{g/cm}^2$; X_0 is computed following Tsai(1974). Other numbers are from (Barnett *et al.*, 1996).

Material	Z	ρ (g/cm ³)	X_0 (cm)	E_{LPM} (TeV)	y_{die}	E_p
hydrogen(liq. BP)	1	0.07	865	6.6 PeV	1.4×10^{-5}	14 PeV
helium(liq. BP)	2	0.125	755	5.8 PeV	1.5×10^{-5}	13 PeV
carbon	6	2.2	19.6	151	5.5×10^{-5}	1.3 PeV
aluminum	13	2.70	8.9	68	6.0×10^{-5}	620 TeV
iron	26	7.87	1.76	13.6	1.0×10^{-4}	200 TeV
lead	82	11.35	0.56	4.3	1.1×10^{-4}	70 TeV
tungsten	74	19.3	0.35	2.7	1.5×10^{-4}	60 TeV
uranium	92	18.95	0.35	2.7	1.4×10^{-4}	56 TeV
gold	79	19.32	0.33	2.5	1.5×10^{-4}	57 TeV
air(STP)	-	0.0012	30,400	234 PeV	1.3×10^{-6}	47 PeV
water	-	1.00	36.1	278	3.9×10^{-5}	1.6 PeV
std. rock	11	2.65	10.0	77	6.0×10^{-5}	695 TeV

For $k \ll E$, Eq. (29) matches the classical result: photons with $k < k_{LPM} = E^2/E_{LPM}$ are suppressed. For example, for 25 GeV electrons in lead, photon emission below 125 MeV is suppressed. For higher energy electrons, a large portion of the spectrum can be suppressed; for 4.3 TeV electrons in lead, most of the spectrum is suppressed. At the endpoint of the spectrum, $k \rightarrow E$, l_{f0} approaches zero, so the Bethe-Heitler cross section always applies at this point.

Slightly different calculations result in different coefficients in Eq. (29). Eq. (29) matches Landau and Pomeranchuk, but others have found different answers. Feinberg & Pomeranchuk (1956) and the introductions to Anthony (1995, 1997) used the simpler criteria $\langle \theta_{MS} \rangle > 1/\gamma$, leading to a suppression twice that given here. Use of the minimum uncertainty principle $\Delta p \Delta x > \hbar/2$ (Schiff, 1968) in Eq. (5) would shorten l_{f0} and reduce the suppression.

Because $\theta_{MS/2}$ both depends on l_f , and also partly determines l_f , finding the degree of suppression requires solving a quadratic equation for l_f .

$$l_f = \frac{2\hbar E(E-k)}{km^2c^3(1 + E_s^2 l_f / 2m^2c^4 X_0)} = l_{f0} \left[1 + \frac{E_s^2 l_f}{m^2c^4 X_0} \right]^{-1}. \quad (31)$$

If multiple scattering is small, this reduces to Eq. (5). Where multiple scattering dominates

$$l_f = l_{f0} \sqrt{\frac{kE_{LPM}}{E(E-k)}}. \quad (32)$$

Since the formation length is the maximum distance over which the bremsstrahlung amplitudes add coherently, the bremsstrahlung cross section scales linearly with the distance over which coherence is maintained, or the formation length. It is convenient to define a suppression factor S , giving the emission relative to Bethe Heitler:

$$S = \frac{d\sigma/dk}{d\sigma_{BH}/dk} = \frac{l_f}{l_{f0}} = \sqrt{\frac{kE_{LPM}}{E(E-k)}} \quad (33)$$

and the $dN/dk \sim 1/k$ found by Bethe and Heitler (1934) changes to $dN/dk \sim 1/\sqrt{k}$.

Figure 1 compares bremsstrahlung cross sections for 25 GeV and 1 TeV electrons in lead. The Bethe-Heitler unsuppressed cross section is compared with three approaches to suppression: the full semi-classical suppression Eq. (31), the commonly used low energy limit Eq. (33), and Migdals calculation, included as a standard. Eq. (31) predicts considerably more suppression than Migdal. Equation (33) is a better match to Migdal, but the required approximation is unjustified in the transition region $k \sim E(E-k)/E_{LPM}$. Better agreement would be found with a larger E_{LPM} , as would be given by the minimum uncertainty principle. If only S is considered, and the onset of suppression neglected, it is impossible to separate E_{LPM} and the overall cross section normalization. The location of the onset of separation is needed to separate these two factors.

Nevertheless, Eq. (33) demonstrates some implications of bremsstrahlung suppression (Landau and Pomeranchuk, 1953b). With suppression, the number of photons emitted per radiation length is finite, scaling as $\sqrt{E/E_{LPM}}$ for $E > E_{LPM}$. Electron dE/dx due to bremsstrahlung is also reduced; instead of rising linearly with E , it is proportional to $\sqrt{EE_{LPM}}$. Fig. 2 shows the relative bremsstrahlung energy loss, $(dE/dx)_{LPM}$ for Migdal compared with the Bethe-Heitler prediction.

Besides the photon spectrum, LPM suppression also affects the photon angular distribution. When θ_γ is large compared with $1/\gamma$, l_f is reduced. Including θ_γ ,

$$q_{||} = p_e - p'_e - k/c \cos \theta_\gamma = \sqrt{(E/c)^2 - (mc)^2} - \sqrt{[(E-k)/c]^2 - (mc)^2} - k/c \cos \theta_\gamma. \quad (34)$$

The change in electron direction is (correctly) assumed to be negligible. Then,

$$q_{||} \sim \frac{m^2c^3k}{2E(E-k)} + \frac{k\theta_\gamma^2}{c} \quad (35)$$

For $k \ll E$, $l_f = l_{f0}/(1 + \gamma^2\theta_\gamma^2)$. This formula may be used to derive the angular distribution of bremsstrahlung photons (Landau and Pomeranchuk, 1953b). When θ_γ increases $q_{||}$, the

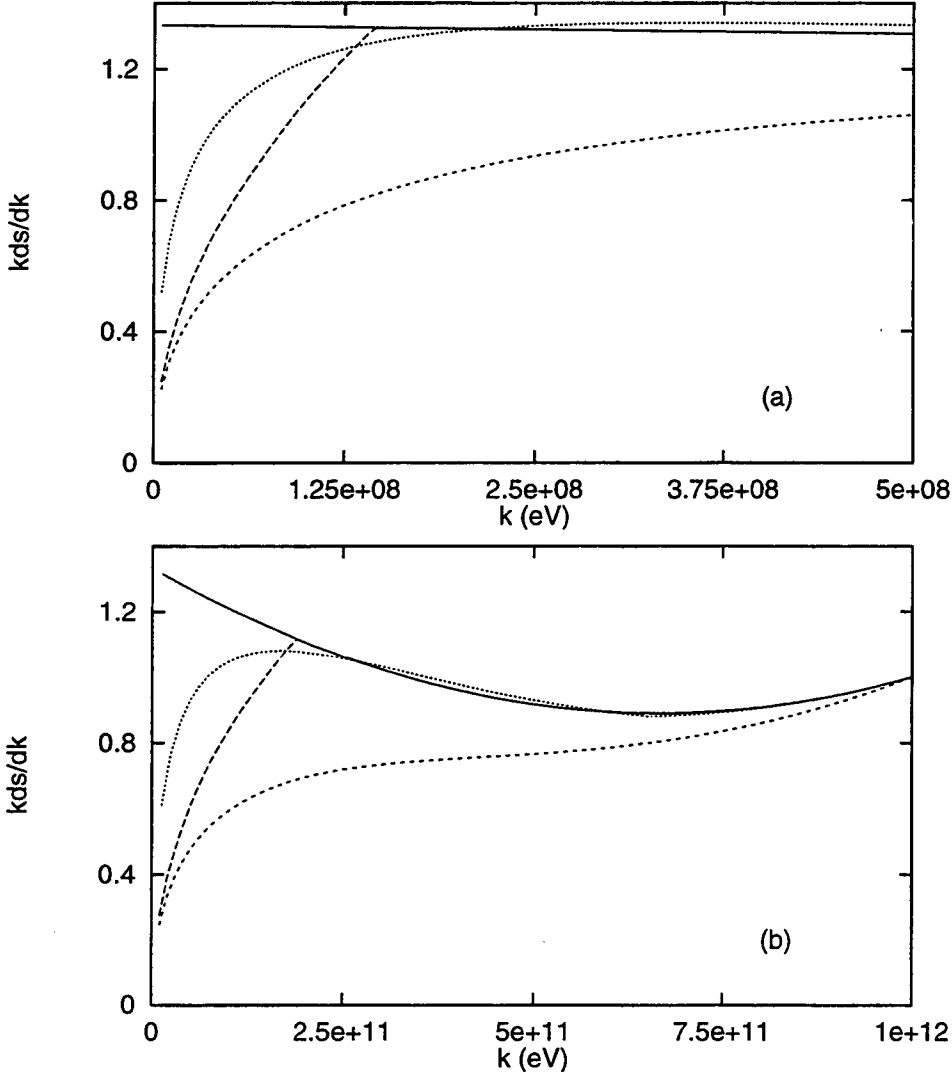


FIG. 1. Comparison of the differential energy weighted cross sections per radiation length, $X_0 n k d\sigma/dk$ for Bethe-Heitler radiation (solid line), Migdals detailed suppression calculation (dotted line), full quadratic suppression from Eq. (31) (short dashes), and the strong suppression limit, Eq. (33) (long dashes), for (a) 25 GeV electrons and (b) 1 TeV electrons incident on a lead target. This gives the differential (with photon energy) number of photons emitted per radiation length.

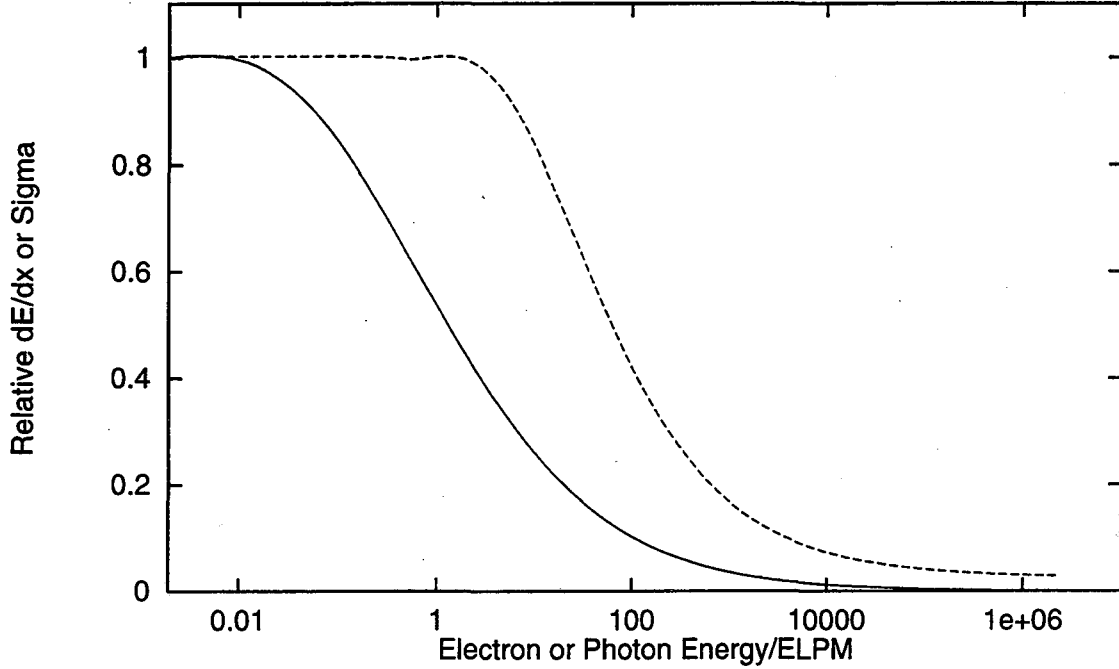


FIG. 2. The relative electron energy loss $dE/dx(\text{Migdal})/dE/dx(\text{Bethe-Heitler})$ from bremsstrahlung (solid line) and the relative photon conversion cross sections $\sigma(\text{Migdal})/\sigma(\text{Bethe-Heitler})$. Both curves are for lead, with electron/photon energy in units of $E_{LPM} = 4.3$ TeV.

multiple scattering term becomes less important, so there is less suppression for $\gamma\theta_\gamma > 1$. With both multiple scattering and a finite θ_γ ,

$$l_f = \frac{2\hbar c E(E-k)}{km^2 c^3} \left[1 + \frac{E_s^2 l_f}{m^2 c^4 X_0} + \frac{\theta_\gamma^2 E(E-k)}{2m^2 c^4} \right]^{-1} \quad (36)$$

Suppression is large only if the multiple scattering term is larger than the '1' plus the angular term. This happens if $k\theta_\gamma^2 < m^2/E_{LPM}$. Then,

$$S(\theta) = \sqrt{\frac{kE_{LPM}(1 + \gamma^2\theta_\gamma^2)}{E(E-k)}}. \quad (37)$$

Suppression disappears rapidly as θ_γ rises.

When $S(0)$ is small, the angular distribution is broadened. It follows simply from Eq. (37) that multiple scattering broadens the angular distribution from $\langle\theta_\gamma\rangle \sim 1/\gamma$ to $\langle\theta_\gamma\rangle \sim 1/\gamma\sqrt{S}$ (Landau and Pomeranchuk, 1953b). Galitsky and Gurevich (1964) found that $\langle\theta_\gamma\rangle$ is determined by the electron multiple scattering over the distance l_f , giving the same algebraic result.

This increase in $\langle\theta_\gamma\rangle$ will be difficult to observe because, in general, the overall photon angular spread is dominated by electron multiple scattering before the emission. For thin enough targets, however, this is not true; if S is small enough, then the photon emission angles dominate over multiple scattering. For thin targets, the reduced suppression for $\theta_\gamma \gg 1/\gamma$ should be experimentally measurable.

C. Photon Interactions with the Medium

Ter-Mikaelian (1953) pointed out that photon interactions can also induce suppression. Photons can interact with the medium by coherent forward Compton scattering off the target electrons, producing a phase shift in the photon wave function. If this phase shift is large enough, it can cause destructive interference, reducing the emission amplitude. Ter-Mikaelian used classical electromagnetism in his analysis, calculating suppression in terms of the dielectric constant of the medium,

$$\epsilon(k) = 1 - (\hbar\omega_p)^2/k^2 \quad (38)$$

where ω_p , the plasma frequency of the medium, is $\sqrt{4\pi nZe^2/m}$. This is equivalent to giving the photon an effective mass $\hbar\omega_p/c^2$. The relationship between photon energy k and momentum p_γ becomes $p_\gamma c = \sqrt{\epsilon}k$ and the momentum transfer is

$$q_{\parallel} = p_e - p'_e - k\sqrt{\epsilon}/c = \frac{k}{2c\gamma^2} + \frac{(\hbar\omega_p)^2}{2ck}. \quad (39)$$

The formation length is then

$$l_f = \frac{2\hbar ck\gamma^2}{k^2 + k_p^2} \quad (40)$$

where $k_p = \gamma\hbar\omega_p$. When dielectric suppression is strong, q_{\parallel} is dominated by the photon and l_f becomes independent of E : $l_f = 2ck/\hbar\omega_p^2$. As with LPM suppression, the cross section is proportional to the path length that can contribute coherently to the emission, so S is the ratio of the in-material to vacuum formation lengths:

$$S = \frac{k^2}{k^2 + k_p^2}. \quad (41)$$

For $k < \gamma k_p$, bremsstrahlung is significantly reduced. This happens for $y < y_{die}$, where

$$y_{die} = \hbar\omega_p/mc^2 \quad (42)$$

is a material dependent constant. For lead, $\hbar\omega_p = 60$ eV, so $y_{die} \sim 10^{-4}$. Table I lists y_{die} for a variety of materials.

Dielectric suppression can be found classically by including the dielectric constant in Eq. (1), so the phase is $\Phi = \exp\{ikt[1 - |\mathbf{v}|\epsilon \cos(\theta_\gamma)/c]/\hbar\}$. The classical calculation gives the same results. It is worth noting that the case $\cos(\theta_\gamma) = c/|\mathbf{v}|\epsilon$, which gives an infinite formation length, corresponds to Čerenkov radiation (Ter-Mikaelian, 1972, pg. 196).

Because photon emission angles are determined by the kinematics, a finite θ_γ affects dielectric suppression the same way as it does LPM suppression. Including θ_γ ,

$$l_f = \frac{2\hbar ck\gamma^2}{k^2(1 + \gamma^2\theta_\gamma^2) + k_p^2}. \quad (43)$$

For large suppression and $\theta_\gamma\gamma > 1$, many terms cancel, and $S = k^2\theta_\gamma^2/\hbar\omega_p$ is independent of E . In this limit, the angular spread is $\langle \theta_\gamma \rangle \sim \hbar\omega_p/k$ (Galitsky and Gurevich, 1964).

Ter Mikaelian (1972, pg. 127) pointed out that dielectric suppression also affects q_{min} in the form factor logarithm. The complete cross section for $k \ll E$ is then

$$\frac{d\sigma}{dk} = \frac{16Z^2\alpha r_e^2 k}{3k_p^2} \ln \left(184Z^{-1/3} \sqrt{1 + \left(\frac{k_p}{k}\right)^2} \right). \quad (44)$$

Because $k_p^2 \sim n$, except for the logarithmic term, photon emission is independent of the density! As the density rises, increasing the number of scatters, suppression rises in tandem, leaving the total photon production constant.

This suppression is sometimes known as the longitudinal density effect, by analogy with the transverse density effect (Jackson, 1972, pg. 632) which reduces ionization dE/dx . It is also known as dielectric suppression. Unfortunately, a quantum mechanical calculation of dielectric suppression has yet to appear, nor has dielectric suppression been described in terms of Compton scattering.

Because dielectric suppression and the LPM effect both reduce the formation length, the effects do not merely add; the total $q_{||}$ must be calculated, and from that l_f and hence the suppression found. Feinberg and Pomeranchuk (1956) showed that when $k_p > k_{LPM}$ ($E > E_{LPM}\omega_p/mc^2$), then dielectric suppression overwhelms LPM suppression, and only the former is observable. Because dielectric suppression has a stronger k dependence than LPM suppression, the converse is not always true when $k_{LPM} > k_p$.

D. Bremsstrahlung Suppression due to Pair Creation

Landau and Pomeranchuk (1953a) pointed out that, at the highest energies, l_f can approach a radiation length. Then, the partially created photon can pair create partway through the formation zone. This destroys the coherence between different parts of the formation zone, reducing the amplitude for photon emission.

Unlike Compton scattering, above a certain photon energy, the pair creation cross section is independent of energy: $\sigma_\gamma = (28/9)\alpha r_e^2 Z^2 \ln(184Z^{-1/3})$. This constant cross section limits the formation length to roughly X_0 . When this limit applies, radiation is suppressed by l_{f0}/X_0 , and the photon spectrum $d\sigma/dk$ becomes constant. This suppression is stronger than multiple scattering, where l_f can still rise, as \sqrt{k} , so it will dominate at high enough energies.

Neglecting other suppression mechanisms, $l_{f0} > X_0$ when

$$k < \frac{2\hbar E(E - k)}{X_0 m^2 c^3}. \quad (45)$$

However, dielectric suppression and LPM suppression limit the range of applicability. With these mechanisms considered, suppression due to pair creation is present when (Galitsky and Gurevich, 1964):

$$\frac{E^2}{E_s^2} \left(\frac{\hbar c}{X_0 k} - \frac{\hbar^2 \omega_p^2}{k^2} \right) > 1. \quad (46)$$

If $E > E_p$, where

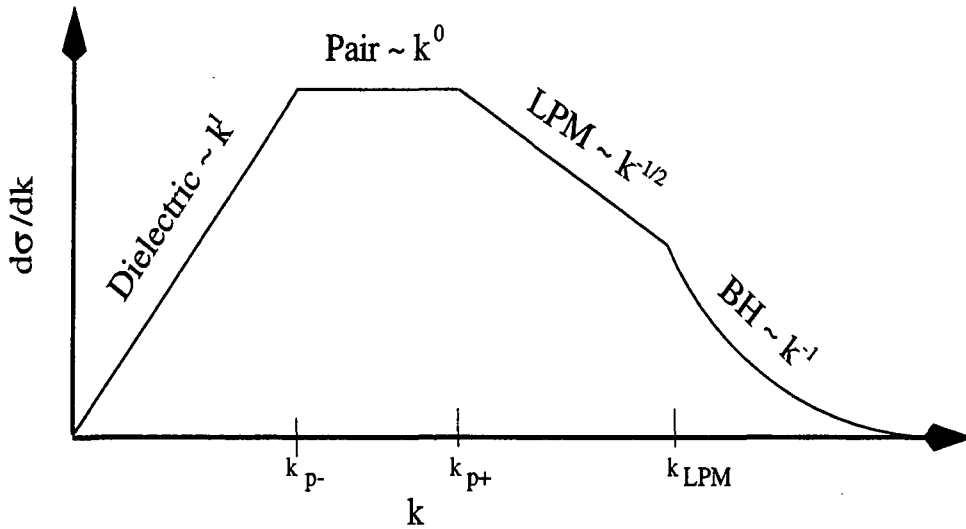


FIG. 3. Schematic view of bremsstrahlung $d\sigma/dk$ when several suppression mechanisms are present. For electron energies below E_p , the pair creation suppression disappears and LPM suppression connects with dielectric suppression.

$$E_p = \frac{2X_0\omega_p E_s}{c} \quad (47)$$

is a material dependent constant, then there will be a 'window' in k where this mechanism applies, $k_{p-} = X_0\omega_p^2/2\hbar c < k < k_{p+} = 2\hbar c E(E - k)/(X_0 E_s^2)$, as is shown in Fig. 3. In this window, the suppression factor is

$$S = \frac{m^2 c^3 k X_0}{2\hbar E(E - k)} \quad (48)$$

and $d\sigma/dk$ is independent of k . For $k < k_{p-}$, dielectric suppression dominates, while for $k > k_{p+}$, LPM suppression is dominant. E_p ranges from 70 TeV for lead to 42 PeV for sea level air; other values are given in Table I. For lead, the photon 'window' is $5 \times 10^7 \text{ eV} < k < 1.6 \times 10^{-19} E^2 (\text{eV})$, while for air it is $3.3 \times 10^8 \text{ eV} < k < 3.0 \times 10^{-24} E^2 (\text{eV})$.

Similarly, bremsstrahlung of a sufficiently high energy photon can suppress pair production. The bremsstrahlung can affect the overall pair production rate if the emitted photon contributes significantly to q_{\parallel} of the entire reaction.

These formula must be considered only a rough approximation. At high enough energies, the pair creation cross section is itself significantly reduced because of LPM suppression and X_0 in Eq. (45) should be increased to account for this. As Fig. 2 shows, for energies significantly above E_{LPM} , the pair conversion length rises significantly. At this point, when bremsstrahlung and pair creation suppress each other, the simple separation of showers into independent bremsstrahlung and pair creation interactions becomes problematic, and a new, unified approach is needed.

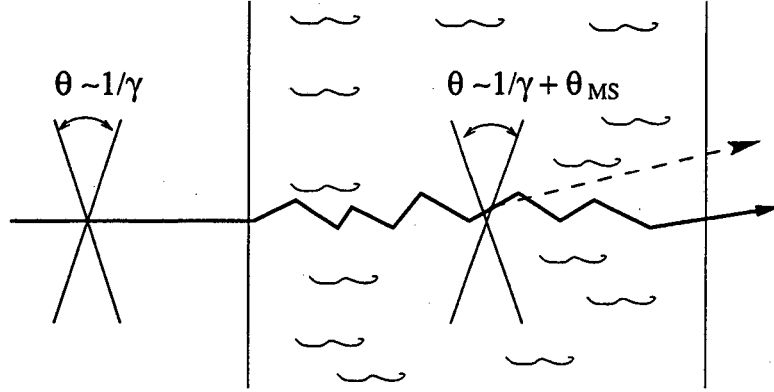


FIG. 4. Diagram of transition radiation caused by multiple scattering. The pancaked electromagnetic fields are broadened by multiple scattering from their free space width $1/\gamma$ to $\sqrt{1/\gamma^2 + \theta_{MS}^2}$, where θ_{MS} depends on l_f , and hence on k .

E. Surface effects and Transition Radiation

The discussion so far has been aimed at infinitely thick targets. With finite thickness targets, the effects of the entry and exit surfaces must be considered. At first sight, this appears straightforward: the only effect being a reduction in the multiple scattering when the formation zone sticks out of the target, and hence there is less suppression. However, in addition to reduced suppression, multiple scattering produces a new kind of transition radiation.

Conventional transition radiation occurs when an electron enters a target, and the electromagnetic fields of the electron redistribute themselves to account for the dielectric of the medium. In the course of this rearrangement, part of the EM field may break away, becoming a real photon. Because transition radiation has been extensively reviewed elsewhere (Artru, Yodh and Mennessier, 1975), (Cherry, 1978), (Jackson, 1975), it will not be further discussed. However, the formula for radiation, neglecting interference between nearby edges, is given here for future use (Jackson, 1975, pg. 691):

$$\frac{dN}{dk} = \frac{\alpha}{\pi k} \left[\left(1 + \frac{2k^2}{k_p^2} \right) \ln \left(1 + \frac{k_p^2}{k^2} \right) - 2 \right] \quad (49)$$

per edge.

Transition radiation occurs because multiple scattering changes the trajectory of the electron. The variation in electron direction widens the directional distribution of the electromagnetic fields carried by the electron, as is shown in Fig. 4. Scattering broadens the EM fields from their free space width $1/\gamma$ to a l_f (and hence k) dependent value. As the EM field enters the target and realigns itself, it can emit transition radiation.

Classically, this new form of transition radiation is closely related to the old. Both depend on the difference in l_f in the two materials (Ter-Mikaelian 1972, pg. 233), with the complete radiation

$$\frac{dN}{dkd\theta_\gamma} = \frac{2\alpha k \theta_\gamma^3}{\pi \hbar^2 c^2} (l_f - l'_f)^2 \quad (50)$$

where l_f and l'_f are the formation lengths in the two media. If $l_f = l'_f$, then there is no transition radiation. Conventional transition radiation can be derived from this formula by focusing on ϵ for the media, while multiple scattering transition radiation can be calculated by focusing on θ_{MS} . Of course, the complete spectrum includes both contributions.

When multiple scattering dominates, the photon spectrum given by Eq. (50) is

$$\frac{dN}{dkd\theta_\gamma} = \frac{2\alpha\theta_\gamma^3\gamma^2}{\pi\hbar c}(1 - S^2) \quad (51)$$

The spectrum is given by integrating over θ_γ ; this is complicated because the maximum θ_γ depends on k . With this considered, for $E > E_{LPM}$ and $k > k_p$, (Ter-Mikaelian, 1972, pg. 235)

$$\frac{dN}{dk} \sim \frac{\alpha}{\pi k} \left(\ln \left(\frac{1 + \sqrt{1 + 4k_{LPM}/k}}{2} \right) + \frac{2}{1 + \sqrt{1 + 4k_{LPM}/k}} - 1 \right) \quad (52)$$

per edge. The total radiation may be found by integrating dN/dk up to k_{LPM} . Since $k_{LPM} \sim E^2$, the total energy lost by the electron ΔE rises as E^2 , in contrast to conventional transition radiation, where the loss is proportional to E . When ΔE becomes a significant fraction of E , quantum effects must become important.

This transition radiation has yet to be adequately studied experimentally. There are also a number of caveats. These calculations assume that the transition is instantaneous, completely neglecting the sharpness of the surface. They also neglect coherence between nearby edges. More quantitative estimates are discussed in Sec. IV.C. For pair creation, one expects similar surface effects; unfortunately these have yet to be worked out.

F. Thin Targets

In extremely thin targets, neither dielectric effects nor multiple scattering produce enough of a phase shift to cause suppression. Suppression due to multiple scattering disappears when the total scattering, taken over the entire target thickness, is less than $1/\gamma$. This occurs for targets with $T < (mc^2/E_s)^2 X_0 \approx X_0/1720$. With dielectric suppression, $l_f \rightarrow 0$ as $k \rightarrow 0$, so for very small k , less than $Tk_p^2/2\hbar c$, there will always be dielectric suppression. Of course, for extremely thin targets at low energies, transition radiation will dominate over bremsstrahlung.

For multiple scattering, an interesting intermediate case applies for slightly thicker targets where $X_0/1720 < T < l_{f0}$. Then, the entire target acts as a single radiator. The emission can be found from the probability distribution for the total scattering in the entire target, either classically (Shulga and Fomin, 1978) or using quantum calculations (Ternovskii, 1960). These calculations are more complex than those presented earlier, because the scattering angle is represented by a probability distribution, rather than an average angle. As such, this can serve as an introduction to Migdals calculations, which will be discussed in the following section. The total radiation from the target is (Ternovskii, 1960)

$$\frac{dN_T}{dk} = \frac{2\alpha}{\pi k} \int_0^\infty d^2\theta f(\theta) \left(\frac{2\zeta^2 + 1}{\zeta\sqrt{\zeta^2 + 1}} \ln(\zeta + \sqrt{\zeta^2 + 1}) - 1 \right) \quad (53)$$

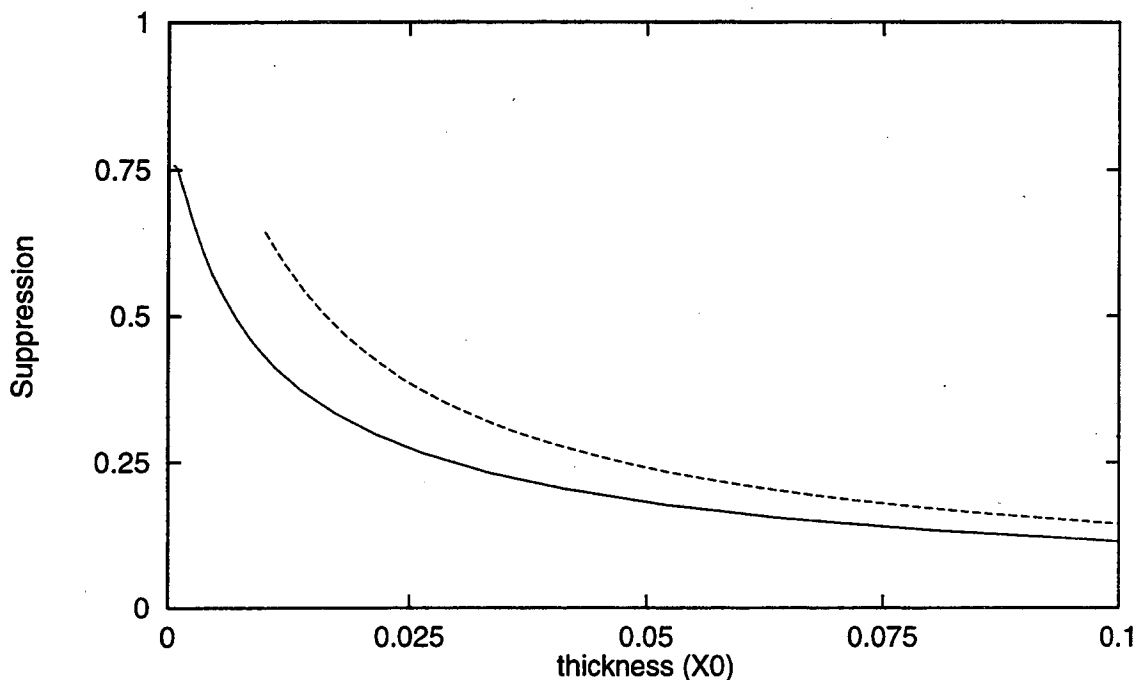


FIG. 5. Suppression factor σ_T/σ_{BH} for thin targets. The solid line follows Eq. (53) for $E=25$ GeV, but is only slightly energy dependent, as long as $T > X_0/1720$ and $T < l_f$. The dashed curve is the logarithmic approximation, Eq. (55).

where $\zeta = \gamma\theta/2$, and θ is the scattering angle. Since θ is independent of k , this formula has the same k dependence for $k \ll E$ as the Bethe-Heitler calculation. Assuming that the scattering is Gaussian with rms scattering angle θ_0 , where, for thin targets (Barnett *et al.*, 1996)

$$\theta_0 = \frac{E_s}{E} \sqrt{\frac{T}{X_0}} \left(1 + 0.038 \ln \frac{T}{X_0} \right). \quad (54)$$

For the relevant range of thicknesses, neglecting the second, logarithmic term changes the suppression factor by at most a few percent.

Eq. (53) can be evaluated numerically. For very thin targets, it matches the Bethe-Heitler spectrum, except for a factor of 4/3. For thicker targets, the suppression factor, $S = N_T/T\sigma_{BH}$ is shown in Fig. 5.

In the limit $T \gg (m/E_s)^2 X_0$, (but with $T < l_{f0}$), $dN/dk \sim \ln T$ (Ternovskii, 1960). The intensity varies logarithmically with the target thickness! A slightly more detailed calculation finds (Shulga and Fomin, 1996)

$$\frac{dN}{dk} = \frac{2\alpha}{\pi k} \left(\ln \frac{E_s^2 T}{m^2 c^4 X_0} - 1 \right). \quad (55)$$

This approximation, shown by the dashed line in Fig. 5, overestimates Eq. (53) by 10-20%. Suppression should broaden the photon angular distribution, as with thicker targets.

A similar expression should apply for pair creation - the formation length is the same.

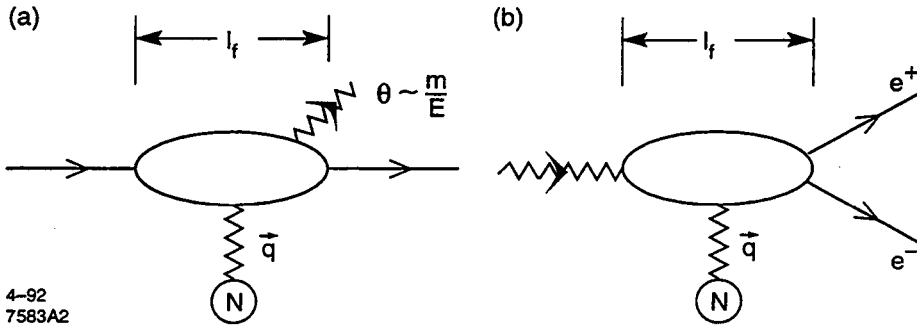


FIG. 6. Schematic representations of the l_f s for bremsstrahlung and pair conversion, showing their relationship.

G. Suppression of Pair Creation

Multiple scattering can also suppress production of e^+e^- pairs from photons. The relationship between the two Feynman diagrams, shown in Fig. 6, is clear, and the two reactions are easily mapped into each other. The crossing does change the kinematics of the process. Since it is the electron and positron that multiple scatter, and they must have energies lower than that of the initial photon, suppression occurs only at higher incident particle energies. To avoid confusion, k will continue to refer to photon energy, with the produced pair having energies E and $k - E$.

Pair production is not possible classically. However, Landau and Pomeranchuk (1953b) give some simple arguments that it should be suppressed along with bremsstrahlung. This can be demonstrated by considering the kinematics of the process. The momentum transfer is

$$q_{\parallel} = k/c - \sqrt{(k - E)/c^2 - m^2c^2} - \sqrt{E^2/c^2 - m^2c^2} = \frac{m^2c^3k}{2E(k - E)}. \quad (56)$$

Because q_{\parallel} is unchanged when E and $k - E$ are interchanged, either can represent the electron or positron. The formation length can be expressed in terms of the two final state momenta or in terms of the invariant mass of the created pair. Not surprisingly, l_{f0} for pair production is similar to the bremsstrahlung case:

$$l_{f0} = \frac{2\hbar E(k - E)}{m^2c^3k}. \quad (57)$$

It might seem surprising that k is in the denominator here. But, l_{f0} is a maximum for $E = k - E = k/2$; then $l_{f0} = 2\hbar ck^2/m$, and it is clear that l_{f0} rises with k . If $E \ll k$, then this equation reduces to $l_{f0} = 2\hbar cE/m^2$, and l_{f0} is very short. This asymmetric energy division corresponds to a pair with a large invariant mass. In terms of pair mass, M_p ,

$$l_{f0} = \frac{2\hbar k}{M_p^2c^3}. \quad (58)$$

One difference between pair creation and bremsstrahlung is that the multiple scattering now applies to two separate particles. The lower energy particle scatters more, and hence dominates the additional q_{\parallel} . The scattering is taken over $l_f/2$, as if the charged particles

appear suddenly in the middle of the formation zone, and the result is very similar to Eq. (31):

$$l_f = l_{f0} \left[1 + \frac{E_s^2 l_f}{m^2 c^4 X_0} \right]^{-1} \quad (59)$$

where l_{f0} now refers to Eq. (57). When the second term is dominant,

$$l_f = l_{f0} \sqrt{\frac{k E_{LPM}}{E(k-E)}} = \frac{2\hbar k}{M_p m c^3} \sqrt{\frac{E_{LPM}}{k}}, \quad (60)$$

similar to Eq. (31). Then,

$$S = \sqrt{\frac{E_{LPM} k}{E(k-E)}} = \frac{M_p}{m} \sqrt{\frac{E_{LPM}}{k}}. \quad (61)$$

For a given k , the suppression is largest when $E \approx (k-E) \approx k/2$. There is no suppression for $E \approx 0$ or $E \approx k$. For $E \gg E_{LPM}$, the total cross section scales as $\sqrt{E_{LPM}/k}$. Figures 2 and 10 show how suppression increases as k rises.

As with bremsstrahlung, the emission angles can affect suppression. The relevant angular variables are θ_{e+} and θ_{e-} , the angles between the outgoing particles trajectories and the incoming photon path. If either angle is larger than k/m , then the formation length is shortened and suppression reduced.

Because of the high photon energy, there is no apparent analogy to dielectric suppression for pair creation.

H. Muons and Direct Pair Production

Electromagnetic processes involving muons are also subject to suppression. However, because $m_\mu \gg m_e$, the effects are greatly reduced. For a given lepton energy, the formation length is reduced by $(m_e/m_\mu)^2 \sim 1/40,000$. For muons, Eqs. (29) and (33) hold, but with E_{LPM} replaced by

$$E_{LPM(\mu)} = \frac{m_\mu^4 c^7 X_0}{\hbar E_s^2} \approx 1.38 \times 10^{22} \text{eV/cm} \cdot X_0. \quad (62)$$

This energy is high enough that LPM suppression is generally negligible for muon bremsstrahlung and pair creation.

For muons, dielectric suppression still occurs for $k < \gamma\omega_p$. For solids, suppression typically sets in for $k/E < 7 \times 10^{-7}$. This is very small, but perhaps not unmeasurable.

Unlike electrons, high energy muons have a significant cross section for direct pair production, $\mu^- N \rightarrow \mu^- e^+ e^- N$. This process is similar to bremsstrahlung followed by pair creation, except that the intermediate photon can be virtual. Both the μ and the final state electrons are subject to multiple scattering. The formation length can be calculated by treating the pair as a massive photon. Then,

$$l_f = \frac{2\hbar c \gamma^2}{k} \left[1 + \frac{\gamma^2 M_p^2 c^4}{k^2} \right]^{-1} \quad (63)$$

where γ is for the incoming muon, k is the virtual photon energy and M_p is the pair mass. Compared to the bremsstrahlung case, l_f is affected only for $k < \gamma M_p c^2$, or $y < M_p/m_\mu$. Since the incoming muon has a very high energy, it exhibits little multiple scattering. The electron multiple scattering is larger because $E_e \ll E_\mu$. Suppression is possible if the electron multiple scatters by an angle larger than m/E_e , which happens when $l_f > X_0/1720$. Assuming that the pair mass does not reduce l_f (i.e. $y > M_p/m_\mu$), then S is given by Eq. (33), with $E_{LPM(\mu)}$ replacing E_{LPM} . The required energies are high enough that they are rarely reached.

Although it is much less probable, electrons can also lose energy by direct pair production, $e^-N \rightarrow e^+e^-e^-N$. For electrons, the pair mass is larger than the incoming particle mass, so the M_p term dominates in q_{\parallel} and $l_f = 2\hbar k/M_p^2 c^3$. Suppression is possible if $l_f > (E_s/mc^2)^2 X_0$. Even in dense materials, this requires $k > 5 \times 10^{18}$ eV (with, of course $E > k$), energies unlikely to be reached except perhaps in astrophysical situations. The lack of suppression for direct pair production is an early demonstration that higher order diagrams typically involve larger q_{\parallel} than simpler reactions. Because of this, higher order processes are less subject to suppression; when suppression is large they become more important.

I. Magnetic Suppression

External magnetic fields can also affect the electrons trajectory, and hence its radiation. This section will consider the effect of the change in electron trajectory on bremsstrahlung emission, neglecting the closely connected synchrotron radiation emitted by the same field.

An electron will be bent by an angle

$$\theta = \frac{\Delta p}{p} = \frac{eBl_f \sin \theta_B}{E} \quad (64)$$

over a distance l_f in a uniform magnetic field B . Here, θ_B is the angle between the electron trajectory and the magnetic field. As with multiple scattering, if the bending, taken over $l_{f0}/2$ is larger than $1/\gamma$, then bremsstrahlung can be suppressed. This can happen if (Klein, 1993)

$$y < y_B = \frac{\gamma B \sin \theta_B}{B_c} \quad (65)$$

where B_c is the critical magnetic field, $B_c = m^2 c^3 / e\hbar = 4.4 \times 10^{13}$ Gauss.

The bending angle accumulates linearly with l_f , in contrast to the LPM case where $\theta \sim l_f^2$; this will lead to a stronger k dependence than with LPM scattering. If θ_B is treated in the same manner as θ_{MS} in Eq. (27), then

$$l_f = l_{f0} \left[1 + \left(\frac{eB \sin \theta_B l_f}{mc^2} \right)^2 \right]^{-1}. \quad (66)$$

This leads to a quartic equation for l_f , compared with the quadratic found with multiple scattering. In the limit of strong magnetic suppression ($l_f \ll l_{f0}$), the suppression factor l_f/l_{f0} has a form similar to the LPM effect (Klein, 1997):

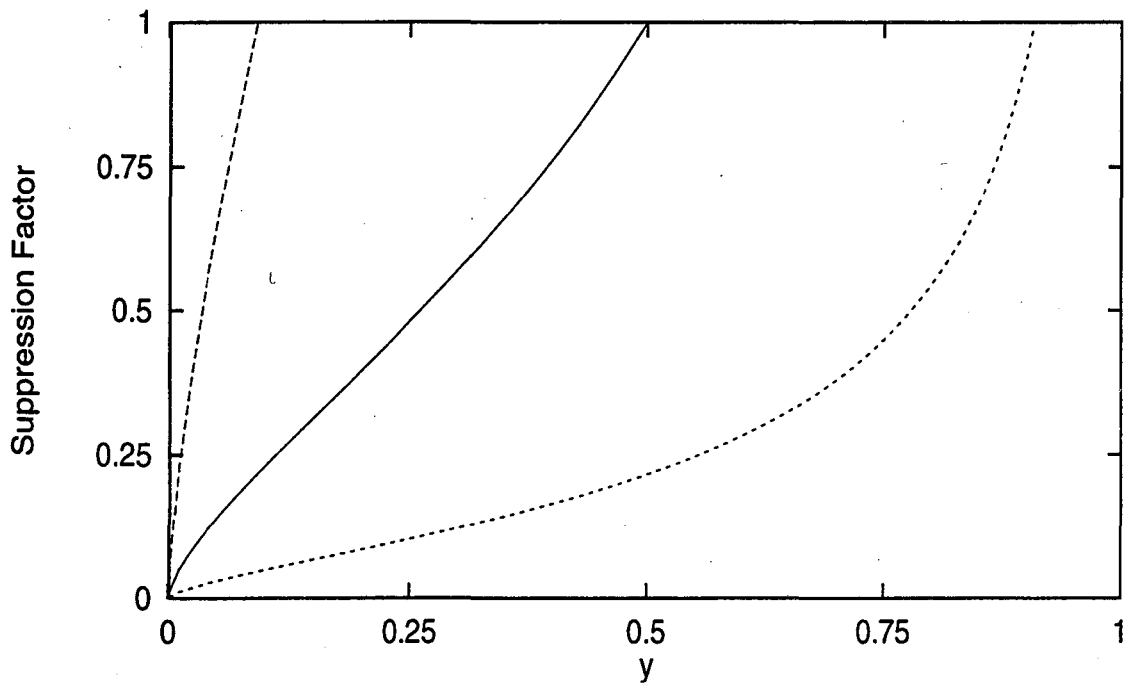


FIG. 7. Suppression factor S for magnetic suppression, for $E = 0.1E_B$ (long dashes), $E = 1E_B$ (solid line) and $E = 10E_B$ (short dashes).

$$S = \left(\frac{kE_B}{E(E-k)} \right)^{2/3} \quad (67)$$

where $E_B = mc^2 B_c / B \sin \theta_B$. Suppression is shown as a function of k in Fig. 7 for three different values of E/E_B .

Because magnetic suppression has a weaker k dependence than dielectric suppression, it is only visible when dielectric suppression does not apply, i.e. for $y_B > y > y_{die}$. For 25 GeV electrons in saturated iron (~ 20 kG), $E_B \approx 1.5$ PeV and $y_B \sim 2.5 \times 10^{-5}$, so the magnetic effect will be hidden. At higher electron energies, it becomes quite visible. For a 1 TeV electron in a 4T field, as will be found at in the CMS detector at LHC, photons with energies below 900 MeV are suppressed.

Suppression should also occur for pair production. A similar calculation finds

$$S = \left(\frac{kE_B}{E(k-E)} \right)^{2/3} \quad (68)$$

For symmetric pairs (maximum suppression), $S = (4E_B/k)^{2/3}$. Because the magnetic bending is quite deterministic, in contrast to multiple scattering which is statistical, this semi-classical calculation may be more accurate than that for multiple scattering.

Baier, Katkov and Strakhovenko (1988) considered bremsstrahlung suppression in a magnetic field, for both normal matter (screened Coulomb potentials) and e^+e^- colliding beam machines. They used kinetic equations to find the radiation to power law accuracy, in both strong and weak field limits. These results are similar to Eq. (67).

When the magnetic field is confined to the material, magnetic suppression should also produce transition radiation. This can happen with ferromagnetic materials. Eq. (50) could be used to find the spectrum.

Both the semi-classical calculation and the more accurate result neglect synchrotron radiation. Because the length scales are similar, synchrotron radiation is important in the same kinematic regions where bremsstrahlung suppression is large. A complete calculation should treat them both similarly, calculating the electron trajectory due to the combined field, and then calculating the radiation for that trajectory.

J. Enhancement and Suppression in Crystals

So far, we have considered only amorphous materials. In crystals, however, the atoms are regularly spaced. The regular lattice allows a huge range of phenomena, because the interactions with the different atoms can add coherently (Williams, 1935). When the addition is in phase, enhanced bremsstrahlung or pair production results, while out of phase addition results in a suppression.

The phase relationship depends on the spacing between atoms, measured along the direction of electron motion. The relative phase for interactions with two different atoms is $\Phi = \exp \{i[kt - \mathbf{k} \cdot \mathbf{r}(t)]/\hbar\}$ where \mathbf{r} is the atomic position. If Φ has the same phase for two nuclei, then the emission amplitudes add coherently.

Including θ_γ , the phase is

$$\Phi = \exp \{ikt[1 - |\mathbf{v}|a \cos(\theta_\gamma)]/\hbar\} \quad (69)$$

where a is the spacing between two atoms along the direction of electron motion. If the nuclei are spaced so that

$$ak \cos(\theta_\gamma)/\gamma^2 = 2\pi n \quad (70)$$

where n is an arbitrary integer, then the exponential is one and the addition is coherent. As with Čerenkov radiation, for the correct θ_γ , the exponential phase is always zero, and $l_f \rightarrow \infty$, implying infinite emission (from an infinite crystal). Conversely, if $ak \cos(\theta_\gamma)/\gamma^2 = (2n + 1)\pi$, there is complete destructive interference.

The large set of variables in Eq. (70) gives rise to a variety of effects. As \mathbf{k} , the incident electron direction (affecting a) or θ_γ vary, the interference will alternate between constructive and destructive, producing peaks in the photon energy spectrum for most sets of conditions.

Although Eq. (69) predicts infinite coherence, several factors limit the coherence length in a real crystal. One of these is the thermal motion of the atoms. When the rms thermal displacement of the atoms is larger than $1/k_{||}$, the coherence is lost. Changes in the electron trajectory can also limit the coherence length. The crystalline structure can generate very high effective fields, causing strong bending, known as channeling (Sørensen, 1996); this bending often limits the coherence length. Multiple scattering can also change the electron direction, and limit the coherence (Bak *et al.*, 1988). Finally, crystal defects and dislocations can also limit coherence. Because this is a vast subject, with several good reviews available (Palazzi, 1968) (Akhiezer and Shulga, 1987) (Baier, Katkov and Strakhovenko, 1989) (Sørensen, 1996), this article will not consider regular lattices further.

K. Summary & Other suppression mechanisms

The suppression mechanisms discussed so far are summarized in Table II, in order of increasing strength. Many other physical effects can lead to suppression of bremsstrahlung and pair production. Many of them involve partially produced photon interactions with the medium. Some of the interactions that can affect bremsstrahlung are photonuclear interactions, real Compton scattering, and, at lower energies, a host of atomic effects including K and L edge absorption and a variety of optical phenomena.

TABLE II. Summary of different bremsstrahlung suppression mechanisms.

Region	Source	dN/dk scaling	Maximum k
Bethe-Heitler	-	k^{-1}	E
LPM	multiple scattering	$k^{-1/2}$	k_{LPM}
Magnetic	magnetic field	$k^{-1/3}$	$y_B E$
Pair Creation	pair creation	k^0	k_{c+}
Dielectric	photon interactions	k^1	$y_{die} E$

Photonuclear interactions have an effect on bremsstrahlung similar to that of pair conversion - the partly created photon is destroyed. However, because the photonuclear cross section is small compared with the pair conversion cross section, this is a small correction. Real Compton scattering can also effectively destroy the photon. Toptygin (1964) treated these reactions as imaginary (absorptive), higher order terms to the dielectric constant of the medium. The bremsstrahlung plus real Compton scattering of the partially produced photon is in some sense a new class of radiation, with its own Feynman diagram. Because Compton scattering involves momentum transfer from the medium, l_f is short, and so, in some regions of phase space (when dielectric suppression is large), Toptygin found that this diagram can be the dominant remaining source of emission.

Other photon absorption mechanisms occur at lower photon energies. For example, K or L edge absorption produces a peak in the photon absorption spectrum. These peaks are difficult to observe because of competition from transition radiation, which is affected by the same peaks (Bak *et al.*, 1986). If, over a formation length, the absorption probability due to these peaks is significant, then suppression can occur. Variations in the dielectric constant due to optical effects can also introduce suppression (Pafomov, 1967).

III. MIGDAL FORMULATION

Beyond these semi-classical approaches, calculations get much more difficult. The first quantum calculation, by Migdal (1956, 1957) is still considered a standard. Migdal treated the multiple scattering as diffusion, calculating the average radiation per collision, and

allowing for interference between the radiation from different collisions. When collisions occur too close together, destructive interference reduces the radiation.

This approach replaces the average multiple scattering angle used earlier with a realistic distribution of scattering, and, hence, of the electron path. Migdal also allows for the inclusion of quantum effects, such as electron spin and photon polarization.

Migdal treated multiple scattering using the Fokker-Planck technique (Scott, 1963). This technique is used to solve the Boltzmann transport equation for $F(\theta, z)$, where F is the probability distribution of particles moving at an angle θ with respect to the initial direction. The equation is:

$$\frac{\partial F(\theta, z)}{\partial z} = -\omega_0(z)F(\theta, z) + \int_0^\infty \theta' d\theta' \int_0^{2\pi} d\beta' W(\chi, z) F(\theta', z) \quad (71)$$

where ω_0 is the scattering probability per unit thickness, given by the integral of $W(\theta, z)$ over all angles. Here, θ is the scattering angle and β' is the azimuthal angle. $W(\chi, z)$ is the single scatter angular distribution. The angle χ is the angular opening between vector representing θ and θ' : $\chi^2 = \theta^2 + \theta'^2 - 2\theta\theta' \cos \beta'$. The W dependence on z allows for inhomogeneity in the material; otherwise W is independent of z . For each of the trajectories allowed by the diffusion, Migdal calculated the photon radiation, including electron spin and photon polarization effects.

The Fokker Planck method is valid if $W(\chi, z)$ is sufficiently sharply peaked at $\chi = 0$, so that it has a finite mean square $\langle \chi^2 \rangle_z$ and that $F(\theta', z) - F(\theta, z)$ can be accurately approximated by a second order Taylor expansion in $\theta' - \theta$. Some calculations (Scott, 1963) lead to a Gaussian distribution for F , with a mean multiple scattering angle $\langle \chi^2 \rangle_z$. Unfortunately, a Gaussian distribution underestimates the number of scatters at angles larger than a few times θ_0 . This failure may limit the accuracy of Migdal's calculation.

This approach also assumes that the number of scatterings is very large. Since l_f is relatively short, this may entail some loss of accuracy.

A. Bremsstrahlung

With these calculations, updated with a more modern form factor, the Migdal cross section for bremsstrahlung is

$$\frac{d\sigma_{LPM}}{dk} = \frac{4\alpha r_e^2 \xi(s)}{3k} \{y^2 G(s) + 2[1 + (1 - y)^2] \phi(s)\} Z^2 \ln \left(\frac{184}{Z^{1/3}} \right) \quad (72)$$

where $G(s)$ and $\phi(s)$ are the suppressions of the electron spin flip and no spin flip portions of the cross section respectively. They are given by

$$G(s) = 48s^2 \left(\frac{\pi}{4} - \frac{1}{2} \int_0^\infty e^{-st} \frac{\sin(st)}{\sinh(t/2)} dt \right) \quad (73)$$

$$\phi(s) = 12s^2 \left(\int_0^\infty e^{-sx} \coth(x/2) \sin(sx) dx \right) - 6\pi s^2 \quad (74)$$

where

$$s = \sqrt{\frac{E_{LPM} k}{8E(E - k)\xi(s)}} \quad (75)$$

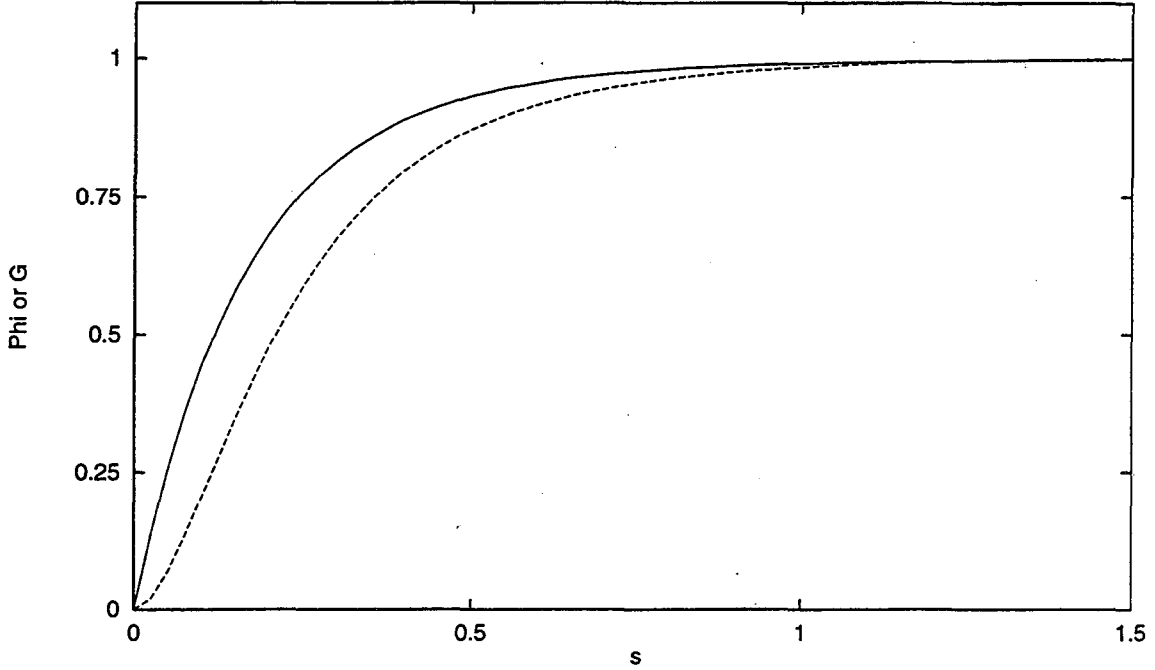


FIG. 8. Migdals $G(s)$ (dashed line) and $\phi(s)$ (solid line). ϕ governs the suppression for $y \ll 1$.

For $k \ll E$, $s \sim 1/\langle \gamma \theta_{MS} \rangle$. For $s \gg 1$, there is no suppression, while for $s \ll 1$, the suppression is large. $\phi(s)$ and $G(s)$ are plotted in Fig. 8.

Migdal found infinite series solutions for G and ϕ . In the region of no suppression ($s \rightarrow \infty$), $G(s) = \phi(s) = 1$, he reproduced the Bethe-Heitler formula. For small suppression, where s is large, $G(s) = 1 - 0.22/s^4$ and $\phi(s) = 1 - 0.012/s^4$. For strong suppression, $s \rightarrow 0$, $G(s) = 12\pi s^2$ and $\phi(s) = 6s$.

Multiple scattering also affects the electron scattering angles, and hence the form factor $\ln(\theta_{max}/\theta_{min})$. Migdal accounted for the changing angular distribution with a variable $\xi(s)$, given by

$$\begin{aligned}
 \xi(s) &= 2 & (s < s_1) \\
 \xi(s) &= 1 + \ln(s)/\ln(s_1) & (s_1 < s < 1) \\
 \xi(s) &= 1 & (s \geq 1)
 \end{aligned} \tag{76}$$

where $s_1 = Z^{2/3}/184^2$. The logarithmic rise in ξ reflects the increasing electron scattering angles. For sufficiently high energies, q_{max} is limited by the size of the nucleus R_A to $q_{max} = \hbar/R_A$; Migdal approximated $R_A = 0.5\alpha r_e Z^{1/3}$. This limit is reached for $s = s_1$; at this point the form factor of the nucleus becomes important and Migdals approach loses accuracy. The fortuitously simple '2' coefficient comes from the chosen approximation for R_A . The exact cutoff is of limited importance because it is only reached for extremely large suppressions, where higher order diagrams are likely to dominate.

One calculational difficulty with these formulae is that ξ depends on s , which itself depends ξ , so the equations must be solved recursively. To avoid this difficulty, Stanev and collaborators (1982) developed simple, non-iterative formulae for $G(s)$, $\phi(s)$ and $\xi(s)$. They found accurate approximations for $\phi(s)$ and $G(s)$:

$$\begin{aligned}
\phi(s) &= 1 - \exp\left(-6s[1 + (3 - \pi)s] + s^3/(0.623 + 0.796s + 0.658s^2)\right) \\
\psi(s) &= 1 - \exp\left(-4s - 8s^2/(1 + 3.96s + 4.97s^2 - 0.05s^3 + 7.5s^4)\right) \\
G(s) &= 3\psi(s) - 2\phi(s).
\end{aligned} \tag{77}$$

These equations were used to produce the curves in Fig. 8. To avoid recursion, they removed $\xi(s)$ from the equation for s , defining

$$s' = \sqrt{\frac{E_{LPM}k}{8E(E-k)}}. \tag{78}$$

Modified formulae for ξ depend only on s' :

$$\begin{aligned}
\xi(s') &= 2 & (s' < \sqrt{2}s_1) \\
\xi(s') &= 1 + h - \frac{0.08(1-h)[1 - (1-h)^2]}{\ln \sqrt{2}s_1} & (\sqrt{2}s_1 < s' \ll 1) \\
\xi(s') &= 1 & (s' \geq 1).
\end{aligned} \tag{79}$$

where $h = \ln s' / \ln(\sqrt{2}s_1)$. This transformation is possible because ξ depends only logarithmically on s .

The energy weighted cross sections per radiation length, $X_0 n k d\sigma/dk$ from Eq. (72) are shown for a number of electron energies in Fig. 9. As E rises, the cross section drops, with low energy photons suppressed the most. The number of photons with $k < E(E-k)/E_{LPM}$ is reduced.

One weakness of Migdals approach is that, while it reproduces the main terms of the Bethe-Heitler equation, it does not include all of the corrections that are typically used today. In the Bethe Heitler limit, Migdals finds,

$$\frac{d\sigma_{LPM0}}{dk} = \frac{4\alpha r_e^2}{3k} \{y^2 + 2[1 + (1-y)^2]\} Z^2 F_{el}, \tag{80}$$

matching the Bethe and Heitler (1934) result. In comparison a modern bremsstrahlung emission cross section (Tsai, 1974) (Perl, 1994)

$$\frac{d\sigma_{BH}}{dk} = \frac{4\alpha r_e^2}{3k} \left[\{y^2 + 2[1 + (1-y)^2]\} [Z^2(F_{el} - f) + ZF_{inel}] + (1-y)\frac{(Z^2 + Z)}{3} \right] \tag{81}$$

includes several additional terms. F_{el} is the elastic form factor from Sec. 2, $\ln(184/Z^{1/3})$, for interactions with the atomic nucleus. F_{inel} is an inelastic form factor, $\ln(1194/Z^{2/3})$ that accounts for inelastic interactions with the atomic electrons. Newer suppression calculations, discussed later, treat inelastic scattering separately.

The f term accounts for Coulomb corrections because the interaction takes place with the electron in the Coulomb field of the nucleus. For lead $f = 0.33$, while $F_{el} = 3.7$. The Coulomb correction may be incorporated into suppression calculations by adjusting the form factors (Sec. VII; Baier and Katkov, 1997a).

These corrections may be simply accounted for with a simple assumption (Anthony *et al.*, 1995) that, since the momentum transfer to the target is small compared with the

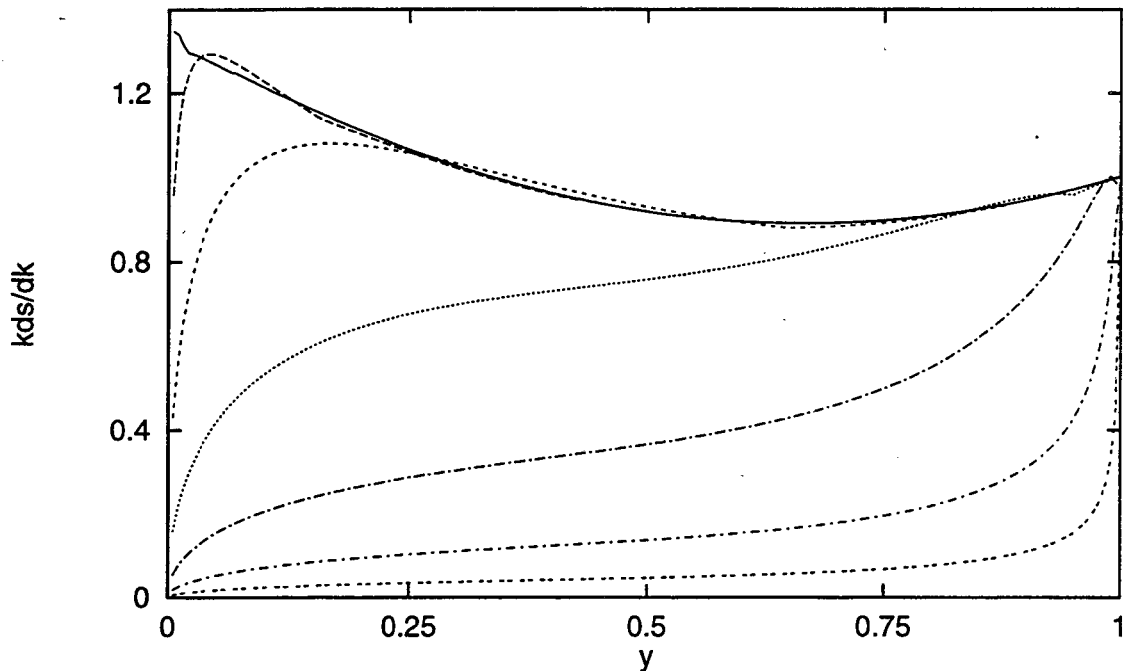


FIG. 9. $d\sigma_{LPM}/dy$ for bremsstrahlung as a function of y for various electron energies in a lead target, showing how the spectral shape changes. Electrons of energies 10 GeV (top curve), 100 GeV, 1 TeV, 10 TeV, 100 TeV, 1 PeV and 10 PeV (bottom curve) are shown. The units are photons per radiation length.

electron mass, the lighter (electron) target is irrelevant, and the electron scattering term and Coulomb corrections can be merely lumped into Migdals form factor. This is equivalent to scaling the radiation length to include these corrections; the standard tables of radiation lengths (Barnett, 1996) include these factors.

The other difference, the final $1 - y$ term, is problematic because of the different y dependence. In a semi-classical derivation (Ter-Mikaelian, 1972, pg. 18-20), this term only appears in the limit where there the atomic electrons do not screen the nucleus. This is the small impact parameter, high momentum transfer, short formation length limit. With full screening (small momentum transfer, large formation length), this term is not present. So, if the semi-classical result holds, this term represents a part of the cross section that involves large momentum transfers, and so is not subject to suppression. Because it is only about a 2.5% correction for large Z nuclei, current experiments have limited sensitivity to this point.

In the strong suppression limit, for $y \ll 1$, the small s approximations for $\phi(s)$ and $\xi(s)$ lead to the semi-classical scaling

$$S = 3\sqrt{\frac{kE_{LPM}}{E(E-k)}}. \quad (82)$$

Because $\xi(s)$ varies only logarithmically with s , this limit, corresponding to $\xi(s) = 2$, is only reached for very strong suppressions, $S < 10^{-3}$. As Fig. 1 shows, the normalization differs from the semi-classical results, but, as previously mentioned, can depend on the how the absolute cross section is treated. Moreover, for a direct comparison, it might be fairer to use

$\xi = 1$, since the semi-classical calculations do not consider the form factor. This changes the coefficient to $3/\sqrt{2} \sim 2$.

For lower energies, the strong suppression limit is

$$S \sim \sqrt{\frac{36kE_{LPM}}{8E(E-k)}} \left(1 - 0.13 \ln S\right) \quad (83)$$

where the recursion for $\xi(s)$ has been removed, and s_1 calculated for lead. It is clear that the correction for ξ is significant, particularly for small S .

The uncertainties in Migdals calculation are problematic. Because of the Fokker-Planck method and the consequent poorly handled mean scattering angle; these results are of only logarithmic accuracy. One numerical hint of inaccuracy can be seen by comparing Migdals formula as written with the Bethe-Heitler limit. Figures 1 and 9 show that, for $k_{LPM} < k < 1.3k_{LPM}$, the Migdal curve is slightly above the Bethe Heitler result; the excess occurs when $\phi(s)\xi(s)$ rises slightly above 1; the maximum cross section excess is about 3%. This gives a crude estimate of the expected accuracy of Migdals methods.

Migdal accounted for dielectric suppression in his formulae. Since dielectric suppression only occurs for $y \ll 1$, only the ϕ term is affected; Migdal replaced $\phi(s)$ with $\phi(s\Gamma)/\Gamma$, where $\Gamma = 1 + k_p^2/k^2$, to get

$$\frac{d\sigma_{LPM}}{dk} = \frac{16\alpha r_e^2 \xi(s)}{3k} \frac{\phi(s\Gamma)}{\Gamma} Z^2 \ln \left(\frac{184}{Z^{1/3}} \right). \quad (84)$$

The same substitution applies for the simplified polynomials (Stanev *et al.*, 1982). When dielectric suppression is strong, this does not completely match the Ter-Mikaelian form factor in Eq. (44).

Similar results may also be obtained with a functional integral approach (Akhiezer and Shulga, 1987).

Migdal comments that, for thick slabs, the photon angular distribution is dominated by the electron multiple scattering. However, nothing in Migdals calculation should change the semi-classical result that suppression should be reduced for photons with $\theta_\gamma > 1/\gamma$; this effect may be visible in thinner targets. Pafomov (1965) discussed the energy and angular distribution of photons emerging from thin slabs ($T \ll X_0$), producing a complex set of results.

B. Pair Creation

The cross section for pair production may be found simply by crossing the Feynman diagram for bremsstrahlung, as shown in Fig. 6. Migdal used this crossing to calculate the cross section for pair production:

$$\frac{d\sigma_{LPM}(\gamma \rightarrow e^+e^-)}{dE} = \frac{4\alpha r_e^2 \xi(\tilde{s})}{3k} \left(G(\tilde{s}) + 2 \left[\frac{E^2}{k^2} + \left(1 - \frac{E}{k}\right)^2 \right] \phi(\tilde{s}) \right) \quad (85)$$

where

$$\tilde{s} = \sqrt{\frac{E_{LPM}k}{8E(k-E)\xi(\tilde{s})}} \approx \frac{m}{k\gamma} \quad (86)$$

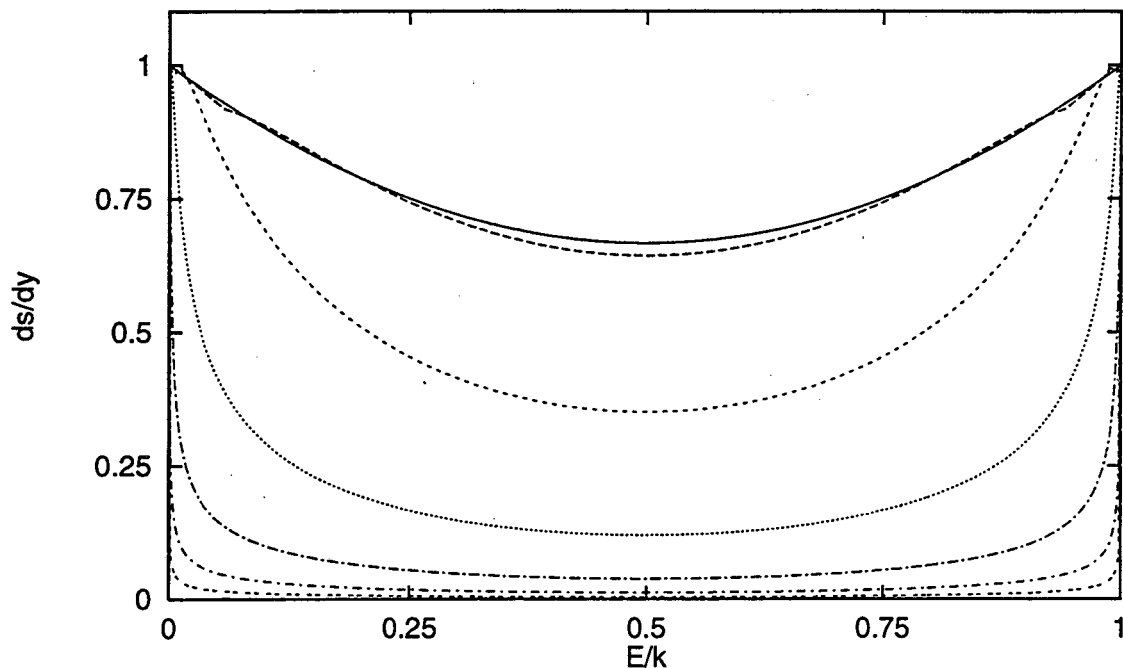


FIG. 10. $X_0 n d\sigma_{LPM}/dy$ for pair production in lead, as a function of y for various photon energies, showing how the spectral shape changes. Cross sections are plotted for photons of energies 1 TeV, 10 TeV, 100 TeV, 1 PeV, 10 PeV, 100 PeV and 1 EeV, with the cross section decreasing as k increases. The differential conversion probability is given per radiation length.

and G and ϕ are as previously given. In the limit $\tilde{s} \gg 1$ there is no suppression, while $\tilde{s} \rightarrow 0$ indicates large suppression, both leading to the appropriate semi-classical result. These equations can be simplified as was done with bremsstrahlung (Stanev, 1982).

Figure 10 gives the pair production cross section in lead for a number of photon energies. As k increases above E_{LPM} , the cross section drops, with asymmetric pairs increasingly favored. For the regions $E_{LPM} < E(k - E)/k < 1.3E_{LPM}$, the Migdal cross section rises above the Bethe-Heitler case, matching the bremsstrahlung $\phi(s)\xi(s) > 1$ overshoot. It also causes the 'hiccup' present at $k = E_{LPM}$ in Fig. 2.

C. Surface Effects

Migdals calculations only apply for an infinite thickness target. Several authors have calculated the transition radiation due to multiple scattering, based on a Fokker-Planck approach. Although these calculations begin with the same approach, the details differ significantly, as do the final results. Gol'dman (1960) added boundaries to Migdals Fokker-Planck equation, calculating the emission inside and outside the target, and an interference term. Outside the target, there is no emission, while inside he reproduced Migdals result. For the surface terms, the photon flux for $y \ll 1$ and $s \ll 1$ is

$$\frac{dN}{dk} = \frac{\alpha}{\pi k} \ln \frac{1}{s} \approx \frac{\alpha}{2\pi k} \ln \left(\frac{8k_{LPM}}{k} \right) \quad (87)$$

per surface. This result is similar to the semi-classical result in Eq. (52).

Ternovskii (1960) considered the effect of the dielectric constant of the medium together with the multiple scattering, again working from Migdals kinetic equation. He considered the entire range of target thicknesses, including interference between closely spaced boundaries. By comparing the radiation inside the target with an interference term, he found that for targets with $T < \alpha X_0/2\pi$, multiple scattering is insignificant, and the Bethe-Heitler spectrum is recovered. This covers much thicker targets than the limit $T < X_0/1720$ presented in section II.F. His results for intermediate thickness targets, Eq. (53), apply for $\alpha X_0/2\pi < T < \alpha X_0/2\pi s$, also a wider range than in Sec. II.F.

For thicker targets, with $T \gg \alpha X_0/2\pi s$, if the dielectric dominates ($s > 1$ or $s(k_p/k)^2 > 1$), he obtains Eq. (49). Where multiple scattering dominates ($s < 1, s(k_p/k)^2 \ll 1$), then

$$\frac{dN}{dk} = \frac{\alpha}{2\pi k} \left(\frac{k^2}{E^2} + 2 \frac{E^2 + (E-k)^2}{E^2} \right) \ln \frac{\chi}{\sqrt{s}} \quad (88)$$

where $\chi \approx 1$. This result is similar to that of Gol'dman, but covers the complete range of y . Neglecting the logarithmic term, the spectrum matches that of unsuppressed bremsstrahlung for a target of thickness $\sim 0.5\alpha X_0$, or roughly one mean free path; this is a very different E and k dependence than would result from $1l_f$ of Bethe-Heitler radiation.

Unfortunately, Eq. (88) is difficult to use. It only applies for $s(k_p/k)^2 \ll 1$; no solution is given for the intermediate region $s(k_p/k)^2 \approx 1$. Also, χ is poorly defined. If the equation is extended to $s(k_p/k)^2 = 1$, then setting $\chi = 1$ creates a large discontinuity. The discontinuity disappears if one chooses $\chi = 0.42$, but this also eliminates transition radiation in the region $0.17 < s < 1$.

Garibyan (1960) extended his previous work with transition radiation to include multiple scattering. He found that multiple scattering dominates when

$$k > k_p (k_p/k_{LPM})^{1/3}. \quad (89)$$

If $\xi(s)$ is neglected, this is the same cutoff found by Ternovskii. Where multiple scattering dominated, he reproduced Gol'dmans result. Elsewhere, he found the usual transition radiation from the dielectric of the medium.

These formulae can produce negative results for $s > 1$; common sense indicates that they should be cut off in this region where no transition radiation is expected. However, Pafomov (1964) stated that this was evidence that these previous works were wrong. The problem is that the radiation was incorrectly separated into transition radiation and bremsstrahlung. Pafomov calculated the transition radiation as the difference between the emission in a solid with and without a gap, again starting with the initial formulae of Gol'dman. Pafomov found the same $(k_p^4/k_{LPM})^{1/3}$ threshold for multiple scattering dominated transition radiation as Garibyan. He found a different magnitude; for $k < k_{LPM}$,

$$\frac{dN}{dk} = \frac{\alpha}{\pi k} \ln \frac{2}{3} \sqrt{\frac{k_{LPM}}{k}}. \quad (90)$$

Counterintuitively, Pafomov predicted that for $k > k_{LPM}$, there is still transition radiation, given by

$$\frac{dN}{dk} = \frac{\alpha}{\pi k} \frac{8k_{LPM}^2}{21k^2}. \quad (91)$$

These two equations do not match in the region $k \approx k_{LPM}$. However, a numerical formula, not given here, covers the entire range smoothly. It is worth noting that Eq. (91) is quite close to the semi classical result for $k < k_{LPM}$.

Fig. 11 compares the transition radiation from a single surface predicted by Gol'dman/Garibyan, Ternovskii (using $\chi = 1.0$), and Pafomov. Except for Pafomov, these calculations predict radiation up to $k = k_{LPM} = E^2/E_{LPM}$. For a flat kdN/dk spectrum, the total energy radiated per surface rises as E^2 , as with the semi-classical approach. For large enough E , electrons lose most of their energy to radiation when crossing an interface.

However, these equations fail before this point. For high enough electron energies, these calculations predict that each electron should emit several photons per edge traversed. Since the formation lengths for the various photon emissions will overlap at the edge, this is really a higher order process, not yet treated properly by calculations.

Unfortunately, these calculations appear to do a poor job of fitting the data. Fig. 19 shows that they predict transition radiation considerably above the data from SLAC E-146.

IV. BLANKENBECLER AND DRELL FORMULATION

Blankenbecler and Drell (1996) calculated the magnitude of LPM suppression with an eikonal formalism used to study scattering from an extended target. The approach was originally developed to study beamstrahlung. One major advantage of their approach is that it naturally accommodates finite thickness slabs, automatically including surface terms.

They begin by calculating the scattering of a wave packet moving through a random medium. For each electron path, they calculate the radiation, based on the acceleration of the electron. The radiation is calculated for all possible paths and averaged. One clear conceptual advantage of this calculation is that it does not single out a single hard scatter as causing the bremsstrahlung; instead all of the scatters are created equal. This differs from Landau and Pomeranchuk and Migdal, who found the rate of hard scatters which produced bremsstrahlung, and then calculated the multiple scattering in the region around the hard scatter to determine the suppression. For a thick target, in the strong suppression limit $s \ll 1$, they predict that the radiation is $\sqrt{3\pi/8}$ (about 8%) larger than that of Migdal.

One advantage of this calculation is that it treats finite thickness media properly. There are three relevant length scales: l_{f0} (Eq. (5)), T and the mean free path αX_0 . These variables are combined into two ratios:

$$N_{BD} = \frac{\pi l_{f0}}{3\alpha X_0} \quad (92)$$

and

$$T_{BD} = \frac{\pi T}{3\alpha X_0} \quad (93)$$

where T_{BD} is the target thickness, in mean free paths, while N_{BD} is the number of formation lengths per mean free path; when N_{BD} is large suppression is strong, while $N_{BD} < 1$ corresponds to a single interaction per electron, and hence the Bethe Heitler regime.

The eikonal approach finds the wave function phase and momentum difference between different points on the electron path. These differences are then used to find the radiation for that length scale. The emission is

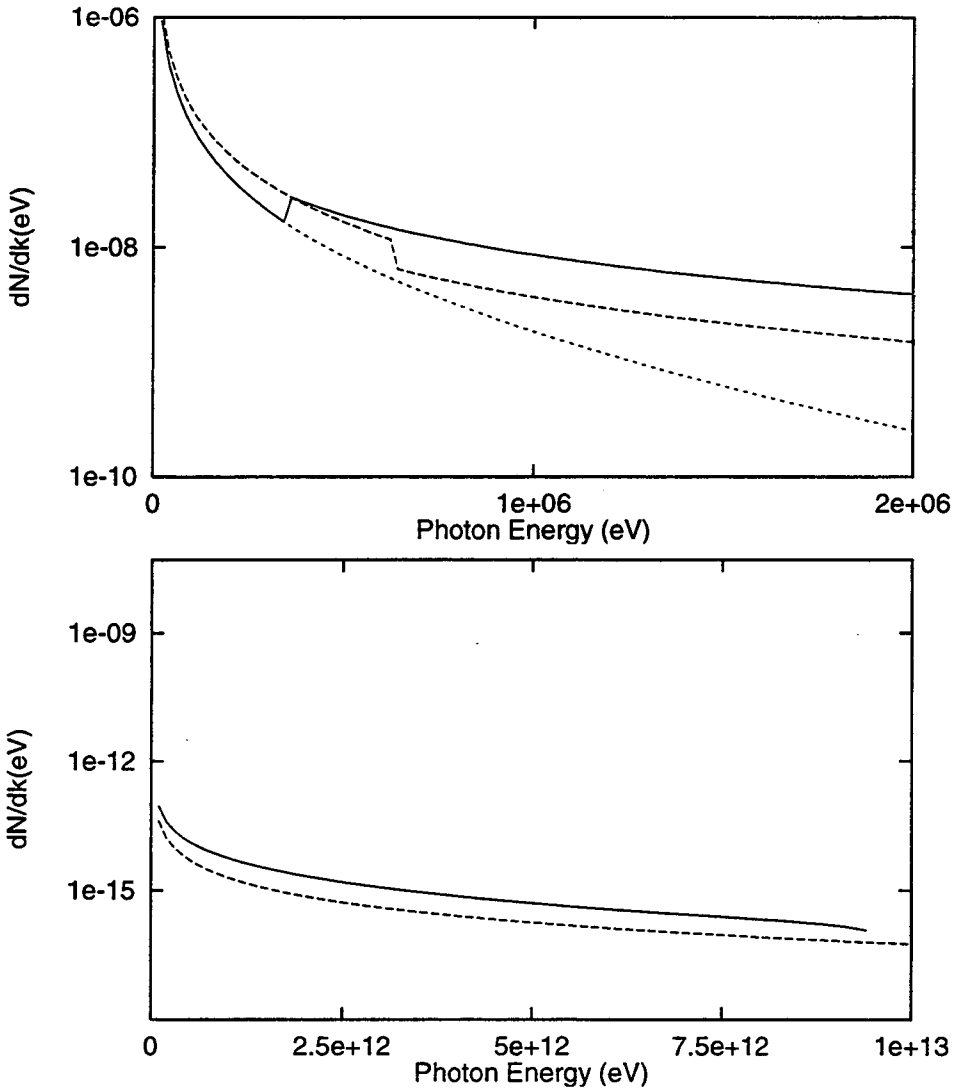


FIG. 11. Comparison of the edge effects predicted by Ternovskii (with $\chi = 1$) (solid line) and Pafomov (long dashes), for a single independent edge, compared with conventional transition radiation (short dashes). (a) shows the radiation from a 100 GeV electron in lead. The jump in the Ternovskii curve at $k = 350$ keV is at $s(k_p/k)^2 = 1$, while the drop in the Pafomov curve at 630 keV occurs for $k_p^4/k_{LPM} = 1$. Panel (b) shows the Pafomov and Ternovskii predictions for a 10 TeV electron in lead; both curves are much smoother. Conventional transition radiation is negligible in (b).

$$\frac{d\sigma_{BB}}{dk} = \frac{\alpha}{2k(E-k)nX_0} \int \frac{d^2k_{\perp}}{4\pi^2} \int_{-\infty}^{+\infty} dz_2 \int_{-\infty}^{z_2} dz_1 S(z_2, z_1) \cos \left(\int_{z_1}^{z_2} dz \frac{d\Phi(z, 0)}{dz} \right). \quad (94)$$

Here, $k_{\perp} = k \cos(\theta_{\gamma})$ is the photon perpendicular energy, $S(z_2, z_1)$ is a sum over electron polarization (spin flip and no spin flip), and $d\Phi/dz$ is the differential phase difference due to multiple scattering. The d^2k_{\perp} integration is equivalent to an integration over photon angles. In the absence of scattering, $d\Phi/dz$ is constant, and then the integrals must be carefully evaluated; Blankenbecler and Drell introduce a convergence factor to insure that the boundary conditions are correct.

Because the integrals include all possible values of z , three regions must be considered: before the target (denoted +), inside the target (denoted 0), and after the target (-). For the double integral, there are 9 possible combinations, of which two (++) and (--) are clearly zero. Time ordering eliminates (-+), (-0) and (0+), leaving the bulk term (00), two single surface terms (+0) and (0-) and the interference term (+-). For thick targets with $T_{BD} \gg 1$, the interference term vanishes, and the bulk term dominates over the single surface terms. In this case, their calculations reproduce the Migdal results, with the 8% higher cross section. For thinner targets, the surface terms are more important. The relative importance of these terms is shown in Fig. 12, which gives their results in terms of a suppression form factor $S = F(N_{BD}, T_{BD})$, relative to Bethe-Heitler.

For thin targets, $T_{BD} < 1$, where $N_{BD} > 1$, the surface interference term (+-) dominates, because of the large transition radiation. $N_{BD}/T_{BD} < 1$ reduces to the Bethe Heitler free particle case.

For a thick target, $T_{BD} > 1$, the central interaction (00) region is important. For large N_{BD} , their results are similar to those of Migdal. For very large N_{BD} , with $N_{BD}/T_{BD} > 1$, the formation length is longer than the target, and both the (00) and mixed regions contribute. Fig. 13 compares the suppression as a function of N_{BD} (which is proportional to $1/k$), for a variety of T . For large T_{BD} , suppression increases with N_{BD} . When T_{BD} decreases, suppression drops, eventually reaching a value that is almost independent of N_{BD} , and similar to that predicted by Shulga and Fomin (1996).

There are a few caveats in this calculation. The eikonal approach assumes that the potential is smooth enough. Blankenbecler and Drell used a Gaussian scattering potential, which underestimates the rate of large angle scattering. Second, they assumed that the wave function phase and amplitude fluctuate independently. Blankenbecler (1997b) showed that accounting for the correlation between amplitude and phase reduces the emission by a further 5-15%. Fig. 13 shows curves with and without the correlation. The calculation has also been extended to include multiple slabs separated by a gap (Blankenbecler, 1997a).

Calculating the emission from a slab as a whole introduces a problem, because it assumes that there is either zero or one interaction per incident electron. But, neglecting correlation effects, with a typical bremsstrahlung cross section of 10 photons per X_0 , the relative probability of getting 2 interactions compared with 1 interaction is $\sim 20T/X_0$, so single interactions are only prevalent for slabs with $T < 0.05X_0$. This problem makes it difficult to use these results in many real-world situations.

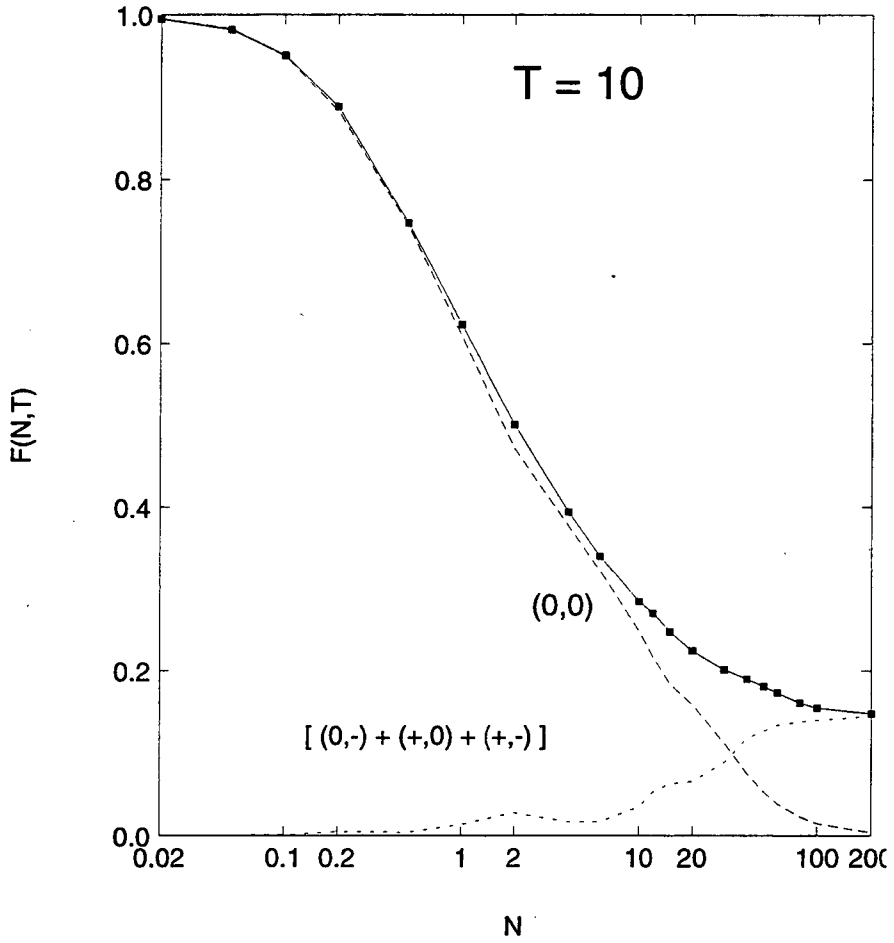


FIG. 12. The Blankenbecler and Drell form factor $F(N_{BD}, T_{BD})$ for a target with $T_{BD} = 10$, showing the contributions for the bulk emission (00) and the transition and interference terms (0-), (+0) and (+-). For a fixed target thickness, $N_{BD} \sim 1/l_{f0} \sim k/E^2$; the edge effects are largest for small N_{BD} corresponding to small k . From Blankenbecler and Drell (1996).

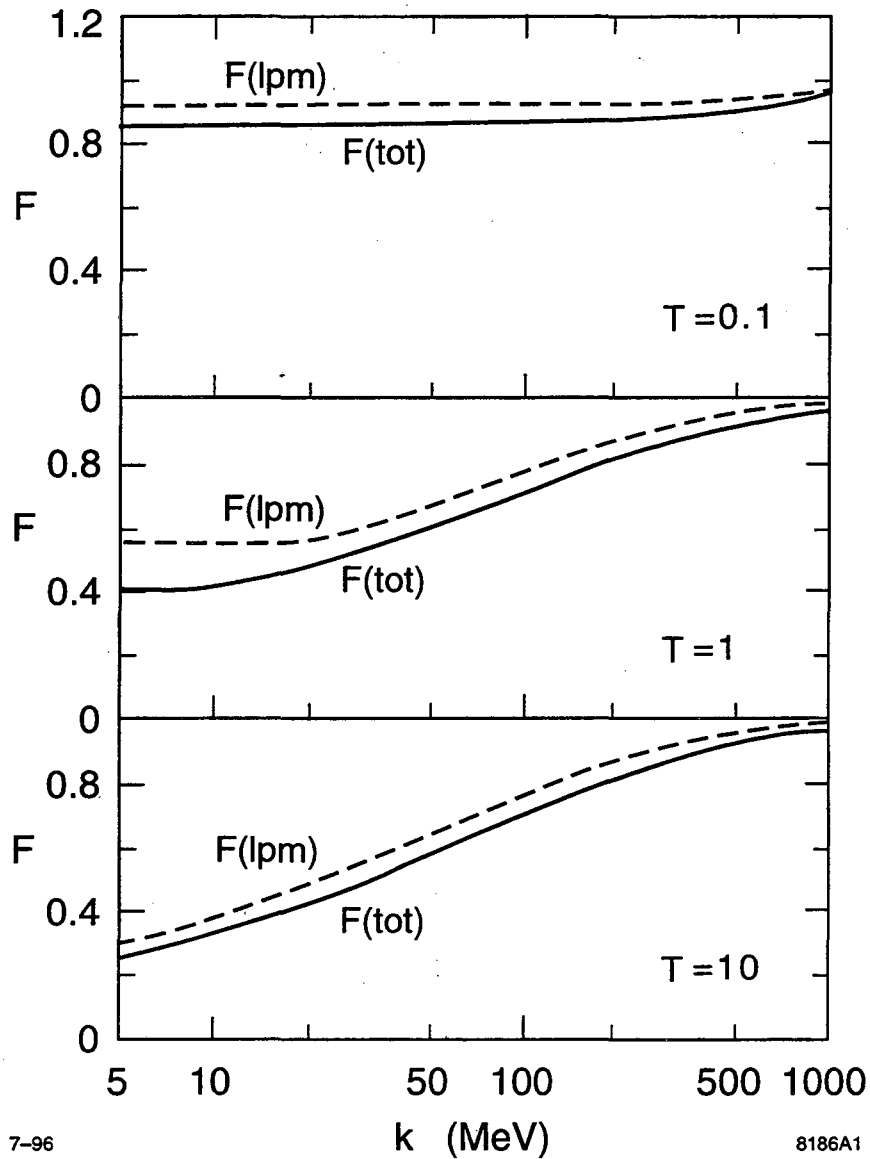


FIG. 13. The Blankenbecler and Drell form factor $F(N_{BD}, T_{BD})$ for 25 GeV electrons in 3 thicknesses of gold targets. $F(\text{lpm})$, assumes that the wave function amplitude and phase fluctuate independently, while $F(\text{tot})$ includes the correlation between amplitude and phase, further reducing the emission. From Blankenbecler (1997b).

V. ZAKHAROV CALCULATION

Zakharov (1996a,b, 1998) transformed the problem of multiple scattering into a two dimensional (impact parameter and depth in the target) Schröedingers equation. This equation was solved using a transverse Greens function based on a path integral. This impact parameter approach is complementary to Migdals momentum space approach. Because this approach allows for arbitrary target density profiles, it naturally accomodates finite thickness targets.

Zakharov (1996a) calculated the radiation due to a simple Coulomb potential. The calculation is keyed to the scattering cross section for a e^+e^- dipole of separation ρ , where the scattering cross section is simply related to the bremsstrahlung cross section. He parameterized the cross section as $\sigma(\rho) = C(\rho)\rho^2$. In the strong suppression limit, C varies slowly with ρ . Zakharov then found the frequency Ω for a harmonic oscillator in a potential which would reproduce this scattering cross section. This is roughly equivalent to describing the multiple scattering with a Gaussian. The radiation is governed by a parameter $\eta = \Omega l_f$. For an infinitely thick target, the results are almost identical to Migdal (Zakharov, 1998); functions of η that match Migdals ϕ and G , for $\eta = 1/\sqrt{8}s$. The only difference is the slowly varying part of the cross section: $\xi(s)$ for Migdal and $C(\rho_{eff}y)/C(1/m)$ for Zakharov; ρ_{eff} is the impact parameter where radiation is largest. In the Bethe-Heitler limit, $\rho_{eff} \sim 1/ym$.

In the limit $y \rightarrow 0$, for strong suppression

$$\frac{d\sigma_Z}{dk} = \frac{2\alpha^2 Z}{E} \sqrt{\frac{2\hbar c \log(2a/y\rho_{eff})}{\pi n k}} \quad (95)$$

where

$$\rho_{eff} = \left(\frac{\pi Z^2 \alpha^2 n E y^3 \log(2/\alpha Z^{1/3})}{\hbar c} \right)^{1/4} \quad (96)$$

where a is the Thomas-Fermi screening radius from Section II. Numerically, $\rho_{eff}(m) \sim 10^{-9}/[E(eV)y^3]^{1/4}$ for lead. These equations are valid for $200/Z^{1/3} < \log(2a/y\rho_{eff}) < 1.5 \times 10^5/Z^{2/3}$; corresponding to $\xi(s) = 1$ and $\xi(s) = 2$ for Migdal.

Except for the '1' in $\xi(s)$, this equation has the same form as Eq. (83) from Migdal. Although unimportant to the theory, the '1' greatly reduces the effect of the slowly varying term. Numerically, $2a/y\rho_{eff} = 6.8 \times 10^{-7} E(eV)/y$ for lead; other solids aren't too different. For a 1 TeV electron beam, as y varies from 10^{-4} (y_{die}) to 10^{-2} (an arbitrary upper limit to 'low y '), the Zakharov logarithm varies by about 20%, while the change in $\xi(s)$ is much smaller. This variation should be large enough to measure. With the lower energy electron beams currently available, the usable y range is probably too narrow to measure this variation.

Zakharov (1996b) considered several additions required for calculations involving smaller suppressions. Instead of the harmonic oscillator approach, he used the actual potential. This required additional integrations, and hence a finite thickness targets. The potential must be treated more accurately because, for moderate suppression, $C(\rho)$ varies more quickly with ρ . He used separate screened elastic ($a = 0.83a_0 Z^{-1/3}$) and inelastic ($a = 5.2a_0 Z^{-2/3}$) potentials, reproducing the appropriate unsuppressed bremsstrahlung cross sections. The separate potentials would have the largest effect for low Z nuclei. However, because of the

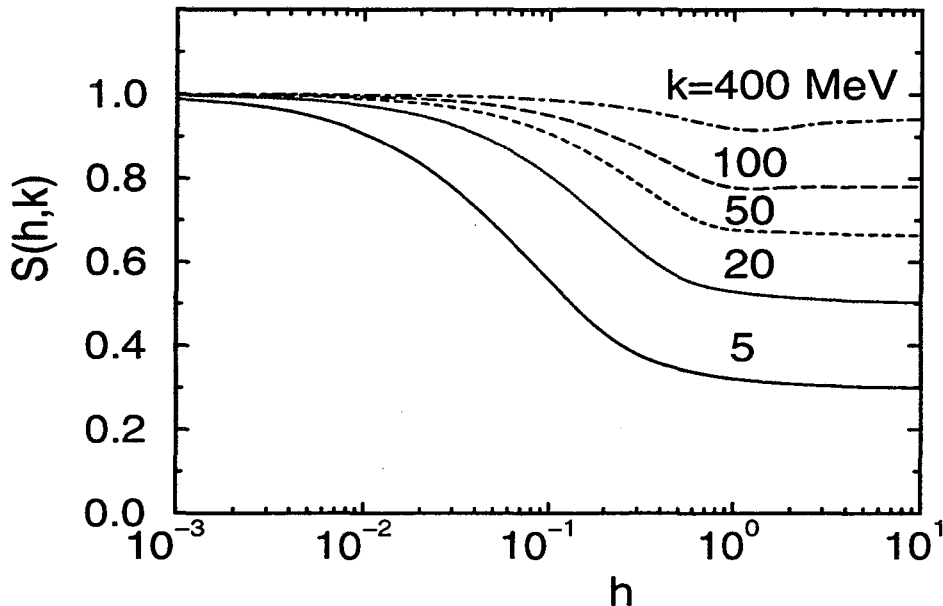


FIG. 14. Suppression factor $S(h, k)$ found by Zakharov. The curves are for a 25 GeV electron, with $h = T/l_{f0}$. The $h = 10$ results are very close to the infinite thickness limit. The dip around $h = 1$ for the highest photon energies is due to interference between the two target surfaces. From Zakharov (1996b).

small recoil, the separate form factors have a small effect on suppression. Because of the more accurate overall potential, this calculation may be more accurate than Migdals.

Figure 14 shows Zakharov suppression factors for finite target thicknesses, for various photon energies in a 25 GeV electron beam. This shows nicely how the suppression increases with target thickness; the upper limit of the plot $h = 10$ is very close to the infinite thickness limit. Like Blankenbecler and Drell, this calculation suffers from its inability to handle thick targets with multiple photon emission, and does not include dielectric suppression. Zakharov (1997b) presents a few results for multiple-slab configurations, finding a smaller interference term than Blankenbecler (1997a); the two results would agree better if Blankenbecler included the amplitude-phase correlation in his multiple slab calculations.

Zakharov's results for gluon bremsstrahlung from a quark will be discussed in Sec. XII.

VI. BDMS CALCULATION

The BDMS group (R. Baier *et al.*, 1996) started with the Coulomb field of a large number of scatterers, with the atomic screening modelled with a Coulomb potential cut off with a Debye screening mass μ . An eikonal approach is used to account for the large number of scatters.

The critical variable in this calculation is the (dimensionless) phase difference between neighboring centers,

$$\kappa = \frac{X_0 \mu^2 c^3 k}{2\hbar E^2} \quad (97)$$

For QED calculations, $\mu = \hbar Z^{1/3}/a_0 c$ reproduces Thomas-Fermi screening. The authors also define a coherence number $\nu = \alpha l_{f0}/X_0$, the number of scatters required for the accumulated phase shift to equal 1. This coherence number is similar to Blankenbecler and Drells N_{BD} . A large phase shift between interactions, $\kappa > 1$, corresponds to the Bethe-Heitler limit. Because this approach assumes massless electrons, the 'Bethe-Heitler limit' does not completely match the usual Bethe-Heitler formula.

In the factorization limit, $T < l_{f0}$, where the entire target reacts coherently, their results match Ternovskii (1960):

$$\frac{dN}{dk} = \frac{2\alpha}{\pi k} \langle \ln(\frac{q_{tot}^2}{m^2 c^2}) \rangle \quad (98)$$

where q_{tot} is the total perpendicular momentum acquired by the particle while traversing the target due to multiple scattering. Here, the mass m was required to remove a collinear divergence.

In the LPM regime, ($\kappa \ll 1$), they find a bremsstrahlung cross section similar to Eq. (95). They attribute the logarithmic term to occasional non-Gaussian large angle ($\theta > 1/\gamma$) Coulomb scatters. Because of these large scatters, the mean squared momentum transfer is poorly defined, and, in fact, diverges logarithmically; this logarithm appears in the suppression formula.

$$\frac{d\sigma}{dk} = \frac{\alpha}{\pi k X_0} \sqrt{\kappa \ln(1/\kappa)}. \quad (99)$$

They comment that they neglect a logarithmic factor under the logarithm; if the corresponding term is removed from Zakharov's formula, the two results have the same functional dependence. If one identifies $E_{LPM} = \kappa \mu^2/2$, as their paper indicates, then the radiation takes the form

$$\frac{d\sigma}{dk} \sim \frac{\alpha}{\pi k} \sqrt{\frac{k E_{LPM}}{E^2} \log \frac{E^2}{k E_{LPM}}}. \quad (100)$$

A later paper (R. Baier *et al.*, 1997) expands the calculation to include finite thickness single slab targets, again in the strong suppression limit.

VII. BAIER & KATKOV

Baier and Katkov (1997a) also calculated suppression due to multiple scattering, trying to reach an accuracy of a few percent, by including several corrections omitted from previous calculations. They begin by calculating the scattering from a screened Coulomb potential, in the same impact parameter space used by Zakharov. Coulomb corrections are included to account for the motion of the screening electrons, along with separate potentials for elastic and inelastic scattering. Finally, they allow for a nuclear form factor, with an appropriately modified potential for impact parameters smaller than the nuclear radius.

They begin by calculating an electron propagator for a screened Coulomb potential, in the Born approximation, which assumes Gaussian distributed scattering. This produces the Migdal result. The electron propagator is then expanded perturbatively, with a correction

term which accounts for both large angle scatters and Coulomb corrections to the potential. Without the Coulomb corrections, the first order result is similar to that of Zakharov (V. Baier, 1998).

Coulomb corrections are incorporated by adjusting the parameters in the potential. With Coulomb corrections, the screening radius becomes $a_2 = 0.81Z^{-1/3}a_0 \exp[0.5 - f(Z\alpha)]$, while the characteristic scattering angle changes from $\theta_1 = 1/Ea_0$ to $\theta_2 = 1/Ea_0 \exp[f(Z\alpha) - 0.5]$. Here, $f(Z\alpha)$ is the standard Coulomb correction (Tsai, 1974). This simple scaling accounts for the extra terms in Eq. (81) compared with Eq. (80). For heavy nuclei, a_2 is about 20% larger than the standard Thomas-Fermi screening radius.

Higher order terms may also be calculated for the electron propagator. The ratio of the first two terms of the expansion is 0.451 divided by a logarithmic term, so the series should converge reasonably rapidly.

Inelastic scattering can be incorporated into the calculations by adding a term to the scattering potential, changing the charge coupling from Z^2 to $Z^2 + Z$ and further modifying the characteristic angle, to $\theta_e = \theta_1 \exp[Z/(1+Z)(f(\alpha Z) - 1.88) - 0.5]$.

Dielectric suppression is included by modifying the potential, with a replacement similar to Migdal's. For $k \ll k_p$, the spectrum is similar to Ter-Mikaelian's, but to power law accuracy and including Coulomb corrections:

$$\frac{d\sigma}{dk} = \frac{16Z^2\alpha r_e^2 k}{3k_p^2} \left[\ln \left(\frac{184k_p}{kZ^{1/3}} \right) + \frac{1}{12} - f(Z\alpha) \right] \quad (101)$$

where $f(Z\alpha)$ is the standard Coulomb correction (Tsai, 1974).

Baier and Katkov considered the case where suppression is very strong and the finite nuclear radius becomes important. This is where Migdal cut off q_{max} by limiting $\xi(s) = 2$. However, Baier and Katkov only consider the small y regime. There, with dielectric suppression taken into account, limiting the maximum momentum transfer to \hbar/R_A changes the form factor for $k < k_p R_A \lambda_e$. This affects the cross section in lead for $y < 2 \times 10^{-6}$. In this region,

$$\frac{d\sigma}{dk} = \frac{16Z^2\alpha r_e^2 k}{3k_p^2} \left(\ln \left(\frac{a}{R_A} \right) - 0.02 \right). \quad (102)$$

For $y = 10^{-6}$ in lead, this is about 25% larger than Eq. (101). This is probably measurable, although transition radiation and backgrounds will be very large.

Baier and Katkov then considered targets with finite thicknesses, breaking down the possibilities in a manner similar to Blankenbecler and Drell, with a similar double integral. For relatively thick targets, $T > l_{f0}$, the results are consistent with Ternovskii (1960), but with additional terms for the Coulomb correction. For $T < l_{f0}$ and strong suppression,

$$\frac{dN}{dk} = \frac{\alpha}{\pi k} \left[\frac{k^2}{E^2} + \left(1 + \frac{(E-k)^2}{E^2} \right) \left(\left(1 + \frac{1}{2A} \right) [\ln(4A) - 0.578] + \frac{1}{2A} - 1 + \frac{0.578}{L_t} \right) \right] \quad (103)$$

where $A = \pi Z^2 \alpha^2 n T / m^2 (L_t + 1 - 2 \times 0.578)$ and $L_t \sim 2 \ln(2a_2 / \lambda_e \rho_t)$, with ρ_t the (scaled) minimum impact parameter that contributes to the form factor integral. Unfortunately, this equation diverges as $T \rightarrow 0$. V. Baier and Katkov (1997b) expanded their treatment to include targets with $T \sim l_{f0}$.

V. Baier and Katkov (1997a) compared their photon spectrum calculation with SLAC E-146 data from a 2% of X_0 thick tungsten target in 25 and 8 GeV electron beams, and find good agreement. However, for a target this thick, there is a substantial (roughly 20%) correction to the photon spectrum to account for electrons that undergo two independent bremsstrahlung emissions. Baier and Katkov do not include this correction, so it is very surprising that their calculations show such a good agreement with data. V. Baier and Katkov (1997b) compare their calculations for a 0.7 % X_0 thick gold targets in 8 and 25 GeV beams with E-146 data, and also find good agreement. Because these targets are much thinner, the multiple interaction probability is greatly reduced and the agreement is much less surprising.

VIII. THEORETICAL CONCLUSIONS

A. Comparison of Different Calculations

The theoretical calculations discussed here used a variety of approaches to solve a very difficult problem. Because the underlying techniques are so different, it is difficult to compare the calculations themselves. However, some general remarks are in order.

All of the post-Migdal calculations are done in the paradigm of a finite thickness slab, integrating both bulk emission and transition radiation. Unfortunately, the finite thickness slab calculations are not easily usable by experimenters. The problem is that they do not allow a single electron to undergo two independent interactions while in the target. This is easily handled with a Monte Carlo simulation. However, these calculations do not localize the photon emission; without localizing the first emission, it isn't possible to know when to start looking for a second one. Because of the edge terms, it isn't correct to simply spread the emission evenly through the slab. So, they can only be compared with data for thin slabs, where the multiple interaction probability is low. However, in this region, the edge terms are comparable to the bulk emission, complicating any comparison.

In some ways, Zakharov's result builds on Migdal; although the basic approach is very different, Zakharov reproduces Migdal's result, and then adds further refinements. Baier and Katkov have a similar approach, and introduce further refinements. The other calculations have very different genealogies. Because the BDMS calculation does not reproduce the Bethe-Heitler limit, it will not be further considered here. For Blankenbecler and Drell, the only obvious point of comparison is the potential; Zakharov (1996b) states that the Blankenbecler and Drell potential does not match the Coulomb potential, and will not show the logarithmic dependence given by the slow variation of $C(\rho)$ or $\xi(s)$.

Another way to compare results is numerically. Unfortunately, these calculations are very complex and the descriptions lack adequate information to repeat the calculations. So, it is necessary to rely on the results given by the authors. One point of comparison is defined by SLAC E-146 data on a thin target: 25 GeV electrons passing through a 0.7 % X_0 thick gold target. The E-146 collaboration showed that Migdal agreed well with the data as long as $T > l_f$; at lower k , Ternovskiis Eq. (53) matched the data. Blankenbecler and Drell, Zakharov, and Baier and Katkov all showed good agreement with this data. Zakharov added in a 7% normalization factor to get total agreement; the other authors do not mention any normalization. Interestingly, the 7% normalization is just about the magnitude change

introduced by the logarithmic $\xi(s)$. Some correction is required, because, even for a 0.7% X_0 target, the multiphoton pileup 'correction' is still several percent. Overall, this demonstrates agreement at this one point to the $\sim 5\%$ level.

Agreement or disagreement under other conditions has yet to be demonstrated. Because of the different logarithmic treatment, Migdal, Blankenbecler and Drell, and Zakharov will also scale slightly differently with energy. Changes depending on target thickness are more complicated; the very surprising agreement found by Baier and Katkov for the 2% of X_0 tungsten data, where multiple interactions are a 20% correction, shows that there are significant uncertainties in scaling the results with target thickness. It would also be very interesting to compare the different new calculations for a lower Z target, where the E-146 data showed some disagreement with Migdal.

B. Very Large Suppression

One weakness of all of these calculations is that they only consider the lowest order diagrams. For fixed y , l_f rises with E , even with LPM suppression. At high enough energies, the formation zones from different emissions will overlap, causing any lowest order calculations to fail. Dielectric suppression is strong enough that l_f decreases and localization improves with increasing suppression, so it is less subject to this problem. However, for multiple scattering, a method of dealing with higher order terms is needed. While the radiative corrections to bremsstrahlung are known (Fomin, 1958), they were not computed with suppression mechanisms in mind.

Even neglecting the overlapping formation zones, when suppression is large, higher order terms are important, because these processes involve larger q_{\parallel} , and hence are less subject to suppression; Sec. II.H illustrated this for direct pair production. So, when suppression is strong ($S \sim \alpha$), current calculations of LPM suppression are suspect. For QCD calculations, discussed in Sec. XII the problem is much worse because of the large coupling constant, α_s .

It is important to note that suppression can affect other processes, via radiative corrections. The total cross section for Coulomb scattering, for example, is the sum of the elastic cross section plus the cross section for bremsstrahlung where the photon is not observable. Since suppression can affect the latter process, it can indirectly change the elastic scattering cross section (Ter-Mikaelian, 1972, pg. 135). Inelastic processes, which leave the target atom in an excited state can also contribute significantly to the cross section when suppression of the lowest order diagrams is large.

C. Classical and Quantum Mechanical Approaches

There has been some controversy as to how well classical electrodynamics can predict LPM suppression. It is important to note that the original Landau and Pomeranchuk (1953a,b) calculations were completely classical; they failed at the same point that classical bremsstrahlung calculation fail: when $k \sim E$. Of course, at least semi-classical calculations are necessary for pair production.

The main advantage of quantum mechanical calculations is that it covers the complete range of y . It is true that newer calculations based on various types of quantum scattering or diffusion equations are more accurate than the classical calculations. However, classical

scattering calculations using diffusion approaches might be made similarly accurate in the $k \ll E$ region. In the future, quantum approaches are necessary to calculate the higher order terms that become important at extremely high energies, when formation lengths from different emissions begin overlapping. Unfortunately, these calculations seem extremely difficult, and are probably a long way off.

However, the classical approach to LPM suppression was not universally accepted. Bell (1958) stated that Migdal's predictions conflicted with classical electrodynamics, and concluded that "any real effect of this kind is of essentially quantal origin." He pointed out that the classical radiation, Eq. (6), is positive definite, and hence monotonically increasing for increasing pathlength. However, Bell neglected to account for the fact that, in a dense solid, the electron trajectory $\mathbf{r}(t)$ changes, and one cannot simply sum the radiation due to interactions with separate nuclei. Even classically, emission from the different pieces of electron pathlength can interfere, in a manner similar to other classical interference effects.

IX. EXPERIMENTAL RESULTS

Bremsstrahlung or pair creation suppression can be studied with high energy electron or photon beams. Because pair creation suppression requires photons with $k > E_{LPM}$, beyond the reach of current accelerators, pair creation has been studied only with cosmic rays, with consequently very limited statistics. The best suppression studies have used electron beams at accelerators. Besides the LPM effect, these beams have been used to study dielectric suppression.

A. Cosmic Ray Experiments

The first tests of LPM suppression came shortly after Migdal's paper appeared. These experiments used high energy ($k > 1$ TeV) photons in cosmic rays, and studied the depth of pair conversion in a dense target. The earliest experiments looked for a deficiency of low energy electrons in electromagnetic cascades (Miesowicz, Stanisiz and Wolther, 1957). This analysis is difficult because of uncertainties in the incoming photon spectrum and electron energy measurement.

Fowler, Perkins and Pinkau (1959) studied isolated pair production in an emulsion stack. They measured the shower energy and the distance between the initial conversion and the first daughter pair resulting from the primary. They observed 47 showers with $k > 1$ TeV. As k increased, the distance between the conversions rose, as predicted by Migdal, contrasting with the decrease predicted by Bethe-Heitler.

Varfolomeev and collaborators (1960) used a similar tack, albeit on a smaller data set, with similar results. They selected events where the energy of the daughter pair was very small ($y \ll 1$), and found qualitative evidence for suppression; they did not differentiate between LPM and dielectric suppression.

Lohrmann (1961), studied emulsion exposed on high altitude balloon flights. He used lower energy photons than earlier groups, with correspondingly better statistics. He used a variety of analyses, all of which supported Migdal's calculations. More recently, long duration balloon experiments have gathered somewhat larger data samples, up to 120 events, with similar results (Strausz *et al.*, 1991).

All of the air shower experiments suffered from some common problems, by far the largest being the poor statistics; high enough energy photons are not common. In addition, because of the limited emulsion thickness, they did not consider surface effects. Finally, uncertainties in the photon spectrum complicated the analysis. For these reasons, these experiments are at best qualitative verifications of LPM suppression.

B. Early Accelerator Experiments

By the 1970's, 40 GeV electron beams were available at Serpukhov, and the first accelerator based test of LPM suppression was done there (Varfolomeev *et al.*, 1975). Bremsstrahlung photons from 40 GeV electron beams hitting dense targets were detected in an sodium iodide calorimeter. The electrons were magnetically bent away from the calorimeter. Photons with $20 \text{ MeV} < k < 70 \text{ MeV}$ emitted from carbon, aluminum, lead and tungsten targets were studied. Below 20 MeV, synchrotron radiation from the bending magnets dominated the measurement, while above 70 MeV, the experiment was insensitive to the spectral change predicted by Migdal.

The experiment suffered from several limitations. Because the electron beamline was in air, and included several scintillation counters used as triggers, there was a significant light element bremsstrahlung background. The experimenters also mention a significant background due to muon contamination in their beam.

The collaboration presented their data in terms of ratios of photon spectra: lead/aluminum and tungsten/carbon. This may have been done to account for events containing several bremsstrahlung photons from a single electron. The results agreed with Migdal.

CERN NA-43 was an experiment dedicated to studying channeling radiation from electrons and positrons in crystals (Bak *et al.*, 1988). In channeling, electrons or positrons travel along the crystal rows, and hence are strongly affected by the coherently adding fields from the atom rows. At large angles to the axes, the coherence disappears, and normal bremsstrahlung occurs. In this large angle regime, they saw suppression which they attributed to LPM suppression. They also observed suppression consistent with multiple scattering for electrons incident along one of the crystal rows. This is slightly different from suppression in an amorphous material; here the suppression is really the loss of coherent enhancement.

The first experimental studies of dielectric suppression were part of a larger study of transition radiation (Arutyunyan, Nazaryan and Frangyan, 1971). Although the experiment focused on studies of emission from stacks of thin radiators, the experimenters also measured the radiation from 0.25 and 2.8 GeV electrons traversing relatively thick glass and aluminum targets. Although few details were given, they appeared to observe suppression in the region where it was expected.

C. SLAC E-146

In 1992, the E-146 collaboration at Stanford Linear Accelerator Center (SLAC) proposed an experiment to perform a precision measurement of LPM suppression, and to study dielectric suppression. (Cavalli-Sforza *et al.*, 1992). The experimental setup was conceptually

similar to the Serpukhov experiment, but heavily optimized to minimize background. The experimenters collected a very large data set. The experiment was approved in December, 1992, and took data in March-April, 1993.

1. Experimental Setup

Figure 15 shows a diagram of the experiment. An 8 or 25 GeV electron beam entered SLAC End Station A and passed through a thin target. The targets used are listed in Table III. The beam was then bent downward by a 3.25 T-m dipole magnet, through six wire chamber planes which measured its momentum and into an array of lead glass blocks which accurately counted electrons. Produced photons continued downstream 50 meters into a BGO calorimeter array. To minimize backgrounds, the electron path visible to the calorimeter and the photon flight path were kept in vacuum.

TABLE III. The targets used in SLAC E-146. These k_{LPM} values are half those used by the E-146 collaboration.

Target Material	Thickness (X_0)	k_{LPM} (25 GeV)	k_{LPM} (8 GeV)
Carbon	2%, 6%	4.3	0.4
Aluminum	3%, 6%	7.8	0.8
Iron	3%, 6%	48	4.8
Tungsten	2%, 6%	236	24
Gold	0.07%, 0.7%, 6%	250	26
Lead	2%	148	15
Uranium	3%, 5%	236	24
Blank	-		

The calorimeter comprised 45 BGO crystals in a 7 by 7 array with missing corners; each crystal was 2 cm square by 20 cm ($18 X_0$) deep. This segmentation provided excellent spatial resolution for separating synchrotron radiation from bremsstrahlung photons. Scintillation light from each crystal was measured separately by a photomultiplier tube (PMT). The light yield was about 1 detected photoelectron per 30 keV, providing good light output down to 200 keV. The resolution was about 8% (FWHM) at 100 MeV, with a nonlinearity of about 3%. The temperature was monitored throughout the experiment, and the data corrected using the measured drifts.

The collaboration used several methods to calibrate the calorimeter, to obtain both an absolute energy calibration and a crystal to crystal intercalibration. The primary tools for

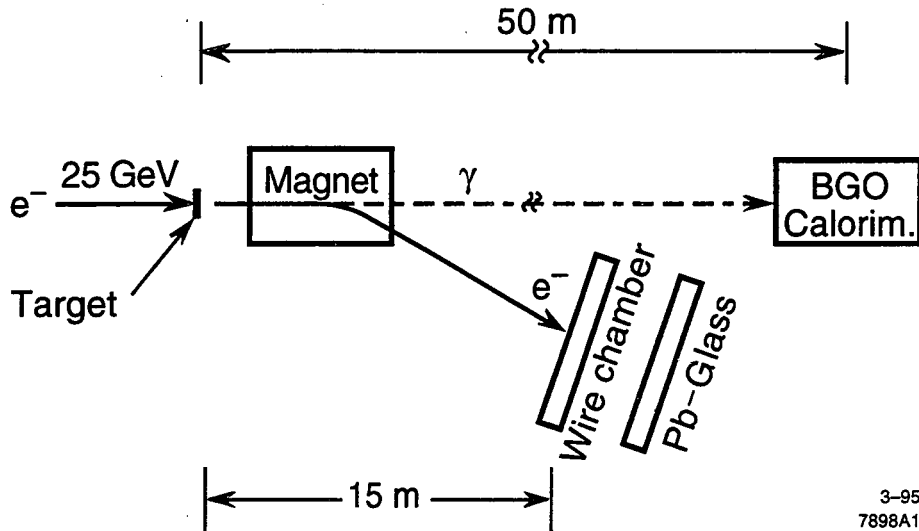


FIG. 15. Diagram of the SLAC-E-146 apparatus. From Anthony *et al.* (1995).

measuring the relative gain were nearly vertical cosmic-ray muons, selected by a plastic scintillator paddle trigger; the gain in each crystal channel was adjusted to produce equal signals.

The absolute energy scale of the calorimeter was primarily determined by putting the calorimeter in a 500 MeV electron beam. This calibration was checked by comparing the electron energy loss, measured by the wire chamber, with the calorimeter energy measurement. Because of the steeply falling photon spectrum and the non-Gaussian errors in the momentum measurement, this was useful only as a cross-check.

Because of the large bremsstrahlung cross section, the experiment required a beam intensity of about 1 electron per pulse. Because it would have been very uneconomical to use the SLAC linac to produce a single electron per pulse, the collaboration developed a method to run parasitically during SLAC linear collider (SLC) operations, by using the off-axis electrons and positrons that are removed from the beam by scrapers in the beam switchyard (Cavalli-Sforza *et al.*, 1994).

Normally, about 10% of the SLC beam is scraped away by collimators in the last 200 meters of the linac. The collimators are only $2.2 X_0$ thick, so a usable flux of high energy photons emerged from their back and sides. Some of these photons travel down the beampipe, past the magnets that bend the electrons and positrons into the SLC arcs, and into the beam switchyard, where a $0.7 X_0$ target converted them into e^+e^- pairs. Some of the produced electrons were captured by the transport line optics, collimated, selected for energy, and transported into the end station.

The beam worked well, with the size, divergence and yield matching simulations. At 8 and 25 GeV, the beam intensity was adjustable up to about 100 electrons/pulse. At 1 electron/pulse, the beam emittance was limited by the optics, with a typical momentum bite of $\Delta p/p < 0.5\%$. The beam optics were adjusted to minimize the photon spot size at the calorimeter; spot sizes there were typically a few mm in diameter. The beam spot was stable enough and small enough that beam motion was not a major source of error.

Data was collected and written to tape on every beam pulse (120 Hz). With the beam

intensity averaging 1 electron/pulse, over 500,000 single electron events could be collected per eight hour shift. The experiment ran for a month, and good statistics were obtained with a variety of targets.

2. Data Analysis and Results

The E-146 analysis selected events containing a single electron, as counted by the lead glass blocks. The photon energy was found by summing the energies of hit BGO crystals using a cluster-finding algorithm. The cluster finding reduced the noise level by eliminating random noise hits.

The experiment studied the photon energy range from 200 keV to 500 MeV, a 2500:1 dynamic range. This exceeded the linear dynamic range of the PMTs and electronics, so data was taken with two different PMT gains, varied by changing the PMT high voltage. The high- k running corresponded to 1 ADC count per 100 keV and the low- k running was 1 ADC count per 13 keV, with the relative gains calibrated with the cosmic ray data. The high- k data was used for $5 \text{ MeV} < k < 500 \text{ MeV}$ while the low- k data covered $200 \text{ keV} < k < 20 \text{ MeV}$, with a weighted average used in the overlap region.

These two sets of data differed in several significant ways. There were large differences in calorimeter behavior and background levels, as well as the physics topics. Above photon energies of several MeV, photons largely lost energy by pair conversion, producing an electromagnetic shower. Showers typically deposited energy in a few to 20 crystals in the calorimeter. At lower energies, the photons typically lost energy by single or multiple Compton scattering. Usually, Compton scattering deposited energy in a single calorimeter crystal. Sometimes, the photon Compton scattered once and then escaped from the calorimeter, taking some energy with it. This produced a low energy tail to the energy deposition curve. While the high- k data had very low backgrounds, the low- k data had significant backgrounds due to synchrotron radiation, at least for the 25 GeV beams. Finally, the two data sets emphasize different physics, with the high- k data most relevant for LPM suppression, with the low- k data more useful for studying dielectric suppression. For these reasons, the two sets of data were analyzed quite independently, and combined in the final histograms.

3. Backgrounds and Monte Carlo

One advance introduced by E-146 was the use of a detailed, high statistics Monte Carlo. The main purpose of the Monte Carlo was to understand multi-photon pileup. This occurred when a single electron passing through the target interacted twice, radiating two photons. The Monte Carlo also simulated photon absorption in the target (Anthony *et al.*, 1997) and modelled the detector. Transition radiation was considered an integral part of the physics, rather than a background. In addition to conventional transition radiation, the predictions of Ternovskii and Pafomov were included as options.

The Monte Carlo tracked electrons through the material in small steps, allowing for the possibility of bremsstrahlung in the material and transition radiation at each edge. LPM suppression was implemented using simple formulae (Stanev *et al.*, 1982) with dielectric suppression incorporated following Migdal(1956). For consistency, the Bethe-Heitler cross

sections were included by turning LPM suppression off from Migdals formulae, rather than using newer calculations.

The expected and measured backgrounds were both small. The major background was synchrotron radiation from the spectrometer magnet. Synchrotron radiation was significant for $k < 1$ MeV in the 25 GeV data. Because the magnet bent the beam downward, the synchrotron radiation painted a stripe in the calorimeter, extending downward from the center. Because of the large lever arm, and because the bending started in the fringe field of the magnet, where the field was low, the synchrotron radiation was small near the center of the calorimeter. Because of the good spatial resolution of the calorimeter, most of the synchrotron radiation was removed with a cut on the photon position in the calorimeter; photons within 45° of a line downward from the calorimeter midpoint were removed; this cut removed most of the synchrotron radiation, along with 25% of the signal.

Non-target related backgrounds were measured with target empty runs. The backgrounds were typically 0.001 photons with $k > 200$ keV per electron, much less than the $\sim 10T/X_0$ bremsstrahlung photons with $k > 200$ keV per electron. Target related backgrounds were expected to be small; photonuclear interaction rates are small, and the events are unlikely to appear in the E-146 analysis.

4. Results

Because of the high statistics and low background, the E-146 data allowed for detailed tests of the theory; photon spectra could be easily compared with different predictions.

Figures 16-20 show a sampling of E-146 results. Photon energies were histogrammed logarithmically, using 25 bins per decade of energy, so that each bin had a fractional width $\Delta k \sim 10\%k$. The logarithmic scale is needed to cover the 2500:1 energy range. The logarithmic binning was chosen so that a $1/k$ Bethe-Heitler (BH) spectrum will have an equal number of events in each bin, simplifying the statistical analysis.

Figure 16 shows the photon spectrum (points with error bars) from 8 and 25 GeV electrons passing through 2% and 6% X_0 carbon targets. Also shown are 3 Monte Carlo (MC) curves. The top curve (dashed line) is from a simulation of BH bremsstrahlung plus conventional transition radiation; the transition radiation is substantial below k_p , 1.4 (0.4) MeV at 25 (8) GeV. Above k_p , the spectrum is sloped because there is a finite probability of a single electron interacting twice while passing through the target. Because the calorimeter cannot separate single photons from multiple hits, but instead measures total energy deposition, this depletes the low energy end of the spectrum (shown here), while increasing the number of calorimeter overflows. In the absence of multiple interactions, the Bethe-Heitler spectrum would be flat at $(1/X_0)dN/d(\log k) = 4/3 \ln(k_{max}/k_{min}) = 0.129$ for bins with logarithmic widths $k_{max}/k_{min} = 10^{1/25} = 1.096$.

The dotted line is from a MC simulation that includes LPM suppression, but not dielectric suppression, plus conventional transition radiation. The solid line is from a simulation that includes LPM and dielectric suppression, along with conventional transition radiation. This curve was adopted by E-146 as their standard curve.

Both suppression mechanisms are required to approach the data. However, there are still significant discrepancies between the LPM plus dielectric MC and the data. Below 800 keV (350 keV) for 25 (8) GeV beams, the upturn in the data may be residual background,

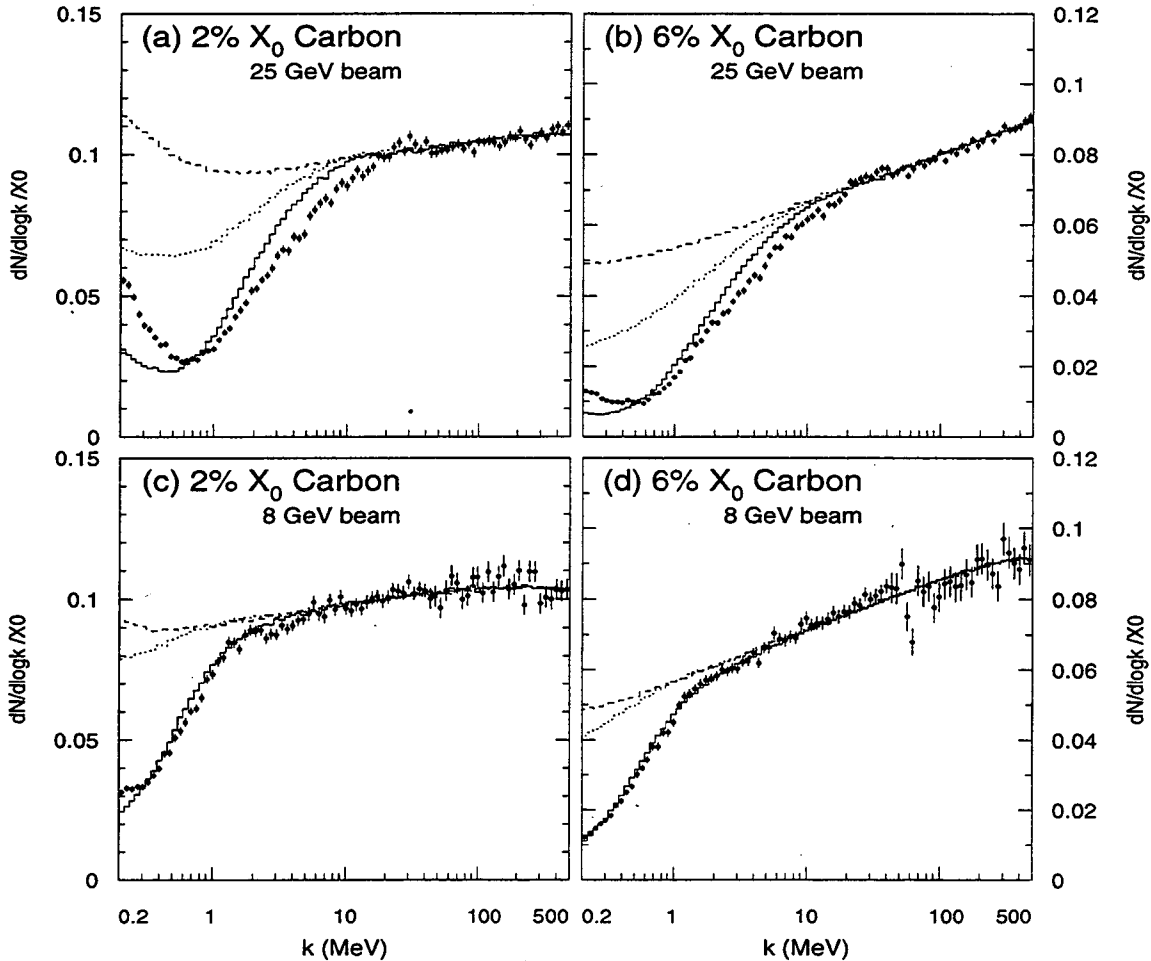


FIG. 16. Comparison of data from SLAC-E-146 with MC predictions for 200 keV to 500 MeV photons from 8 and 25 GeV electrons passing through 2% and 6% X_0 carbon targets. The cross sections are given as $dN/d(\log k)/X_0$ where N is the number of events per photon energy bin per incident electron, for (a) 2% X_0 carbon and (b) 6% X_0 carbon targets in 25 GeV electron beams, while (c) shows the 2% X_0 carbon and (d) the 6% X_0 carbon target in an 8 GeV beam. Three Monte Carlo curves are shown. The solid line includes LPM and dielectric suppression of bremsstrahlung, plus conventional transition radiation. Also shown are the Bethe-Heitler plus transition radiation MC (dashed line) and LPM suppression only plus transition radiation (dotted line). Adapted from Anthony *et al.* (1997).

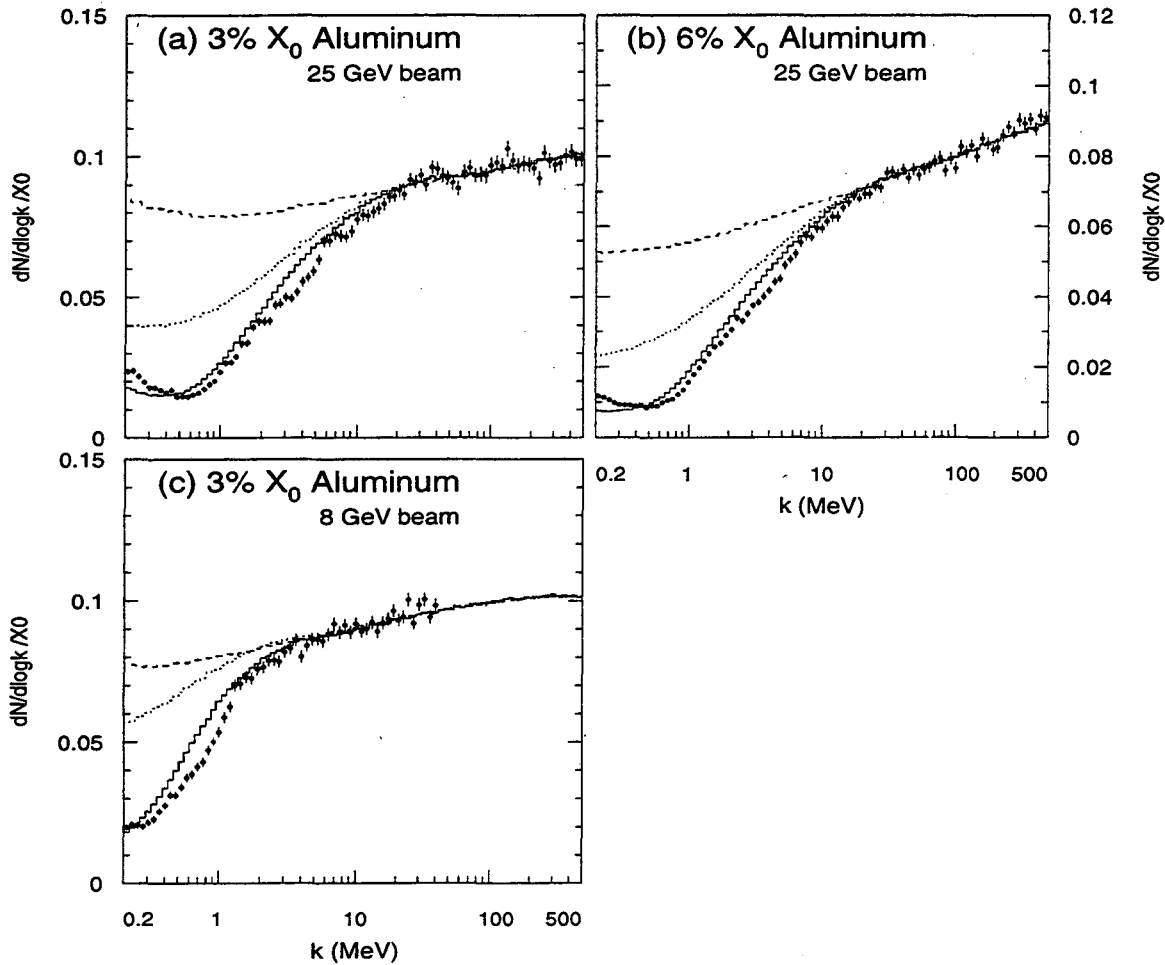


FIG. 17. Comparison of data from SLAC-E-146 with Monte Carlo predictions for 200 keV to 500 MeV photons from 8 and 25 GeV electrons passing through 3% and 6% X_0 aluminum targets. The format and Monte Carlo curves are the same as in Fig. 16. Adapted from Anthony *et al.* (1997).

especially synchrotron radiation. The difference at higher photon energies is more complex, and will be discussed in the following subsection.

Figure 17 shows the spectrum from 8 and 25 GeV electrons passing through 3% and 6% X_0 aluminum targets. The same three MC simulation curves are shown. Because aluminum has twice the Z of carbon, LPM suppression is considerably enhanced, with k_{LPMs} of 8 MeV and 800 keV at 25 and 8 GeV respectively. Because the density is similar, dielectric suppression is similar. Because dielectric suppression has a faster suppression, and hence dominates at low energies, the curve for both suppressions is similar to that of carbon. The agreement between the data and the standard curve is much better than with carbon.

Figure 18 shows the spectrum from 8 and 25 GeV electrons passing through 3% and 6% X_0 iron targets, with just the 'standard' Monte Carlo curve. The general slope of the data matches the simulation, but the behavior at higher k for 25 GeV beams is quite different.

Figure 19 shows the bremsstrahlung spectra in uranium targets. Uranium is dense enough that LPM suppression is dominant, and the E-146 collaboration compared simulations with dielectric and LPM suppression, plus conventional transition radiation (TR), or the cal-

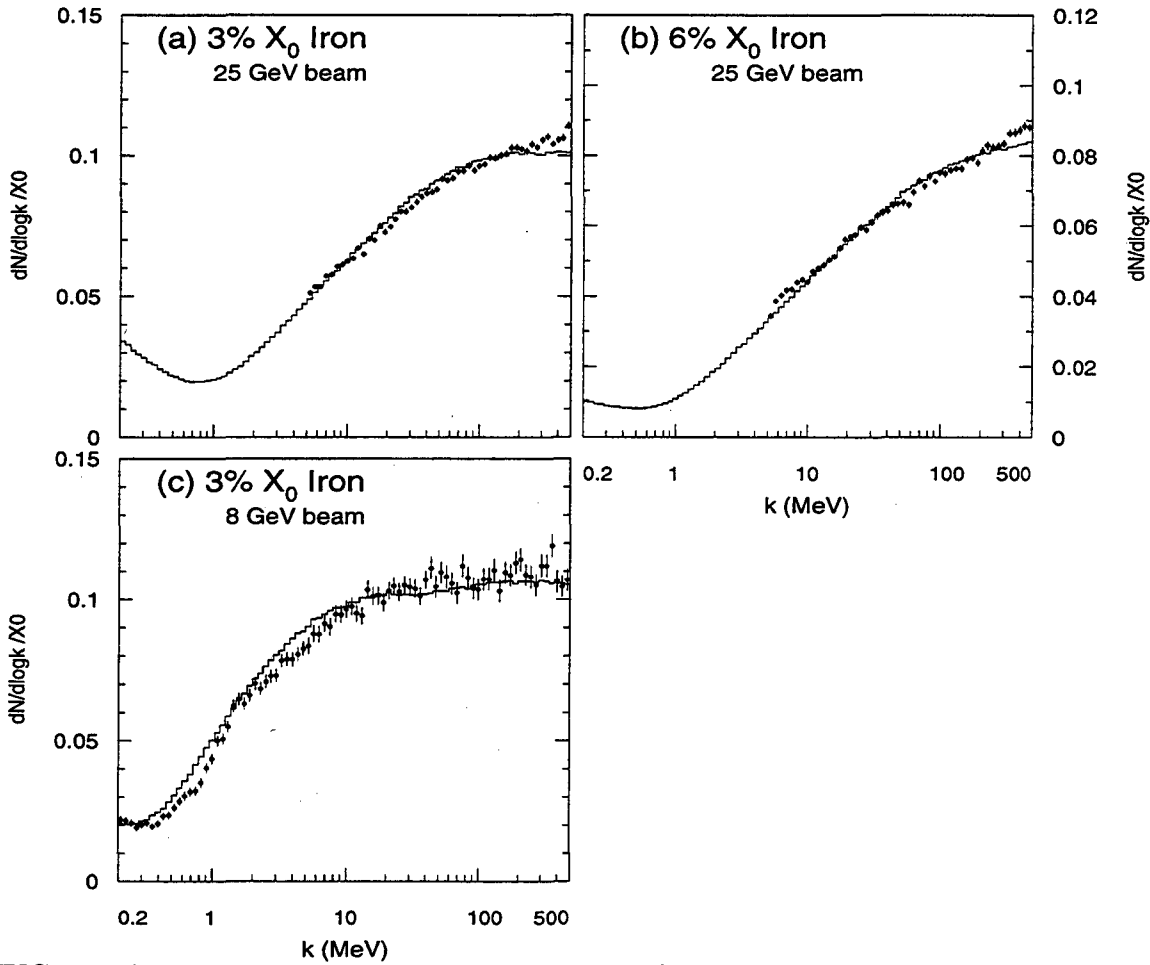


FIG. 18. SLAC-E-146 measurements and Monte Carlo predictions for 8 and 25 GeV electrons passing through a 3% and 6% X_0 iron targets. The Monte Carlo curve is based on LPM and dielectric suppression, plus conventional transition radiation. Adapted from Anthony *et al.* (1997); Panel (c) is mislabelled as 6% X_0 there.

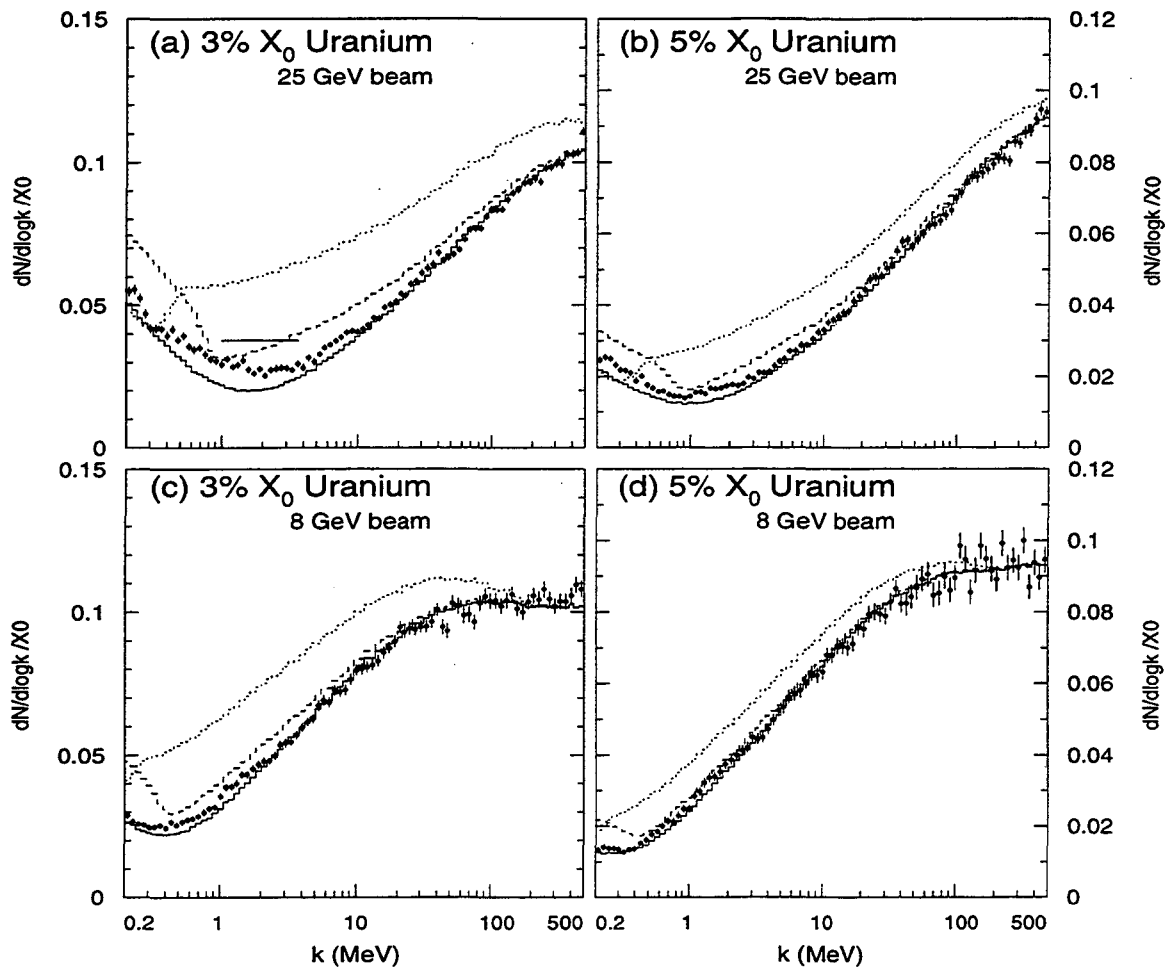


FIG. 19. SLAC E-146 measurements and Monte Carlo for 3% X_0 and 5% X_0 uranium targets in 8 and 25 GeV electron beams. The solid line shows the LPM and dielectric suppression, conventional transition radiation Monte Carlo prediction. The other lines include simulations based on calculations of transition radiation due to Pafomov (dashed line) and Ternovskii (dotted line), Eq. (88), with $\chi = 1$. The flat solid line in panel (a) is a calculation based on Eq. (53). Adapted from Anthony *et al.* (1997).

culations of Ternovskii (1960) or Pafomov (1964) of transition radiation due to multiple scattering.

The Pafomov curve shows a jump around 800 keV (400 keV) at 25 (8) GeV, corresponding to $k = k_p^{4/3}/k_{LPM}^{1/3}$, with the jump corresponding from the switch from Eq. (89) to a smooth numerical approximation, given by Pafomov for Eqs. (90) and (91). Below the jump, Pafomov is considerably above the data and the conventional TR curve. Above the jump, the curve shows a reasonable trend, but the TR appears to be several times too high.

The Ternovskii curve also shows a jump, at about 500 keV (below 200 keV) for the 25 (8) GeV data, corresponding to $sk_p^2/k^2 = 1$. Below the jump, Ternovskii matches conventional TR. Above it, Ternovskii is quite far above the data. Moreover, it extends to too high an energy, above k_{LPM} . The Ternovskii radiation could be brought down by reducing χ below 1 in Eq. (88). However, a considerable adjustment would be required.

Figure 20 shows the spectrum from 8 and 25 GeV electrons passing through a 0.7%

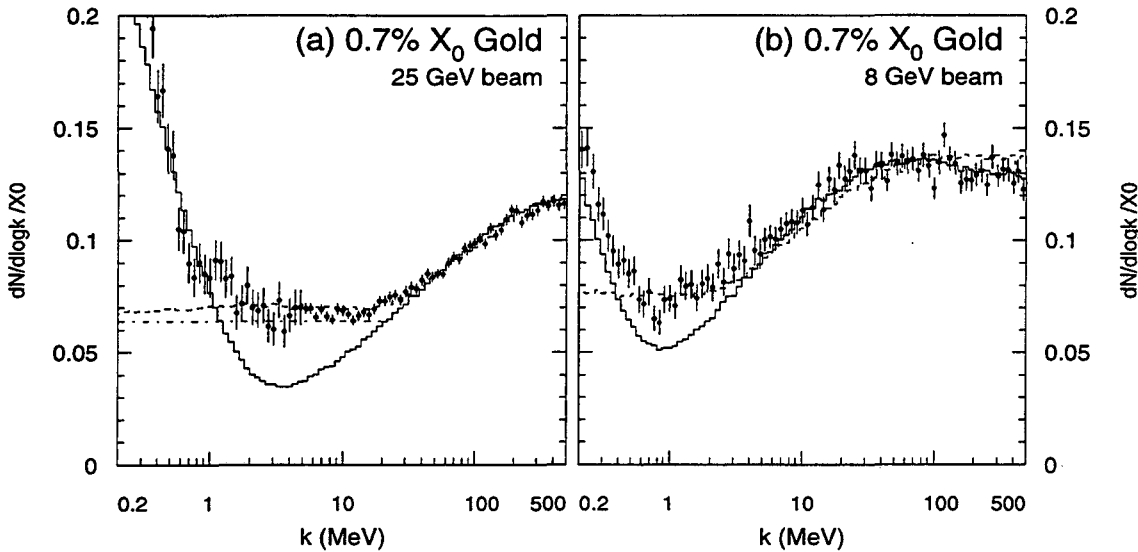


FIG. 20. SLAC E-146 data on 8 and 25 GeV electrons hitting a 0.7% X_0 gold target. Shown are calculations by Blankenbecler and Drell (dashed line), and Shulga and Fomin (dot-dashed line). For comparison, the Migdal MC is shown as the usual solid line. Adapted from Anthony *et al.* (1997).

gold target, with the standard curve is shown by the solid line. This target is especially interesting because, at 25 GeV, for $k < 7$ MeV, $T < l_{f0}$. Including LPM suppression, $T < l_f$ for $k < 3$ MeV. In this kinematic region, the target should interact as a single unit, and the BH $1/k$ spectrum should be recovered, albeit at a reduced intensity. The solid line shows a calculation based on Eq. (53), in good agreement with the flattening observed in the data. For the E-146 2% X_0 lead (not shown here) and 3% X_0 uranium 25 GeV data, Eq. (53) is also applicable, but only for a very limited range of k . However, as Fig. 19 shows, for 3% X_0 uranium, Eq. (53) predicts $dN/d(\log k) = 0.038$ for $1.0 \text{ MeV} < k < 3.7 \text{ MeV}$, considerably above the data. The lead data shows a similar discrepancy. Of course, these discrepancies may be because the equation does not apply so close to $T = l_f$.

Fig. 20 also shows the results of a calculation by Blankenbecler and Drell. Neither prediction has been corrected for multiple interactions in the target or detector resolution. Because neither calculation includes dielectric suppression or transition radiation, they fail for $k < k_p$.

Fig. 21 shows the spectrum from 8 and 25 GeV electrons hitting a 0.07% X_0 target. This target is only about $1.2 \times (X_0/1720)$ thick, so that multiple scattering should produce little suppression, and the Bethe-Heitler simulation (dashed histogram) should be a good match to the data. Dielectric suppression should also be small, because the total phase shift throughout the target, $\hbar\omega_p^2 T/k^2 l_f$, is small for $k > 500$ keV. Transition radiation should also be strongly suppressed, by $(T/l_f)^2$. Without this suppression, transition radiation would completely dominate the data. As expected, the 25 GeV electron data matches the Bethe-Heitler spectrum. However, the 8 GeV data drops off for $k < 2$ MeV. For comparison, a dielectric suppression only Monte Carlo simulation is shown. The data is considerably above this curve.

Blankenbecler and Drell (Blankenbecler, 1997c) predict that, at 25 GeV, emission is

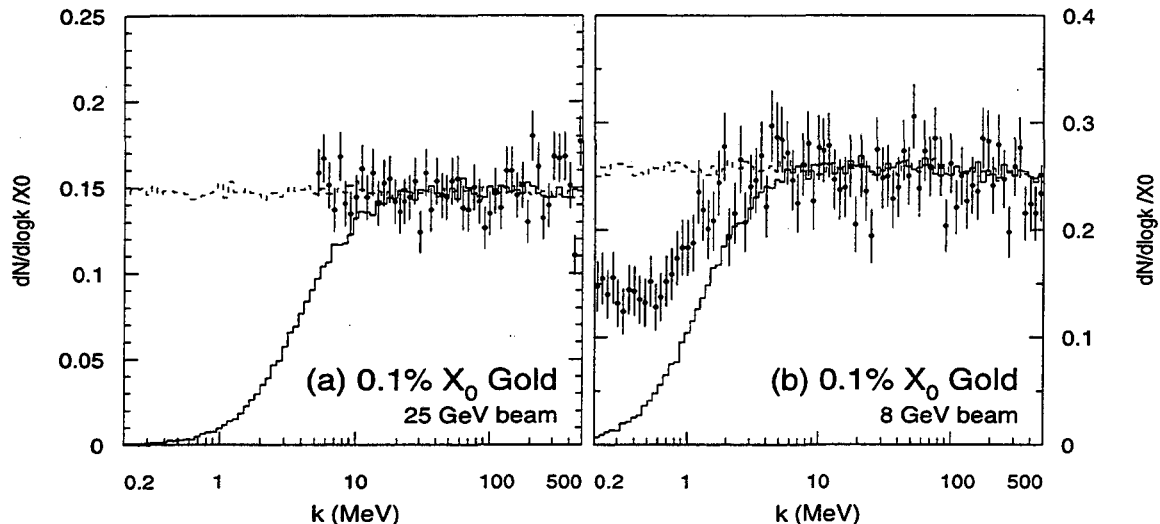


FIG. 21. Measurements and Monte Carlo for a 0.1% X_0 gold target at (a) 25 GeV and (b) 8 GeV. The dashed line is the BH prediction (no suppression), while the solid line is a Monte Carlo which includes dielectric suppression, but not LPM suppression. Because the very thin target should exhibit little transition radiation, no transition radiation is included in these Monte Carlos. From Anthony *et al.* (1997).

suppressed by 10% compared to BH for $k=500$ MeV, rising to 13% at $k=100$ MeV. At 8 GeV, the difference is only a few percent. Unfortunately, these predictions differ from Bethe-Heitler by less than the experimental errors.

For a target this thin, the collaboration has noted that the signal is very small and the potential backgrounds are large. Furthermore, the target thickness and overall normalization between the signal and simulations cannot be well determined.

In all of these plots, the Monte Carlo curves were normalized to the data by multiplication by a constant adjustment, chosen so the MC best matches the data above 20 MeV (2 MeV) at 25 (8) GeV. The low point for the normalization was chosen to avoid thin target corrections for $T < l_{f0}$, backgrounds and transition radiation; for the 0.7% X_0 target, higher limits were chosen, 30 (10) MeV at 25 (8) GeV. Overall, the standard Monte Carlo curves had to be increased by an average of 5% (2σ) to match the data. This discrepancy would likely disappear with an input cross section where the onset of suppression was more gradual around $k \sim k_{LPM}$.

The errors shown on the plots are statistical only. The E-146 collaboration has carefully studied the systematic errors on these measurements. The point-to-point systematic errors vary slowly with k and correspond to a 4.6% uncertainty for $k > 5$ MeV. Below 5 MeV, the systematic errors rise to 9%, because of increased uncertainties in photon energy cluster finding as Compton scattering takes over from showering as the dominant energy loss. The systematic error on the normalization was determined separately; it is $\pm 3.5\%$.

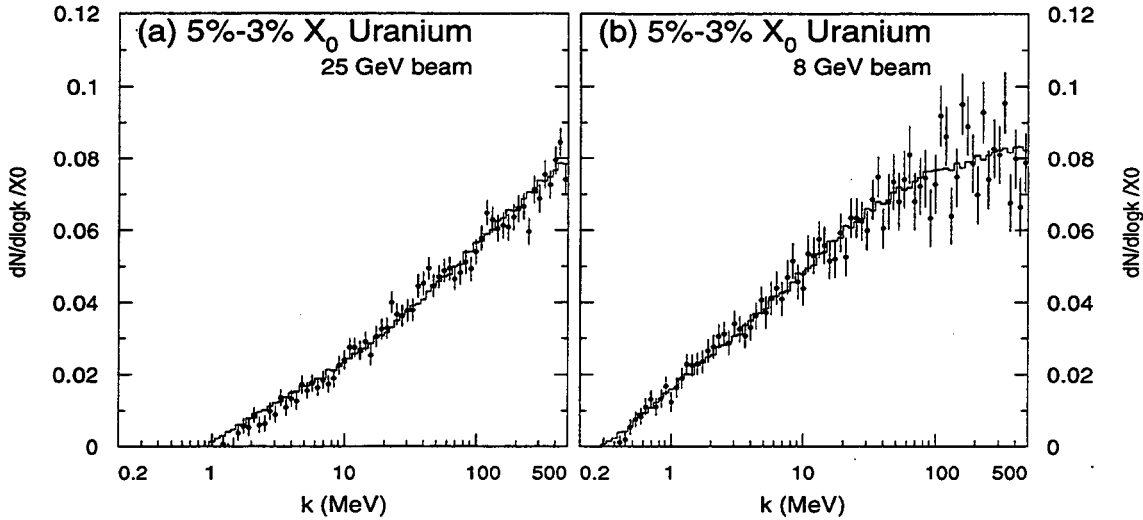


FIG. 22. Bin by bin subtraction of the 3% X_0 uranium data from the 5% X_0 data by SLAC E-146, for 25 and 8 GeV beams. The solid line is the result when the same procedure was applied to their standard Monte Carlo. From Anthony *et al.* (1997).

D. Subtracted Spectra, Bulk and Surface Effects

Although the data clearly demonstrates LPM and dielectric suppression, the data from the thinnest targets shows that there is significant excess photon emission over the bulk LPM predictions. This can easily be ascribed to surface radiation. As long as interference between the two target edges is negligible, the surface and bulk effects can be separated in a model independent way by subtracting spectra from targets made of the same material, but different thicknesses.

Figure 22 shows the results of this subtraction for uranium. The subtracted data and simulations agree much better than the unsubtracted spectra in Fig. 19. Because the subtraction exacerbates the effects multiple interactions in the target, it is necessary to compare the subtracted spectra with similarly treated simulations. For all of the E-146 targets, the subtracted spectra and simulations agree more closely than the unsubtracted spectra, and, for most targets, the agreement is within the statistical and systematic errors. The notable exceptions are the 25 GeV data on the iron and carbon targets,

The improved agreement indicates that the discrepancies in the unsubtracted spectra are due to surface effects. For the denser targets, this is easily explained by transition radiation. However, for the lighter carbon and iron targets, the unsubtracted data indicates more suppression than expected. This is extremely difficult to explain as a surface effect.

The collaboration (Anthony *et al.*, 1997) considered a few explanations for the discrepancies. For carbon, the increased suppression could be due to the crystalline structure of the pyrolytic graphite target. If the target density profile varied, then the higher density regions would show more suppression, and the aggregate would show somewhat higher LPM and dielectric suppression. For iron, magnetization of individual domains could produce some magnetic suppression. Unfortunately, the details depend on the (unknown) domain structure.

The density profile could also vary if the target surfaces were oxidized. For the 2% X_0 tungsten target, the collaboration saw some evidence for this; thickness measurements based on weighing (giving results in g/cm^2) were lower than those obtained with calipers; an oxide layer could explain this. The anomalous normalization on the 2% tungsten target could also be explained by an oxide layer. For the lighter targets, a surface layer could explain the shapes of the curves, but the required thickness seems very unrealistic, and, in any case, such a layer is not supported by the normalization and thickness measurements.

The collaboration considered modifying the subtraction process to measure the transition radiation spectrum due to a single surface. However, the errors are slightly too large for the result to be interesting. Moreover, for the carbon and iron targets, the results would be negative over a large fraction of the spectrum.

A number of the newer theoretical results have pointed to another possibility: the failure of the Migdal theory at the few percent level. Zakharov (1996b) and Baier and Katkov (1997) showed quite good agreement with the densest E-146 targets. Unfortunately, neither group considered the lighter targets. However, a calculation with appropriate form factors for nuclear and electronic interactions might fit low Z data well.

X. LPM EFFECT IN PLASMAS

So far, we have considered the LPM effect for a particle moving through a medium. However, in many cases the particle and medium cannot be distinguished. Instead, the incident particle and the target are both moving, and must be treated on an even footing. If the medium is sufficiently dense, there can be suppression even for non-relativistic particles. In this case, it is useful to consider the formation time t_f instead of the formation length. If t_f is longer than the mean time between collisions $t_c = 1/\Gamma$, Γ being the collision rate, then emission can be suppressed.

One example of a hadronic plasma is a supernova; with the high temperature and density, t_c is very short. For reactions with $t_f > t_c$, suppression may be present. One interesting reaction is the production of right handed neutrinos or axions through $NN \rightarrow NN\nu\bar{\nu}$, $nn \rightarrow npe\bar{\nu}_e$ and $NN \rightarrow NN a$. If these hypothetical particles exist and are produced, they will carry energy away from the explosion, increasing the cooling rate. The measured cooling rate had been used to put limits on these particles. However, Raffelt and Seckel (1991) showed that the high interaction rate can suppress the axion and neutrino production rates, weakening the existing limits.

For axions or neutrinos, $t_f = \hbar/\Sigma E$, where ΣE is the sum of the neutrino energies or the axion energy. When $t_c \ll t_f$, then 'free' collisions are rare. Instead, the interacting nucleons are excited, This can be modelled by giving the nucleon an effective mass, as may be done with photons in dielectric suppression. Two complications come from the possibility of back reactions, and from the degeneracy of the incoming particles. The suppression is the ratio of the emission $Q(\Gamma)$ to $Q(\Gamma = 0)$:

$$S = \frac{t_f}{t_{f0}} = \left\langle \frac{\Sigma E^{n+2}}{\Sigma E^2 + \Gamma^2/4} \right\rangle \left\langle \frac{1}{\Sigma E^n} \right\rangle. \quad (104)$$

Here, n accounts for the multiplicity of the emitted particles, with $n = 2$ for axions and $n = 4$ for neutrino pairs; for axions this equation matches Eq. (41). Because Γ depends

on the local density; finding the overall suppression factor for an entire supernova requires detailed modelling. However, Raffelt and Seckel estimate that S could be as small as 0.1.

The general solution for a non-equilibrium electromagnetic plasma has been elegantly formulated using non-equilibrium quantum field theory (Knoll and Voskresensky, 1995, 1996). By careful classification of diagrams, and appropriate resummation, Knoll and Voskresensky avoided infrared divergences, and reproduced both the classical (non-suppressed) and quasi-particle (low density) limits by appropriate choice of subsets of graphs. In a dense plasma, the quasi-free scattering approximation breaks down, and the reaction rate is reduced by

$$S = \frac{k^2}{k^2 + \Gamma^2}. \quad (105)$$

This equation also matches Eq. (41), with $\gamma\omega_p$ of the medium replaced by Γ , the relaxation rate of the source.

A plasma like this might surround a quantum black hole. Before a quantum black hole explodes, it emits a huge flux of charged particles. This radiation forms a nearly thermal photosphere, consisting of electrons, positrons and photons (Heckler, 1995). The charged particle emission rate and consequent density is high enough that bremsstrahlung and pair production should be suppressed in this plasma. Since most of the emitted particles are hadrons, the black hole may also generate a dense color plasma, akin to a quark gluon plasma, with interactions suppressed as discussed in the following section.

Similar plasma effects probably occurred during the big bang. Unfortunately, we do not know of any calculations involving it.

XI. ELECTROMAGNETIC SHOWERS

Although the LPM effect is best studied using single interactions in thin targets, most real world situations involve thicker targets and consequent electromagnetic showers. Suppression can be important in both natural processes like cosmic ray air showers and neutrino induced electromagnetic showers, and in man-made detectors. Although shower development with the LPM or other suppression effects can only be modelled with complex analytic calculations or Monte Carlo simulations, this section will present some simple calculations that show when suppression effects can be important.

Suppression affects showers in several ways. Besides the obvious elongation when $E > E_{LPM}$ and the radiation length increases, the shower changes form, with the low energy 'fuzz' disappearing, and shower to shower fluctuations become much more important, because the number of interactions drops greatly.

A. Natural Showers

Many calculations have concerned high energy shower development in water or ice, an area relevant to high energy neutrino astronomy, or in air, an application motivated by extremely high energy (EHE) cosmic ray air showers. The latter case is complicated because the air density varies exponentially with altitude.

Water and ice showers are of interest for detecting very high energy astrophysical ν_e through resonant W production, $\nu_e e \rightarrow W \rightarrow e \nu_e$ and similar reactions. This cross section rises rapidly at the W pole, corresponding to a ν_e initial energy of 6.4 PeV, an average of 2.1 PeV of which goes to the outgoing electron. Since $2.1 \text{ PeV} \sim 7E_{LPM}$, LPM suppression is significant. As Fig. 2 shows, at this energy, the electron radiation length is increased by about 35%. This is also above the threshold E_p for suppression due to pair creation.

At similar energies, the search for $\nu_\tau N \rightarrow \tau N \rightarrow e \nu_\tau \bar{\nu}_e N$ events (Learned and Pakvasa, 1995) in ice requires being able to distinguish the τ track from the beginning of an electron shower; because various suppression mechanisms greatly reduce the number of low energy bremsstrahlung photons, this separation becomes much more difficult.

Because both applications involve very high energy showers, direct simulations have been limited by the available computer power; until recently at least partially analytic calculations were needed. These analytic methods owe much of their history to earlier analytic calculations of Bethe-Heitler shower development.

Misaki (1990) used the matrix method to show that EM showers above 10^{15} eV in water are elongated due to the LPM effect. In the tails of the shower, at a given sampling depth, the density is about a factor of 3 higher with the LPM effect than without. This result is typical of the analytic calculations.

Unfortunately, while the analytic calculations can predict the average shower shape, they have limited value for studying shower to shower variations; for this, simulations are needed. To reduce the computing load, hybrid Monte Carlos are often used. A hybrid MC simulates the initial shower development; shower tails are added on based on a library of simulated complete showers. This reduces the computational requirements significantly. Stanev and collaborators (1982) used a hybrid MC to show that the LPM effect elongates showers.

Konishi *et al.* (1991) used a hybrid MC to study fluctuations in showers. He simulated 10^{17} eV showers in lead, where LPM suppression is very strong. In contrast to BH showers, LPM showers showed large shower to shower variations. By eliminating soft bremsstrahlung, the LPM effect greatly reduces the number of interactions per radiation length, so the shower development depends on far fewer interactions, greatly increasing the shower to shower variation. The variation makes shower energy measurement more difficult, especially for a detector with limited sampling. Misaki (1993), quantified the fluctuations, measuring the distribution of the depth of shower maximum, the depth at which the number of shower particles is a maximum. For a 10^{17} eV shower in rock ($E_{LPM} = 77 \text{ TeV}$), he found that shower maximum occurs at 18 ± 13 (FWHM) X_0 for BH showers, compared with 152 ± 176 X_0 for LPM showers. Not only is the maximum deeper, but its position varies much more.

Not considered here is the increased angular spreading caused by suppression. Although it may be not affect the general shower shape, it is probably important in understanding radio waves produced by showers in ice (Zas, 1997), where the spectrum depends on the transverse separation between particles.

B. Cosmic Ray Air Showers

Cosmic ray air showers occur when EHE cosmic rays hit the earth and interacts in the atmosphere to produce a cascade of particles (Sokolsky, Sommers and Dawson, 1992). Showers up to 3×10^{20} eV have been seen (Bird *et al.*, 1994). Two techniques are used to

study the highest energy air showers. Large aperture telescopes, like the Flys Eye (Bird *et al.*, 1994) observe the shower induced fluorescence of the N_2 in air, measuring the shower development in the atmosphere. Ground based arrays of hundreds or thousands of small detectors, spaced up to a kilometer apart, observe the remnants of the shower that reach the ground (Auger, 1996).

Because the detectors are behind such a thick atmospheric absorber, $28 X_0$, or 15 hadronic interaction lengths, λ , ground based arrays have limited resolution. The problem is akin to measuring energy deposition by observing the leakage from the back of a thick calorimeter. Large fluctuations can arise depending on the depth and character of the first interaction in the atmosphere. Determining the energy spectrum of the incoming particles from a sample of events requires a good understanding of the shower process and its fluctuations.

There has been considerable disagreement about whether the LPM effect is important in ultra-high energy showers. Capdevielle and Atallah (1992) predict that LPM suppression has a large effect on 10^{19} to 10^{20} eV proton induced air showers. However, Kalmykov, Ostapchenko and Pavlov (1995) found a much smaller change; for a 10^{20} eV shower, they found a 5% decrease in the number of electrons at shower maximum, and a 15 ± 2 g/cm² downward shift in the position of shower maximum. Although this shift is smaller than the measurement resolution, it is systematic, and important in studies of cosmic ray composition. Neither of these authors considered the effect of other suppression mechanisms, or the effect on higher energy showers.

Although a complete Monte Carlo simulation is required to quantify the effect of suppression, simple calculations can demonstrate some of qualitative features, and give crude estimates of its importance (Klein, 1997). The calculations depend strongly on the identity of the incoming particles, with protons (or neutrons) the most popular, although photons or heavier nuclei cannot be excluded. For heavy ions, any suppression is greatly reduced because of the lower per-particle energy. Because we are considering almost toylike models, the possibility that very high energy photons will pair convert in the earth's magnetic field will be neglected here (Stanev and Vankov, 1997).

Because the atmospheric pressure, $1/X_0$ and $1/E_{LPM}$ decrease exponentially with height, it is convenient to consider shower propagation using an exponential variable; this review will meter depth in terms of column density, in g/cm², with ground level, A_0 at 1030 g/cm². Then, $E_{LPM} = (A_0/A) 234$ PeV, where A is the depth in column density. Similarly, $y_{die} = 1.3 \times 10^{-6}(A/A_0)$ and $E_p = \sqrt{A_0/A} 42$ PeV. Because the atmosphere is much cooler at high altitudes, these numbers underestimate suppression by about 25%. They also neglect the fact that air is composed of diatomic N_2 and O_2 molecules; when an electromagnetic interaction involves one atom of the molecule, the other atom will introduce additional multiple scattering over that expected from a monoatomic gas. This could be a significant effect, but it has yet to be studied.

Incoming photons react by pair production, while protons interact hadronically. A central hadronic collision will produce a shower of several hundred pions; the neutral pions will decay to photons. The highest energy π^0 will have a rapidity near to the incoming proton, and their decay photons will have energies around 2×10^{19} eV. Many diffractive processes, such as Δ production also produce photons with similar energies. Overall, photons from central interactions will have an average energy of about 2×10^{17} eV.

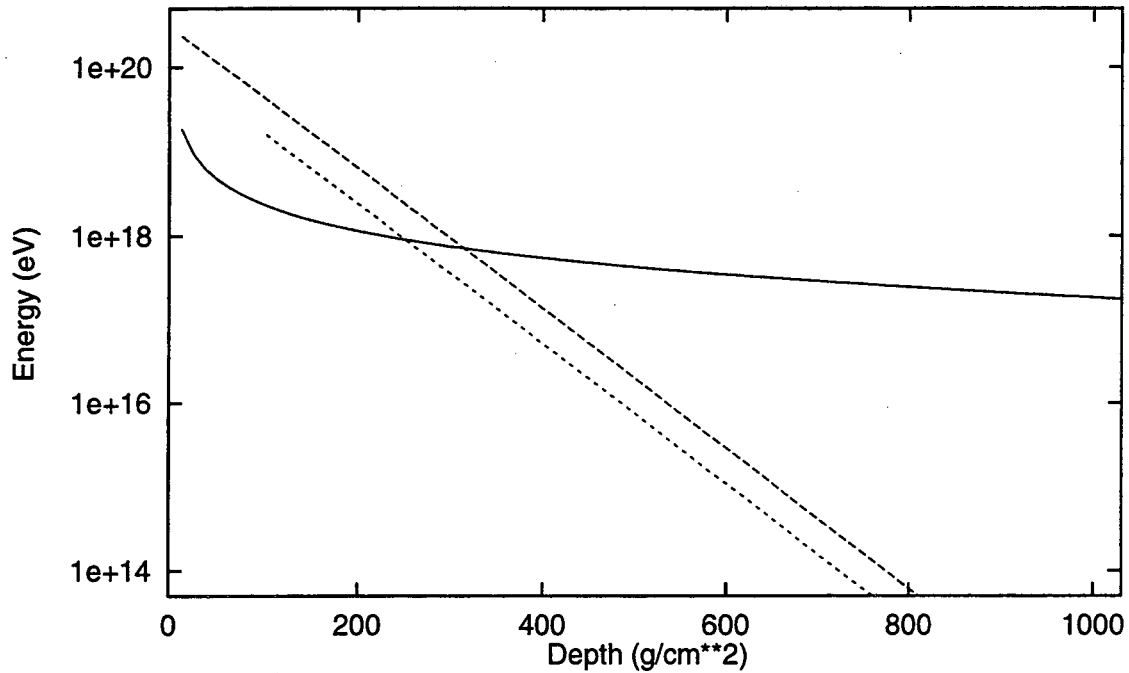


FIG. 23. E_{LPM} (solid line), \bar{E} for a 3×10^{20} eV photon shower (long dashes) and \bar{E} for a 2×10^{19} eV photon created at 1λ (short dashes). The \bar{E} s are based on an idealized Bethe-Heitler shower where the number of particles doubles each radiation length. At altitudes where $\bar{E} > E_{LPM}$, suppression is important; the ratio of the two energies determines the degree of suppression. Here, a temperature correction has been added to E_{LPM} .

Because both E_{LPM} and the average particle energy, \bar{E} , decrease with depth, suppression mechanisms can actually become stronger as a shower moves deeper in the atmosphere. Fig. 23 compares E_{LPM} with \bar{E} for an idealized Bethe-Heitler shower from a 3×10^{20} eV photon. In each successive radiation length, there are twice as many particles with half the energy. The other curve shows a similar cascade, from a 2×10^{19} eV photon starting at 1λ . The electromagnetic interactions at a given depth are determined by the ratio \bar{E}/E_{LPM} . For the photon shower, the maximum suppression occurs around 75 g/cm^2 , where $E \sim 40E_{LPM}$. Electron dE/dx is reduced about 80%, and pair production cross section is reduced by 60%; X_0 has more than doubled. For hadronic showers, the effect is smaller, and, of course, these high energy photons are only a small portion of the total shower. On the other hand, since hadronic interactions are only partially inelastic, the proton may carry a significant fraction of its momentum deeper in the atmosphere, where suppression is larger. In general, at least part of the shower will be suppressed. Because of the large variations in energy deposition depths, it is difficult to give more quantitative estimates.

This simple model underestimates the importance of suppression. When suppression slows shower development, \bar{E} of the remainder of the shower will increase, increasing the suppression in the next radiation length. However, the model shows that suppression is very important in photon showers, and in at least parts of proton initiated showers. However, suppression is clearly less significant for proton showers than predicted by Capdevielle and Atallah (1992). These calculations appear consistent with Kalmykov, Ostapchenko and Pavlov (1995).

Fluctuations are also very important in air showers. Because the cosmic ray energy spectrum falls as $dN/dE \approx 1/E^3$, it is important to understand the tails of the energy resolution distribution; without accurate simulations, showers whose energy is overestimated can skew the measured spectrum. This is especially important with ground based detectors, which measure the leakage through $28 X_0$ of air. The leakage depends critically on the depth and character of the initial interactions. Suppression mechanisms exacerbate the fluctuations, by greatly decreasing the number of interactions in the initial stage of the shower. For example, in sea level air, a 10^{10} electron emits an average of 14 bremsstrahlung photons per X_0 , while a 10^{17} eV electron emits only 3 photons. Pair creation is similarly affected; pairs become more and more asymmetric. The result is that shower to shower fluctuations are much larger.

Suppression also greatly reduces the number of particles in the earliest stages of a shower, eliminating most of the low energy 'fuzz.' The LPM effect, dielectric suppression and pair conversion suppression all contribute to this reduction. Although the LPM effect covers the widest range of energies, the other effects are stronger in the limited range in which they operate. For $E > E_p$, dielectric suppression reduces the number of bremsstrahlung photons with $k < 331$ MeV by two orders of magnitude. None of the current simulation efforts include these other mechanisms. Even relatively late in the shower, there will be a reduction in the number of low energy particles. For example, where $\bar{E} \sim 10^{13}$ eV, the LPM effect suppresses photons below ~ 500 MeV.

Because E_{LPM} drops as altitude decreases, suppression greatly increases the chance of photons penetrating deep in the atmosphere, even if the average interaction depth isn't too different. For example, Bethe-Heitler and LPM predict similar average conversion depths for a 3×10^{20} eV shower, 114 and 122 g/cm² respectively. However, Migdal predicts that the photon has a 7% chance of surviving to a depth of $6X_0$, while Bethe and Heitler predict only a 0.25% survival probability at the same depth. These occasional deep interactions can drastically change the apparent nature of the shower; producing a deep, dense subcore where much more energy will reach the ground. Although the magnitude is smaller, similar effects may be seen for the most energetic photons from proton interactions.

There have also been searches for neutrino interactions with air deep in the atmosphere, producing nearly horizontal air showers. Because the neutrino interaction cross section rises with energy, this becomes especially attractive for very high energy neutrinos, $E \sim 10^{15} - 10^{21}$ eV (Capelle *et al.*, 1998). Since these neutrino interactions occur at low altitudes, where E_{LPM} is a few hundred PeV, suppression is extremely important, especially at the higher energies. For example, a 10^{20} eV electron at sea level has a dE/dx a factor of 10 lower than the Bethe-Heitler prediction.

C. Showers in Detectors

Changes in shower energy deposition may also be important in the next generation of high energy and astrophysics detectors. This review will consider two examples, with a few representative numbers.

Direct cosmic ray composition measurements depend on measuring the cosmic ray charge and energy; the latter in a calorimeter. Because these experiments must be done above much of the atmosphere, either in balloon flights or space based experiments, calorimeter thickness

is limited by the allowable weight. For example, the JACEE collaboration has flown $\sim 6X_0$ thick lead + emulsion/X-ray film calorimeters on long duration balloon flights (Parnell *et al.*, 1989). Protons with energies up to 500 TeV were observed. Since a proton can be diffractively excited to a Δ particle, which can decay $p\pi^0 \rightarrow p\gamma\gamma$, photons with energies up to about 7% of the proton energy, 35 TeV, can be produced. Figure 2 shows that the location of the photon conversion point is not affected since $35 \text{ TeV} \sim 8E_{LPM}$. However, the produced produced electrons and positrons will exhibit reduced energy loss, and overall energy leakage out of the back of the calorimeter may increase. The next generation of space based experiments will detect protons with energies well beyond 1 PeV, with a consequently increased effect (Parnell *et al.*, 1989).

At the Large Hadron Collider, now under construction at CERN, electrons with energies up to about 1 TeV will be produced. Electron identification will be aided by a pre-shower radiator, which will separate electrons from hadrons by measuring the energy radiated in the first 2 or 3 X_0 of a lead calorimeter (Aspell *et al.*, 1996). Because several suppression mechanisms reduce the number of photons emitted by the electron, electrons will interact more like heavier particles like muons and pions. A 1 TeV electron in lead radiates an average of 3 photons per radiation length; with only dielectric suppression it radiates 9 photons per X_0 , while without suppression, the number of photons is infrared divergent: $\ln(E/k_{min})$, where k_{min} is the lowest detectable photon energy. The small average number of photons emitted means that there is a finite probability that the early stages of an electron shower will be indistinguishable from radiation from a pion or muon.

XII. QCD ANALOGS

QCD analogs of the LPM effect involve quarks and gluons moving through a strongly coupling nuclear medium. Because the nuclear medium is so dense, a quark or gluon moving through the medium typically undergoes many soft color exchange interactions, analogous to multiple scattering. Because a nucleus is small, the formation length is often larger than the nucleus, so the nucleus acts as a single radiator.

The literature on this subject is voluminous and this is not the place for a detailed review. Instead, we will discuss a few examples, to illustrate the basic features of the interactions, and also to emphasize the both the similarities and the differences between the QED and QCD cases. Because QCD couples strongly and is non-Abelian, the theoretical calculations are much less robust, and the experimental data is much harder to interpret.

A. Hadron Level Calculations

In hadronic interactions, particle masses play a larger role than they do in electromagnetic interactions. Suppression effects in hadronic interactions can be seen easily by considering the photoproduction of vector mesons, for example $\gamma N \rightarrow \phi N$. This reaction is similar to $\gamma \rightarrow e^+e^-$, with a quark pair produced instead of a lepton pair. One difference is that the interaction between the quark pair and the nucleus is hadronic, rather than electromagnetic.

The formation length for vector meson production is the same as for pair production, $2\hbar k/M_V^2 c$. For a 100 GeV photon producing a ϕ , $l_{f0} = 40 \text{ fm}$, far larger than the nuclear diameter. So, the photon/vector meson interacts with the nucleus as if it is a single particle,

with the interactions determined by Eq. (53). Unfortunately, QCD does not specify $f(\theta)$, but, in principle, this equation could be used to explore how the cross section depends on the nuclear thickness.

Another example where suppression effects can be important is low mass Drell-Yan lepton pair production, $q\bar{q} \rightarrow l^+l^-$. In the rest frame of the target nucleus, the incoming quark or antiquark can be thought of as pair producing the leptons. The momentum transfer from the target quark or antiquark can be small, so the formation zone can extend far outside the nucleus.

B. Quark Level Calculations

More fundamental calculations involve quarks and gluons moving through a possibly very hot nucleus. One focus of recent calculations is the search for the quark gluon plasma; a hadron gas (normal nucleus) may show very different behavior than a quark gluon plasma in which protons and neutrons are replaced by a sea of quarks and gluons. This sea of quarks and gluons, with a longer screening length, should cause fast quarks and gluons to lose energy considerably faster than in medium consisting of confined quarks and gluons. Measurements of high energy jets (or hadrons) energy loss has been proposed as a tool for detecting the quark gluon plasma (Wang, Huang and Sarcevic, 1996).

For the simplest illustration, it is instructive to consider the case of bremsstrahlung energy loss (dE/dx) by a quark with energy E emitting gluons of energy k while moving through a nuclear medium. Including the particle masses

$$l_{f0} = \frac{2\hbar Ek(E-k)}{m_q^2 c^3 k^2 + m_g^2 c^3 E(E-k)} \quad (106)$$

where m_q and m_g are the quark and gluon masses respectively. Unfortunately, these poorly determined masses critically affect l_{f0} . Besides the bremsstrahlung analog, gluons can 'pair create' quark anti-quark pairs, a close analog of pair production. Because of the possibility of experimentally measuring jet or hadron energy loss discussed above, most calculations have focused on the bremsstrahlung analog.

Sørensen (1992) was one of the first to consider this problem. He repeated the Landau and Pomeranchuk semi-classical derivation, and also adapted Migdals formulae to quarks and gluons. Although the calculations were dependent on m_q and m_g , and hence of limited accuracy, he did show that, for reasonable mass choices, suppression was important.

Brodsky and Hoyer (1993) used simple quantum mechanical arguments to find that the energy loss of a parton travelling through nuclear matter is limited by $\Delta E/E < \kappa A^{1/3}/x_1^2 s$ where $\kappa \sim 0.5 \text{ GeV}^2$, x_1 is the fractional energy of the produced parton and \sqrt{s} is the center of mass energy. Here, $x_1\sqrt{s}$ is analogous to E . Since the length of the radiator is proportional to $A^{1/3}$, for high energy partons, the energy loss should be negligible for reasonably high energy hadrons.

Wang, Gyulassy and Plümer (1995) did a detailed calculation of energy loss in a quark gluon plasma. They found that the radiation, while obeying the bound listed above, was very sensitive to the color screening distance in the plasma. The strength of the suppression is given by the ratio of the mean free path λ to an effective formation time t_f ; this is similar to the QED plasma case. When $t_f < \lambda/c$,

$$\frac{dE}{dz} = \frac{C_2 \alpha_s \langle q_1^2 \rangle}{\pi \hbar} \ln \left(\frac{2r_2 E \hbar}{\mu^2 c^3 \lambda} \right) \quad (107)$$

where α_s is the strong force coupling constant, $\langle q_1^2 \rangle$ is the square of the average momentum transfer from a single scattering, which should be proportional to μ^2 , with μ the color screening mass. For quarks, the color factors $C_2 = 4/3$ and $r_2 = 9/8$, while for gluons $C_2 = 3$ and $r_2 = 9/8$. So, the energy loss only grows logarithmically with particle energy; a typical value is $dE/dx \sim 3.6$ GeV/fm. In the opposite case, when $t_f > \lambda/c$, the energy loss is proportional to energy, as with Bethe Heitler bremsstrahlung.

Newer calculations have emphasized the finite size of nuclei. Many of these works have also considered the QED case, useful as a check of their results. Zakharov (1997) applies the techniques of Sec. V to finite thicknesses of both nuclear matter and the quark gluon plasma. For a quark travelling through a nuclear medium, the energy loss is proportional to the distance travelled, $\Delta E/E \sim T/10$ fm, considerably higher than Brodsky and Hoyer. The difference appears to stem from the different treatments of the finite nuclear size. Zakarov found that, because surface effects are so large, LPM suppression plays a minor role.

For high energy quarks ($l_{f0} > R_A$) created inside the nucleus, he found the energy loss $\Delta E \sim T^2$; this dependence is because the quark will take some time to fully create its gluon field; this is analogous to the lower dE/dx observed for newly created e^+e^- pairs. For quarks created at lower energies, where $l_f < R_A$, the energy loss is proportional to the distance travelled, $\Delta E/E \sim T/10$ fm.

R. Baier and collaborators (1995) considered a fast quark or gluon propagating through QCD matter. For an infinite medium, they find a soft gluon spectrum matching their later electrodynamics result (R. Baier *et al.* 1996) result for soft photons, with an energy loss per unit length $dE/dz \sim \sqrt{E}$, similarly to the QED case. This differs from the logarithmic energy dependence found by Wang, Gyulassy and Plümer. The difference is because this work included additional diagrams, such as the non-Abelian 3-gluon vertices; they state that these are the dominant source of emission. A later, expanded collaboration (R. Baier *et al.*, 1997) considered the case of a finite sized quark gluon plasma and found the same energy dependencies are earlier, along with the same R_A^2 dependence found by Zakharov. However, for lower energy emission, they find a much higher energy loss, $\Delta E/E \sim T/4$ fm, much higher than Brodsky and Hoyer or Zakharov. It appears that this difference may be because of the additional diagrams; Zakarov's formalism treats the multiple gluon vertex as a simple modification of the $q\bar{q}g$ vertex, while R. Baier and collaborators have a somewhat more detailed treatment.

While these calculations agree in many ways, there is still some significant disagreement. They generally agree about the appropriate energy scaling in the Bethe-Heitler (no suppression) and strong suppression regimes, and also show a good correspondence with the QED calculations. The disagreement is over where these two regimes apply. Some of this stems from differing treatment of surface terms. Whatever the cause, the numerical results vary greatly. Unfortunately, because of the difficulty of clear experimental tests, it may be some time before data can point to the best result.

XIII. SUPPRESSION IN E^+E^- COLLISIONS

Future high energy electron-positron colliders will collide extremely dense beams of electrons and positrons. When they collide, besides the desired hadronic interactions, large numbers of photons will be created. Photon emission before the desired hadronic interaction can lower the average collision energy. Also, some of the photons will pair convert, introducing a charged particle background into the detector. The photon production can be coherent, a process known as beamstrahlung, or incoherent bremsstrahlung. In beamstrahlung, a single particle interacts with the other beam as a whole to produce a photon. Because of the density of the plasma, multiple scattering, Compton scattering and magnetic suppression can suppress some of these interactions.

Although suppression occurs for similar reasons as in bulk matter, many of the details are different because of the very different medium. Both bremsstrahlung and pair creation are modified because bare charges are involved; q_{min} is governed by the size of the beams. For both, the magnetic fields produced by the opposing beam can have strong effects, and both bremsstrahlung and pair creation are significantly suppressed. (Baier and Katkov, 1973)(Katkov and Strakhovenko, 1977), as is beamstrahlung.

In contrast, because of the low density, LPM suppression is small in currently envisioned machines. Dielectric suppression transfers over rather directly, after adjusting for the differing electron densities. It is in principle strong enough to cause significant suppression. However, because the beams are much shorter than l_{f0} , dielectric suppression is reduced, and of only marginal significance (Chen and Klein, 1993).

XIV. OPEN PROBLEMS AND FUTURE POSSIBILITIES

Theoretically, there has been much progress in the past few years, and several new approaches to LPM suppression have appeared. The problem of radiation from slabs, sets of foils and the like have all been considered for a wide range of kinematic factors. Despite this, these calculations have some limitations. Most are limited to suppression due to multiple scattering, and none cover the full range of suppression mechanisms. None cover pair production; this may no longer be a trivial extension. None of the calculations consider higher order diagrams. Of similar importance, most of the calculations only handle single photon radiation. For slab thicknesses larger than about 10% of X_0 , several photons are likely to be emitted; this requires a difficult extension to the calculation. Finally, the high energy regime when bremsstrahlung and pair creation suppress each other needs to be explored. Even if QED tests are not practical, this may have significant implications for understanding the QCD case.

Even in the absence of a unified approach, a better treatment of dielectric suppression is of interest. To treat multi-GeV bremsstrahlung with classical electromagnetism concepts like the dielectric constant of a medium is rather anachronistic. The dielectric constant comes from photons forward Compton scattering off the electrons in the medium; it would be very nice to see a calculation of dielectric suppression that uses Compton scattering as a starting point; such a calculation might yield some interesting surprises.

All of these recent results need to be made generally accessible. An easily accessible program library would let experimenters compare the different approaches under a variety

of conditions.

Many implications of the LPM effect are poorly appreciated, and there is a need to learn more about them. One 'lesson' from SLAC-E-146 is that there is very little data on small y bremsstrahlung, and consequently little theoretical attention to this area. Of particular concern are radiative corrections to electromagnetic effects. Besides the effect that suppressed bremsstrahlung will have on elastic scattering, little is known about when higher order terms become important.

Experimentally, there is a need to accurately measure suppression at higher energies, and to look at new phenomena. Cosmic ray based experiments have poor statistics, and current accelerators only reach the semi-classical ($k \ll E$) regime. Ideally, a study of quantum bremsstrahlung would use electrons with $E > E_{LPM} \approx 2.6$ TeV. A proposed experiment at Fermilab (Jones *et al.*, 1993) with 250 GeV electrons would be a significant step forward, but would not reach this goal. Unfortunately, a TeV electron beamline seems a long way off. However, because a relatively low flux is sufficient, it might be possible to use electrons and or photons produced in 14 TeV pp collisions at LHC to study bremsstrahlung or pair production. Suppression effects are large enough that they may also be observable in the LHC general purpose detectors. This is particularly likely in apparatus such as pre-shower radiators that look at early shower development.

Any future test of LPM or dielectric suppression must at least match E-146 in statistics, backgrounds and control of systematics. The statistics should be simple, but the backgrounds and systematics will require some effort. It will be necessary to minimize the magnetic fields in the bending magnets, photon angular acceptance, and backgrounds due to the beam transport system. With a higher energy beam, it should also be possible to reduce the systematic errors, by avoiding the calorimetric 'transition region' between energy deposition by Compton scattering and by showering. It would also be very useful to collect data with a wider range of target thicknesses, and also more low Z targets. With an experiment accurate to 1-2%, it should be possible to compare the data with the recent theoretical predictions, assuming that the problems of multiple emission by a single electron can be handled properly, either theoretically or experimentally. While experiments with higher accuracy than E-146 are very desirable, improving the systematic errors by a large factor over E-146 would require extreme attention to detail.

Any new experiment should also investigate other phenomena, such as magnetic suppression. With a 100+ GeV electron beam, magnetic suppression should occur in a broader k range than dielectric suppression, and hence be directly observable. Studies in a constant magnetic field are probably the most interesting, but the effect of randomly ordered domains might also be observable. A similar apparatus could measure emission from targets consisting of stacks of foils, to investigate transition radiation due to multiple scattering. It is desirable to try to push bremsstrahlung measurements to the smallest y possible. As Eq. (102) demonstrates, this is a new regime, and some surprises may await us. One tangible goal would be to reach the point where higher order corrections cause current theories to fail.

There is currently considerable theoretical effort studying LPM-like phenomena in QCD. With the coming data on high energy heavy ion collisions from RHIC, this work will probably continue, with an increasing emphasis on ways to differentiate between suppression in a hadron gas and that of a quark gluon plasma. The biggest need, however, is for a clear

experimental demonstration of suppression involving QCD.

One area where more theoretical work is needed is to understand how suppression phenomena affect many astrophysical phenomena. One down-to-earth subject that needs work is the question of how suppression affects EHE cosmic ray air showers. Other topics, less tied to specific experimental techniques, include the study of suppression in astrophysical regions of extreme density, temperature, and/or magnetic field. This review has discussed a few such areas, but there are many more.

Between the new theoretical approaches and the expanding range of applications in QCD, plasmas and astrophysics, suppression mechanisms seem destined to be a growing area of study over the coming years,

XV. ACKNOWLEDGEMENTS

This review would not have been possible without much help. V. Baier, R. Becker-Szendy, R. Blankenbecler, S. Drell, D. Schiff, N. F. Shulga and B.G. Zakharov explained various theoretical aspects of suppression. V. Baier, R. Becker-Szendy, R. Blankenbecler, S. Drell, R. Engel, L. Kelley, D. Loombha, A. Sørensen, X. N. Wang and D. Zimmerman contributed by reading and commenting on early drafts of this manuscript. Needless to say, any mistakes are my responsibility. I'd also like to thank my E-146 collaborators for continuing discussions of the experiment. Don Coyne, Hans Georg Ritter and Jay Marx provided bureaucratic and moral support. This work was supported by the U.S. D.O.E. under contract DE-AC03-76SF00098.

REFERENCES

- Akhiezer, A. I. and N. F. Shul'ga, 1987, "Influence of multiple scattering on the radiation of relativistic particles in amorphous and crystalline media," *Usp. Fiz. Nauk* **151**, 385 [*Sov. Phys. Usp.* **30**, 197 (1987)].
- Anthony, P. *et al.*, 1995, "An accurate measurement of the Landau-Pomeranchuk-Migdal effect," *Phys. Rev. Lett.* **75**, 1949.
- Anthony, P. *et al.*, 1996, "Measurement of dielectric suppression of bremsstrahlung," *Phys. Rev. Lett.* **76**, 3550.
- Anthony, P. *et al.*, 1997, "Bremsstrahlung suppression due to the LPM and dielectric effects in a variety of targets," *Phys. Rev.* **D56**, 1373.
- Artru, X., G. B. Yodh and G. Mennessier, 1975, "Practical theory of multilayered transition radiation detector," *Phys. Rev.* **D12**, 1289.
- Arutyunyan, F. R., A. A. Nazaryan and A. A. Frangyan, 1972, "Influence of the medium on the emission of relativistic electrons," *Zh. Eksp. Teor. Fiz.* **62**, 2044 [*Sov. Phys. JETP*, **35**, 1067 (1972)].
- Aspell, P., *et al.*, 1996, "Energy and spatial resolution of a shashlik calorimeter and a silicon preshower detector," *Nucl. Instrum. and Meth.* **A376**, 17.
- Auger Collaboration, 1996, "The Pierre Auger project design report," Fermilab-Pub-96-024 (unpublished).
- Baier, R., Yu. L. Dokshitzer, A. H. Mueller and D. Schiff, 1996, "The Landau-Pomeranchuk-Migdal effect in QED," *Nucl. Phys.* **B478**, 577.
- Baier, R., Yu. L. Dokshitzer, A.H. Mueller, S. Peigne and D. Schiff, 1997, "Radiative energy loss of high energy quarks and gluons in a finite volume quark gluon plasma," *Nucl. Phys.* **B483**, 265.
- Baier, R., Yu. L. Dokshitzer, S. Peigne and D. Schiff, 1995, "Induced gluon radiation in a QCD medium," *Phys. Lett.* **B345**, 277.
- Baier, V. N. and V. M. Katkov, 1972, "Production of bremsstrahlung during collisions of high-energy particles in a magnetic field," *Dokl. Akad. Nauk. SSSR* **207**, 68 [*Sov. Phys. Dokl.*, **17**, 1068 (1973)].
- Baier, V. N., V. M. Katkov and V. M. Strakhovenko, 1988, "Radiation at collision of relativistic particles in media in the presence of external field," *Zh. Eksp. Teor. Fiz.* **94**, 125 [*Sov. Phys. JETP* **67**, 70 (1988)].
- Baier, V. N., V. M. Katkov and V. M. Strakhovenko, 1989, "Interaction of high-energy electrons and photons with crystals," *Usp. Fiz. Nauk.* **159**, 455 [*Sov. Phys. Usp.* **32**, 972 (1989)].
- Baier, V. N. and V. M. Katkov, 1997a, "The theory of the Landau, Pomeranchuk, Migdal effect," preprint hep-ph/9709214, to appear in *Phys. Rev. D*.
- Baier, V. N. and V. M. Katkov, 1997b, "The Landau-Pomeranchuk-Migdal effect in a thin target," preprint hep-ph/9712524.
- Baier, V. N., 1998, private communication.
- Bak, J. F., J. B. B. Petersen, E. Uggerhøj, K. Østergaard, S. P. Møller and A. H. Sørensen, 1986, "Influence of transition radiation and density effect on atomic K-Shell excitation," *Phys. Scripta* **33**, 147.
- Bak J. F., *et al.*, 1988, "Channeling radiation from 2 to 20 GeV/c electrons and positrons (II).," *Nucl. Phys.*, **B302**, 525.

- Barnett, R.M. *et al.* (Particle Data Group), 1996, "Review of particle properties," *Phys. Rev.* **D54**, 1.
- Bell, J. S., 1958, "Bremsstrahlung from multiple scattering," *Nucl. Phys.* **8**, 613.
- Bethe, H. A. and W. Heitler, 1934, "On the stopping of fast particles and the creation of positive electrons," *Proc. Royal Soc.* **A146**, 83.
- Bird, D. J., *etal.*, 1994, "The cosmic-ray Energy spectrum observed by the Flys Eye," *Astrophys. J.* **424**, 491.
- Blankenbecler, R. and S. D. Drell, 1996, "The Landau-Pomeranchuk-Migdal effect for finite targets," *Phys. Rev.* **D53**, 6285.
- Blankenbecler, R., 1997a, "Structured targets and the Landau-Pomeranchuk-Migdal effect," *Phys. Rev.* **D55**, 190.
- Blankenbecler, R., 1997b, "Multiple scattering and functional integrals," *Phys. Rev.* **D55**, 2441.
- Blankenbecler, R., 1997c, private communication.
- Brodsky, S. J. and P. Hoyer, 1993, "A bound on the energy loss of partons in nuclei," *Phys. Lett.* **B298**, 165.
- Capelle, K. S., J. W. Cronin, G. Parente and E. Zas, 1998, "On the detection of ultrahigh-energy neutrinos with the Auger Observatory," preprint astro-ph/9801313.
- Capdevielle, J. N. and R. Attallah, 1992, "Limits of classical detection for GAS," *Nucl. Phys. B (Proc. Suppl.)*, **28B**, 90.
- Cavalli-Sforza, M. *et al.*, 1992, "A proposal for an experiment to study the interference between multiple scattering and bremsstrahlung," SLAC-Proposal-E-146, June, 1992.
- Cavalli-Sforza M., *et al.*, 1994, "A method of obtaining parasitic e^+ or e^- beams during SLAC linear collider operation," *IEEE Trans. Nucl. Sci.* **41**, 1374.
- Chen, P. and S. Klein, 1992, "The Landau-Pomeranchuk-Migdal effect and suppression of beamstrahlung and bremsstrahlung in linear colliders," in *Proc. of the Advanced Accelerator Conference Workshop*, ed. J. S. Wurtele (AIP, New York), pg. 921.
- Cherry, M. L., 1978, "Measurements of the spectrum and energy dependence of X-ray transition radiation," *Phys. Rev.* **D17**, 2245.
- Feinberg, E. L. and I. Pomeranchuk, 1956, "High energy inelastic diffraction phenomena," *Supplemento Al Volume III, Series X, Del Nuovo Cimento*, pg 652.
- Fomin, P. I., 1958, "Radiative corrections to bremsstrahlung," *Zh. Eksp. Teor. Fiz.* **35**, 707 [*Sov. Phys. JETP* **35**, 491 (1959)].
- Fomin, S. P. and N. F. Shul'ga, 1986, "On the space-time evolution of the process of ultra-relativistic electron radiation in a thin layer of substance," *Phys. Lett.* **114A**, 148.
- Fowler, P. H., D. H. Perkins and K. Pinkau, 1959, "Observation of the suppression effect on bremsstrahlung," *Phil. Mag.* **4**, 1030.
- Galitsky, V. M. and I. I. Gurevich, 1964, "Coherence effects in ultra-relativistic electron bremsstrahlung," *Il Nuovo Cimento* **32**, 396.
- Gariyban, G. M., 1960, "Radiation of a particle moving across the interface of two media with account of multiple scattering," *Zh. Eksp. Teor. Fiz.* **39**, 332 [*Sov. Phys. JETP* **12**, 237 (1960)].
- Gol'dman, I. I., 1960, "Bremsstrahlung at the boundary of a medium with account of multiple scattering," *JETP* **38**, 1866 [*Sov. Phys. JETP* **11**, 1341 (1960)].
- Heckler, A. F., 1995, "On the formation of a Hawking-radiation photosphere around micro-

- scopic black holes," *Phys. Rev.* **D55**, 480.
- Jackson, J. D., 1975, *Classical Electrodynamics*, (John Wiley and Sons, New York).
- Jones, L. W. *et al.*, 1993, "An experimental test of the Landau-Pomeranchuk-Migdal effect," Fermilab Proposal P-813 (unpublished).
- Kalmykov, N. N., S. S. Ostapchenko and A. I. Pavlov, 1995, "Influence of the Landau-Pomeranchuk-Migdal Effect on the features of extensive air showers," *Yad. Fiz.* **58**, 1829 [*Phys. Atomic Nuclei* **58**, 1728 (1995)].
- Katkov, V. N. and V. M. Strakhovenko, 1977, "Bremsstrahlung in collisions of electrons in a magnetic field," *Yad. Fiz.* **25**, 1245 [*Sov. J. Nucl. Phys.* **25**, 660 (1977)].
- Klein, S. R. *et al.*, 1993, "A measurement of the LPM effect" in *Proc. XVI Int. Symp. Lepton and Photon Interactions at High Energies*, edited by P. Drell and D. Rubin, (AIP, New York), p. 172.
- Klein, S. R., 1997, "Bremsstrahlung and pair creation: suppression mechanisms and how they affect air showers," astro-ph/9712198, to appear in *Observing the Highest Energy Particles ($> 10^{20}$ eV) from Space*, edited by John Krizmanic (AIP, New York), 1998.
- Knoll, J. and D. N. Voskresensky, 1995, "Non-equilibrium description of bremsstrahlung in dense matter (Landau-Pomeranchuk-Migdal effect)," *Phys. Lett.* **B351**, 43.
- Knoll, J. and D. N. Voskresensky, 1996, "Classical and quantum many-body description of bremsstrahlung in dense matter," *Ann. Phys.* **249**, 532.
- Konishi, E., A. Adachi, N. Takahashi and A. Misaki, 1991, "On the characteristics of individual cascade showers with the LPM effect at extremely high energies", *J. Phys. G* **17**, 719.
- Landau, L. D and I. J. Pomeranchuk, 1953a, "The limits of applicability of the theory of bremsstrahlung by electrons and of the creation of pairs at large energies," *Dokl. Akad. Nauk. SSSR* **92** 535. This paper is available in English in (Landau, 1965).
- Landau, L. D. and I. J. Pomeranchuk, 1953b, "Electron-cascade processes at ultra-high energies," *Dokl. Akad. Nauk. SSSR* **92**, 735. This paper is available in English in (Landau, 1965).
- Landau, L. D., 1965, *The Collected Papers of L. D. Landau*, Pergamon Press.
- Learned J. G. and S. Pakvasa, 1995, "Detecting tau-neutrino oscillations at PeV energies," *Astropart. Phys.* **3**, 267.
- Lohrmann, E., 1961, "Investigation of bremsstrahlung and pair production at energies $> 10^{11}$ eV," *Phys. Rev.* **122** 1908.
- Miesowicz, M., O. Stanisiz and W. Wolther, 1957, "Investigation of an electromagnetic cascade of very high energy in the first stage of its development," *Nuovo Cim.* **5**, 513.
- Migdal, A. B., 1956, "Bremsstrahlung and pair production in condensed media at high energies," *Phys. Rev.* **103**, 1811.
- Migdal, A. B., 1957, "Bremsstrahlung and pair production at high energies in condensed media," *Zh. Eksp. Teor. Fiz.* **32**, 633 [*Sov. Phys. JETP* **5**, 527 (1957)].
- Misaki, A., 1990, "A study of electromagnetic cascade showers with the LPM effect in water for the detection of extremely high energy neutrinos," *Forsch. Phys.* **38**, 413.
- Misaki, A., 1993, "The Landau - Pomeranchuk - Migdal (LPM) effect and its influence on electromagnetic cascade showers at extremely high energies," *Nucl. Phys. B (Proc. Suppl.)* **33A,B**, 192.
- Pafomov, V. E., 1964, "Effect of multiple scattering on transition radiation," *Zh. Eksp. Teor.*

- Fiz. **47**, 530 [Sov. Phys. JETP, **20**, 353 (1965)].
- Pafomov, V. E., 1965, "Concerning bremsstrahlung," Zh. Eksp. Teor. Fiz. **49**, 1222 [Sov. Phys. JETP **22**, 848 (1966)].
- Pafomov, V. E., 1967, "Optical bremsstrahlung in an absorbing medium," Zh. Eksp. Teor. Fiz. **52**, 208 [Sov. Phys. JETP, **25**, 135 (1967)].
- Parnell, T. A. *et al.*, 1989, "Spectra, composition and interactions of nuclei with magnet interaction chambers," in *Particle Astrophysics: The NASA Cosmic Ray Program for the 1990's and Beyond*, ed. W. V. Jones, F. J. Kerr and J. F. Ormes, AIP, New York.
- Palazzi, G. D., 1968, "High-energy bremsstrahlung and electron pair production in thin crystals," Rev. Mod. Phys. **40**, 611.
- Perl, M. L., 1994, "Notes on the Landau, Pomeranchuk, Migdal effect: experiment and theory," in *Proc. 1994 Les Rencontres de Physique de la Vallee D'Aoste*, (Editions Frontieres, Gif-sur-Yvette, France.), Ed. M. Grego, p. 567.
- Raffelt, G. and D. Seckel, 1991, "Multiple-scattering suppression of bremsstrahlung emission of neutrinos and axions in supernovae," Phys. Rev. Lett. **67**, 2605.
- Rossi, B., 1952, *High Energy Particles*, Prentice Hall, Inc.
- Schiff, L. I., 1968, "Quantum Mechanics", 3rd edition, (McGraw Hill, New York).
- Scott, W. T., 1963, "The theory of small-angle multiple scattering of fast charged particles," Rev. Mod. Phys. **35**, 231.
- Shul'ga, N. F. and S. P. Komin, 1978, "Suppression of radiation in an amorphous medium and in a crystal," Pis'ma Zh. Eksp. Teor. Fiz. **27**, 126 [JETP Lett. **27**, 117 (1978)].
- Shul'ga, N. F. and S. P. Fomin, 1996, "On the experimental verification of the Landau-Pomeranchuk-Migdal effect," Pis'ma Zh. Eksp. Teor. Fiz. **63**, 837 [JETP Lett., **63**, 873 (1996)].
- Sokolsky, P., P. Sommers and B. R. Dawson, 1992, "Extremely High-Energy Cosmic Rays," Phys. Rep. **217**, 225.
- Sorensen, A. H., 1992, "On the suppression of the gluon radiation for quark jets penetrating a dense quark gas," Z. Phys. C **53**, 595.
- Sorensen, A. H., 1996, "Channeling, bremsstrahlung and pair creation in single crystals," Nucl. Instrum. & Meth., **B119**, 1.
- Stanev T., Ch. Vankov, R. E. Streitmatter, R. W. Ellsworth and T. Bowen, 1982, "Development of ultrahigh-energy electromagnetic cascades in water and lead, including the Landau-Pomeranchuk-Migdal effect," Phys. Rev. D **25**, 1291.
- Stanev, T. and H. P. Vankov, 1997, "Nature of the highest energy cosmic rays," Phys. Rev. **D55**, 1365.
- Strausz, S. C. *et al.*, 1991, "A measurement of the Landau Pomeranchuk Migdal effect in electromagnetic showers," in *Proc. of the 22nd Intl. Cosmic Ray Conf., Dublin, Ireland*, Vol. 4, pg. 233.
- Ter-Mikaelian, M. L., 1954, "Spectrum of damping radiation in a [refracting] medium," Dokl. Akad. Nauk. SSR **94**, 1033.
- Ter-Mikaelian, M. L., 1972, *High Energy Electromagnetic Processes in Condensed Media*, (John Wiley & Sons, New York).
- Ternovskii, F. F., 1960, "On the theory of radiative processes in piecewise homogeneous media," Zh. Eksp. Teor. Fiz. **39**, 171 [Sov. Phys. JETP **12**, 123 (1961)].
- Toptygin, I. N., 1963, "On the theory of bremsstrahlung and pair production in a medium,"

- Zh. Eksp. Teor. Fiz. **46**, 851 [Sov. Phys. JETP **19**, 583 (1964)].
- Tsai, Y. S., 1974, "Pair production and bremsstrahlung of charged leptons," Rev. Mod. Phys. **46**, 815.
- Varfolomeev, R. R. I. Gerasimova, I. I. Gurevitch, L. A. Makar'ina, A. S. Romantseva and S. A. Chueva, 1960, "Influence of the medium density on bremsstrahlung in electron-photon showers in the energy range 10^{11} - 10^{13} eV," Zh. Eksp. Teor. Fiz. **38**, 33 [Sov. Phys. JETP **11**, 23 (1960)].
- Varfolomeev A. *et al.*, 1975, "Effect of the medium on the bremsstrahlung spectrum of 40-GeV electrons," Zh. Eksp. Teor. Fiz. **69**, 429 [Sov. Phys. JETP **42**, 218 (1976)].
- Wang, X. N., M. Gyulassy, and M. Plümer, 1995, "Landau-Pomeranchuk-Migdal effect in QCD and radiative energy loss in a quark-gluon plasma," Phys. Rev. **D51**, 4346.
- Wang, X. N., Z. Huang and I. Sarcevic, 1996, "Jet quenching in the direction opposite to a tagged photon in high-energy heavy-ion collisions," Phys. Rev. Lett. **77**, 231.
- Williams, E. J., 1935, "Correlation of certain collision problems with radiation theory," Kgl. Danske Videnskab. Selskab, Mat. Phys. Medd. **13**, Number. 4, Pg. 1.
- Zakharov B. G., 1996a, "Fully quantum treatment of the Landau-Pomeranchuk-Migdal effect in QED and QCD," Pis'ma v. ZhETF **63**, 906 [JETP Lett. **63** 952 (1996)].
- Zakharov, B. G., 1996b, "Landau-Pomeranchuk-Migdal effect for finite-size targets," Pis'ma v. ZhETF **64**, 781 [JETP Lett. **64**, 781 (1996)].
- Zakharov, B. G., 1997, "Radiative energy loss of high energy quarks in finite-size nuclear matter and quark-gluon plasma," preprint LPTHE-Orsay 97-09, March, 1997.
- Zakharov, B. G., 1998, "Light-cone path integral approach to the Landau-Pomeranchuk-Migdal effect," preprint MPI-H-V44-1997, to appear in Sov. J. Nucl. Phys.
- Zas, E., and J. Alvarez-Muniz, "Čerenkov radio pulses from EeV neutrino interactions: the LPM effect", Phys. Lett. **B411**, 218.

**ERNEST ORLANDO LAWRENCE BERKELEY NATIONAL LABORATORY
ONE CYCLOTRON ROAD | BERKELEY, CALIFORNIA 94720**